THE PERFORMANCE OF HIGH SPEED RECIPROCATING POLYMER SEALS IN WATER

A thesis submitted to the University of Cape Town, towards the degree of Master of Science in Engineering.

Jonathan James Barnes

December 1990

ACKNOWLEDGEMENTS

Without the generous support provided by the Chamber of Mines Research Organization, the work in this thesis would not have been possible. In particular the author would like to thank Mr George Harper for his continued interest in this study together with his valuable criticism and encouragement.

The author also wishes to thank Professor J. B. Martin for his supervision of the thesis.

SYNOPSIS

The elastohydrodynamic lubrication of polymeric piston seals in a water powered rockdrill has been modelled in this thesis. Current seal designs, consist of an Ultra High Molecular Weight Polyethylene (UHMWPE) ring, energised to remain in contact with the reciprocating piston, using a nitrile rubber o-ring. The design of the seals is such that they do not facilitate the formation of a lubricating film, and the high contact stresses at the seal face due to the seal pressure cause excessive wear of the seals.

The elastohydrodynamic model is based on a numerical algorithm in which the elasticity equations for the seal deflection and the one dimensional lubrication equation have been solved simultaneously. The polymeric ring has been simplified due to its axisymmetry, and modelled in cross section as an elastic beam resting on a spring base, while the deformation of the o-ring has been considered independently since the moduli of the two materials differs by nearly two orders of magnitude. The o-ring was modelled using the non-linear Mooney-Rivlin constitutive equation implemented in the finite element code ABAQUS. With this model, the contact stresses existing between the o-ring and the back of the polymer seal have been determined for a range of o-ring squeezes and rubber hardnesses. The resultant lubrication and o-ring forces acting on the rectangular polymer seal have been used in a finite difference formulation of the seal (or beam on a spring base) to determine the seal deflection above the piston.

The numerical algorithm, based on an iterative scheme to calculate the equilibrium position of the seal above the piston, is inherently unstable and does not converge. The instability in the algorithm has been explained in terms of the different stiffnesses of the polymer seal and the lubrication film, and by suitably modifying the deflection of the seal by under-relaxation, it has been possible to achieve a stable and convergent solution.

The performance of existing rockdrill seals in not forming stable hydrodynamic films is due to an unbalanced set of forces acting on the seal, causing the low pressure side

of the seal face to deform and contact the counterface or piston. By suitably modifying the forces acting on the seal it is possible to reverse this action and cause the trailing edge of the seal to deflect away from the counterface and allow for the formation of a full and stable elastohydrodynamic film. If pressure and velocity conditions are favourable, the seal may never contact the piston, but still operate within acceptable leakage limits.

The main controllable factors contributing towards the formation of an elastohydrodynamic film are : the position of the o-ring at the rear of the seal, the length of the seal and the surface roughness of the piston. The position of the o-ring at the rear of the seal limits the penetration of pressure that would normally act along the entire seal length, and reduces the resultant moment on the seal that normally causes the lubrication film to collapse. Increasing the length of the seal has the effect of increasing the average thickness of the fluid film but not necessarily the minimum film thickness, which can be kept constant by adjusting the o-ring position. The surface roughness of the piston is directly related to the minimum film thickness and the fluid film has been shown to collapse when the film thickness is equal to the roughness parameter R_z.

The predictions of the elastohydrodynamic model have been verified in actual seals in a high speed laboratory test rig. Modified seals designed to form a stable elastohydrodynamic film have been run for extended periods showing wear rates eight times lower than current seal designs operating under identical laboratory conditions.

TABLE OF CONTENTS

Chapter I. INTRODUCTION.

The deep and hot conditions in South African gold mines have prompted the development of an alternate form of power for equipment in the stopes - namely hydro-power. In essence this involves using the high pressure head of water, currently used for mine refrigeration, to power stoping equipment in the mine, with the advantage and viability of this method lying in its low cost, high efficiency and safety. The principles of hydraulics fundamental to hydro-power are well known, but the use of mine water as a medium has necessitated extensive research to solve the severe problems of wear and corrosion of internal machine components. One of the main problem areas in harnessing the high pressure head of water is that of dynamic fluid sealing. To maintain a pressure differential of between 15 and 20 MPa across a seal is easily achieved in static or favourably lubricated conditions, since the seal life is not limited by the sliding wear behaviour of the sealing material. Using water as medium means that surface contact, producing high asperity contact pressures cannot be avoided owing to the poor lubricity and low viscosity of water. This thesis addresses the sliding behaviour of piston seals in water powered rockdrills, which results in unacceptably high wear rates of the seals.

The water powered rockdrill is a percussive impacting device wherein the main component, the piston, reciprocates at a frequency of 60 Hz, striking the rear of the drill steel at speeds exceeding 10 m/s each cycle. Water pressure is used to shuttle the piston, with the pressure differential maintained by piston seals situated in the cylinder or piston housing. Operating pressure differentials are nominally 15 MPa, but may exceed 30 MPa, and require PV (pressure x velocity) ratings for seals far greater than those for commercially available piston seals. In addition, the majority of commercial piston seals are designed to be used with more viscous fluids than water. The seals presently used on the rockdrill piston are generally two component seals, consisting of a sealing ring made from Ultra High Molecular Weight Poly-ethylene (UHMWPE), energised against the piston by a nitrile rubber o-ring. Whilst representing the best known material available, the UHMWPE seals still wear at an unacceptably high rate. Current seals lives are of the order of 25 hours before excessive wear causes the seal to fail. In order to ensure complete viability of the rockdrill, seal life needs to exceed 100 hours operation (a total sliding distance approaching 1000 km).

The research effort into piston seals at COMRO has followed two complementary streams. On the one hand, work has been done on the identification of the most suitable sealing materials, and their wear mechanisms sliding in water. The second approach, which is presented in this thesis, involves the modelling and numerical simulation of the behaviour of rockdrill piston seals with a view to improving their wear performance by encouraging elastohydrodynamic lubrication through changes in the seal geometry and design.

The primary objectives of this study are:

1. *To identify and quantify current seal wear, both in the laboratory and in actual operation.*
2. *To model the steady state behaviour of current seals to understand the reasons for their poor wear performance and be able to recommend design improvements.*
3. *To perform laboratory tests on improved seal designs to determine their performance characteristics.*

The approach adopted has been to combine experimental and analytical tools to ensure that the final model of the seals is representative of reality, despite simplifications in both areas.

The first part of this thesis presents on overview of the seal problem, giving details of seals, their operating conditions and characteristic wear modes. The feasibility of modifying seals in order to encourage hydrodynamic or elastohydrodynamic lubrication is also discussed, after preliminary experimental results with polymer slippers sliding in water are shown to correlate well with the theory of lubrication.

The main emphasis of the thesis lies in the development of an elastohydrodynamic model for rockdrill piston seals. The model incorporates a finite difference approximation of the polymer seal, solved simultaneously with the lubrication

equations, and produces results for the final shape of the seal above the counterface (if elastohydrodynamic lubrication is possible). The leakage across the seal face is also modelled. As an input to the model, the contact force profile at the rear of the seal due to the combination of the precompressed o-ring and fluid pressure is also required, and this has been determined experimentally, as well as numerically using the finite element code ABAQUS.

With the solution algorithm running on a personal computer, the formation of a lubricating film in existing piston seals has been modelled. The effects of varying design and geometry parameters have also been modelled and several simple design modifications have been shown to assist in forming a such a lubricating film. In conjunction with the numerical seal model, new and existing seals have been evaluated in a laboratory rig to determine their wear behaviour and leak rates. The results from the experiments are in good agreement with the predictions of the elastohydrodynamic model, and have confirmed the seal modifications which improve the wear of seals by a factor of eight. The results are finally summarised, and recommendations for the improved design of piston seals are made for immediate implementation.

Chapter II. PROBLEM STATEMENT.

In defining the problem, the piston seals currently in use are described, as well as the nature of the environment in which they operate. Their behaviour in terms of the wear of the polymer at the sliding interface is also discussed.

2.1 Current seal types.

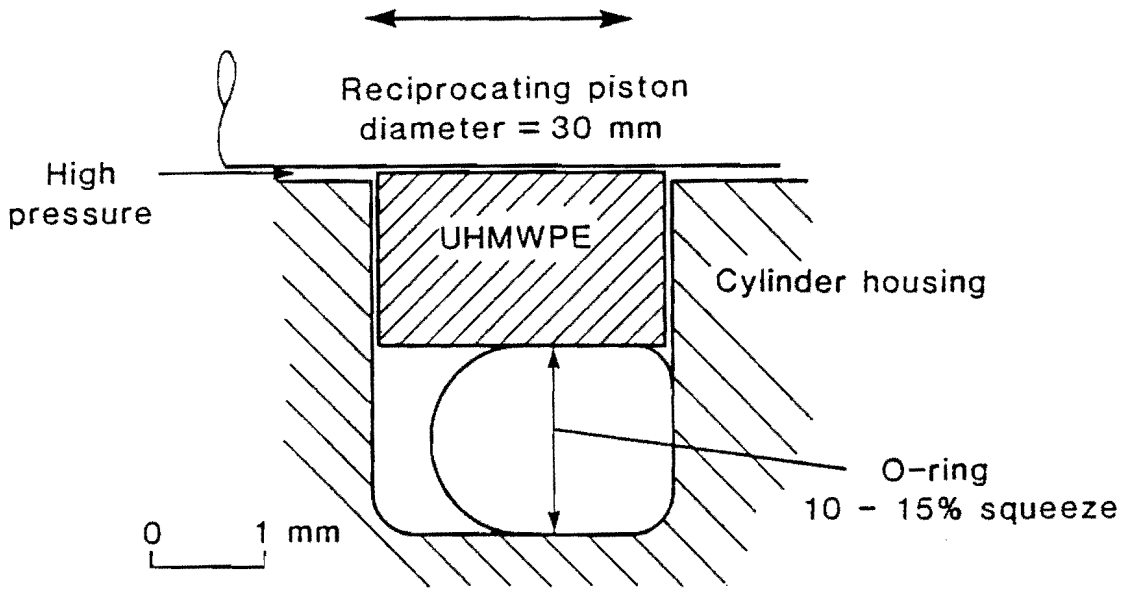

Figure 2.1. TYPICAL NARROW PISTON SEAL

The piston seal has been described as an Ultra High Molecular Weight Polyethylene sealing ring energised against the piston by a rubber o-ring. This is however only one of two current seal configurations used in different rockdrills. The difference in the two seals lies mainly in their length, and for the purposes of this report will be referred to as wide and narrow piston seals respectively. The other major difference between

the two seals is the presence of an energising o-ring. While the narrow seal incorporates an o-ring at the rear of the seal, the wide seal consists only of the polymer ring and relies on the pressure drop across the seal face to cause the seal to remain in contact with the counterface.

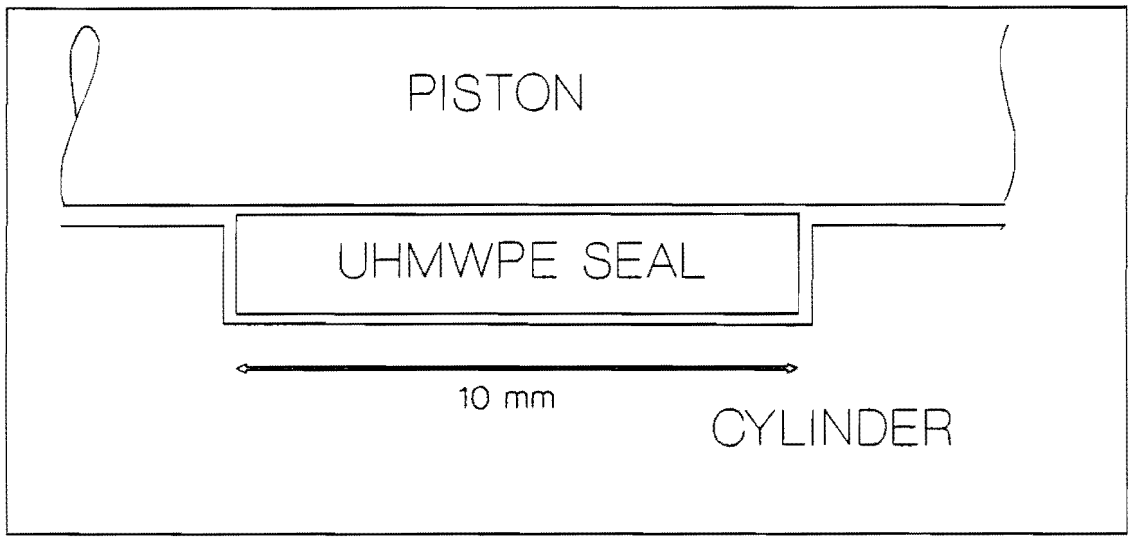

Figure 2.2. WIDE PISTON SEAL

The narrow seal shown in figure 2.1,has a width and thickness of 2mm and nominal diameter of 30mm, corresponding to the piston diameter. The o-ring is typically 70 Shore A nitrile rubber and is inserted behind the polymer ring with a static squeeze of between 10 an 15%. In some instances the round section o-ring is replaced with a square section ring to prevent rolling or spiral failure of the o-ring. Tolerances on the polymer ring are difficult to maintain as each ring is machined rather than moulded, and the polymer deforms under the tool force and associated temperature rise. As a result, the fit of the ring on the piston may vary from a slight interference

fit to a close sliding fit. It may however be assumed that the polymer ring will wear faster with a greater interference fit on the piston, which will result in all seals wearing to the same equilibrium fit regardless of the starting sizes.

The wide seals shown in figure 2.2, are made from the same polymer, UHMWPE, and are usually 5 times wider, although are of similar thickness and diameter to the narrow seals. To ensure that the seal always contacts the counterface, the polymer is machined slightly larger than the seal groove and is compressed against the piston on insertion.

The piston or counterface finish used with the two seals also varies. In conjunction with the narrow seal, the piston is hard chrome plated and surface ground to a roughness of $0.1 \mu m \quad R_a$. The piston used with the wide seals, is made from AISI 431 stainless steel, hardened and ground to a similar surface roughness. Each counterface has its advantages, with the chromed piston exhibiting superior wear performance of the counterface and seals, whereas the softer stainless steel piston is less expensive.

2.2 Operating conditions.

The piston in the rockdrill is driven by high pressure mine water which is controlled by a valve and fed to different chambers surrounding the piston during the reciprocating cycle. The pressure chambers represented in figure 2.3 are labelled the cushion, drive, and return chambers, with pressure in the drive and return chambers effecting the forward and return strokes of the piston. For identification purposes, the piston seals between the chambers are designated by the pressures in the chambers on either side of the seal. Thus the first seal is called the Pa/Pc seal, where P indicates pressure

in all instances, lower case 'a' indicates atmosphere, and lower case 'c' indicates cushion. Similarly the seal separating the drive and return chambers in labelled the Pd/Pr seal.

During one cycle the piston travels a total distance of 60 mm, that is 30 mm forward and 30 mm backwards. The pressures in the various chambers during the forward and return strokes of the piston are shown in figures 2.4 and 2.5, while the absolute velocity of the piston during both strokes is shown in figure 2.6. It will be noted that in the case of the Pr/Pa seal, the pressure drop across the seal is always in the same direction, while the velocity direction of the piston changes. This is important, as the possible formation of a hydrodynamic film at the seal face relies on the pressure drop and piston velocity being in the same direction.

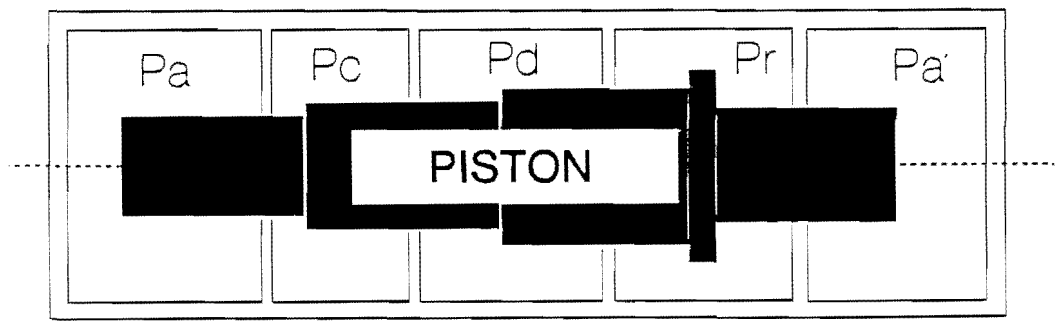

Figure 2.3. PRESSURE CHAMBERS OF A ROCKDRILL PISTON

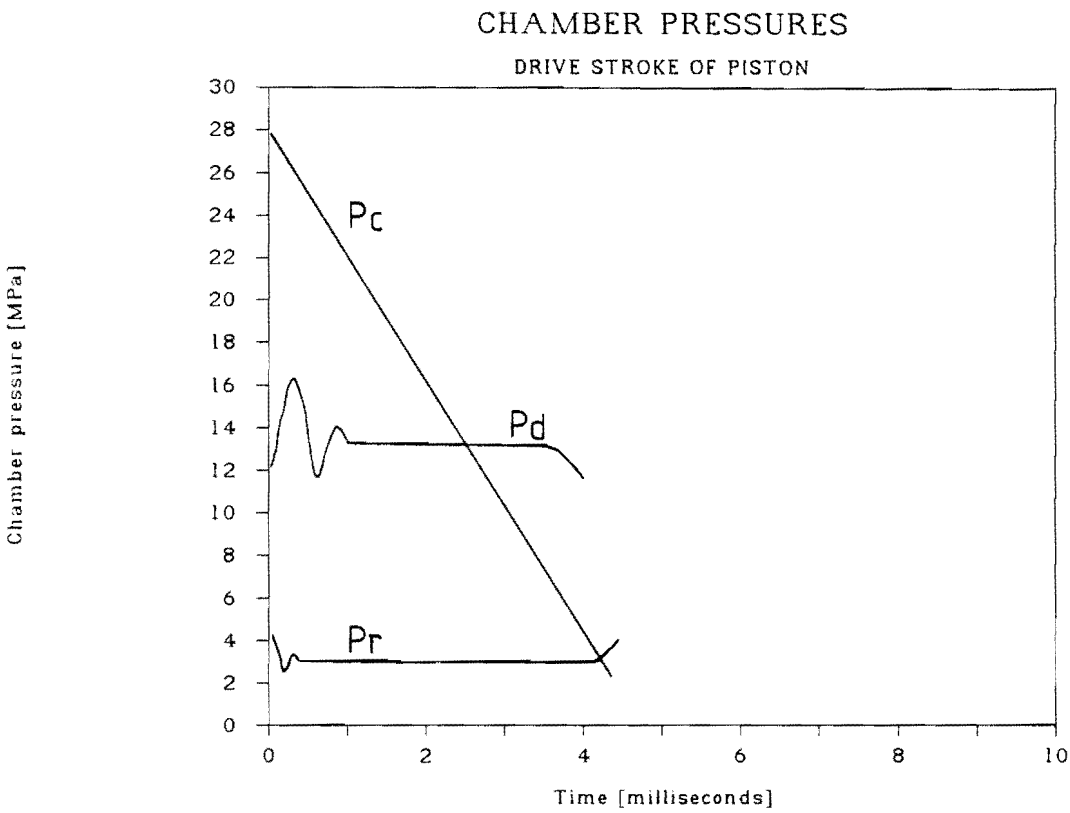

Figure 2.4. DRIVE STROKE - CHAMBER PRESSURES

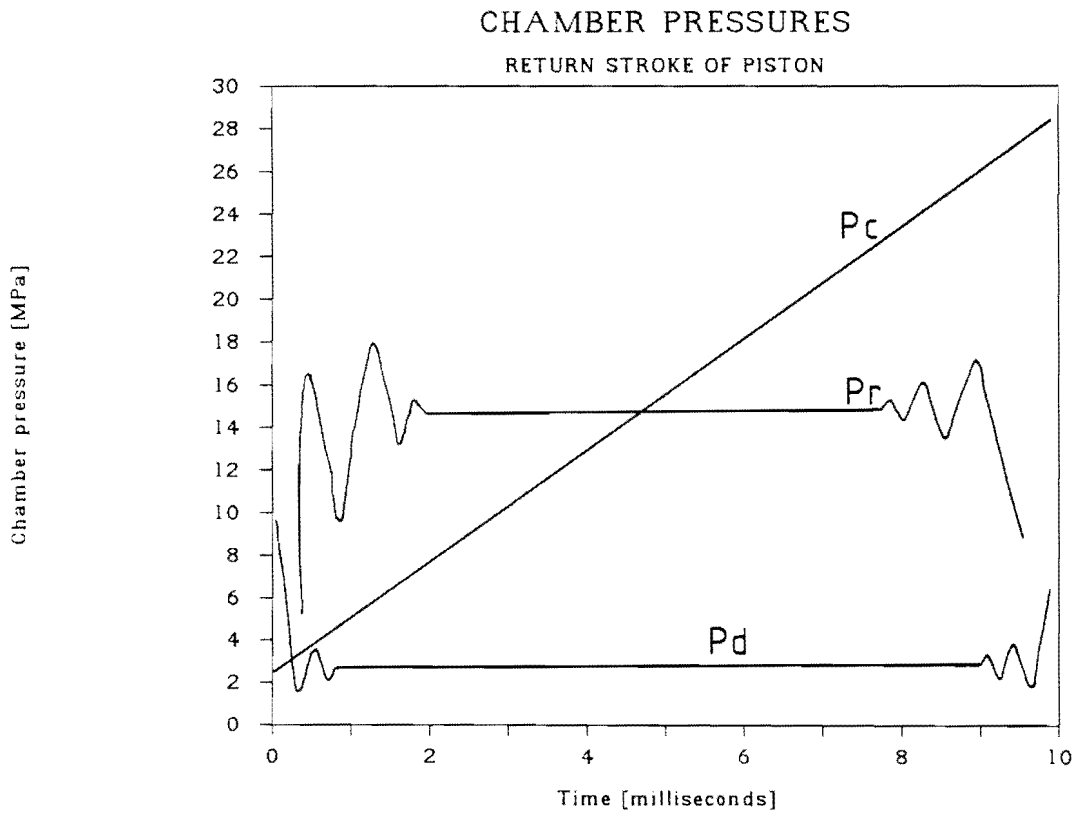

Figure 2.5. RETURN STROKE - CHAMBER PRESSURES

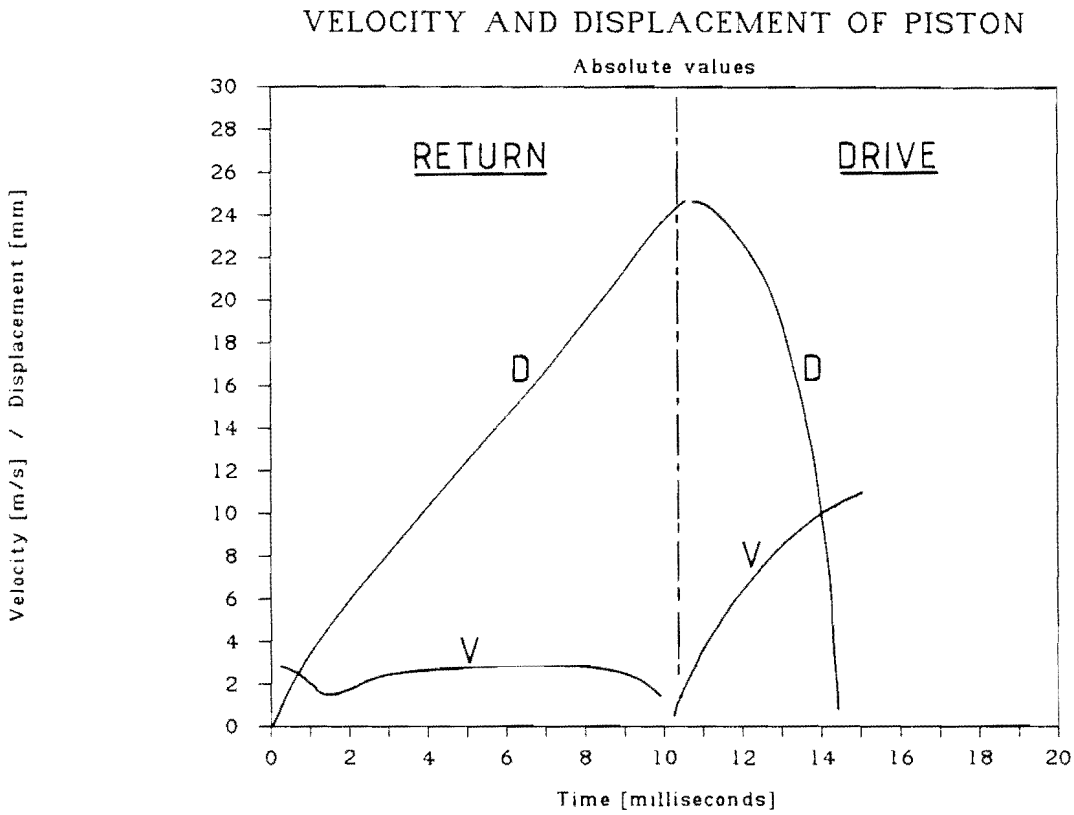

Figure 2.6. VELOCITY AND DISPLACEMENT OF THE PISTON

2.3 Wear performance.

The wear performance of the seals in relation to their design is the key issue in this thesis. However, several other factors affect the wear of the seals. If contact is assumed between the seal and counterface with contact pressures equal to the sealed fluid pressure, then the seal wear is a function of the seal - counterface material couple (the two interacting materials) and the wear rate of the seal or counterface can be improved by controlling material and metrological parameters of the couple.

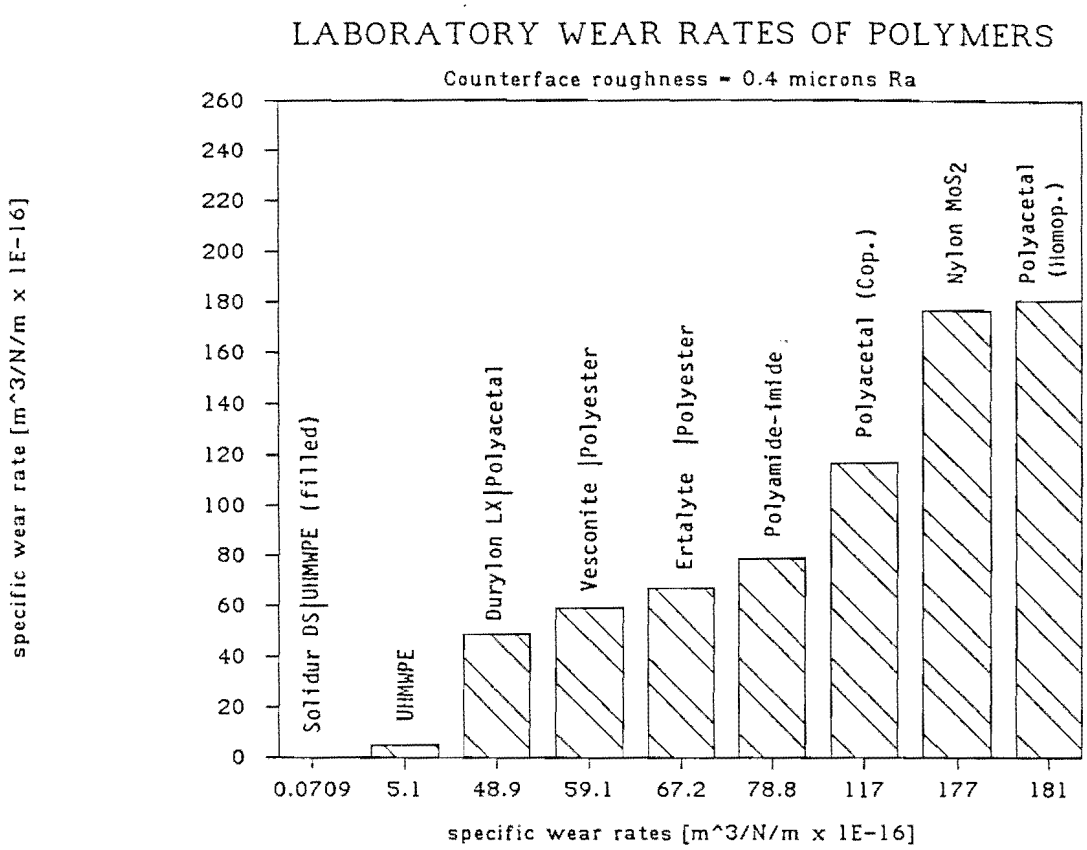

Figure 2.7. POLYMER WEAR RATES

For the seal material, UHMWPE in its virgin or filled state is the best known polymer for the current application in water. Wear test have been performed [1] for numerous potential polymers sliding over a ground AISI 431 counterface in water and the results are shown in figure 2.7. Not clearly visible in the figure, is the wear rate of a filled ultra high molecular weight polyethylene, called Solidur DS. The laboratory wear rate of Solidur DS is 10 times lower than virgin UHMWPE, and as a result the filled polymer is being used in many sealing applications. The superior wear performance of UHMWPE in water is due to its ability to form a coherent transfer film on the counterface. It is of interest to note that PTFE does not perform well in water. In dry applications PTFE performs well because a polymer transfer layer forms on the counterface resulting in material transfer to the counterface and similar transfer back

to the parent polymer with no resultant wear. In water the transfer layer that would form on the counterface is not adherent and material is continually lost from the parent material.

In addition to forming a stable transfer film, the superior performance of UHMWPE can be attributed to its good toughness and fatigue resistance which limit cavitation and abrasive wear [2].

The analysis of worn piston seals shows the seals to wear in a wedge shaped manner (figure 2.8), with the low pressure side of the seal wearing more than the high pressure side. This has previously been attributed to the contact force profile existing between the seal and counterface. However, this is unlikely since the increase in contact pressures due to the o-ring squeeze is small compared with the nominal contact pressure due to the sealed fluid. In addition the specific wear rate of UHMWPE does not vary with applied pressure in this pressure domain [3]. Rather the wear geometry of piston seals has been explained in section 5.2, in relation to the fluid pressures existing in the film at the seal face.

Table 2.1 shows estimates of the specific wear rates of four rockdrill seals, after the used seals were measured and compared with sizes before operation. The specific wear rates are given in the units $m^3 N^{-1} m^{-1}$ (worn volume per unit load per unit sliding distance) and thus take into account the different seal sizes and operating pressures. In comparison to actual seal wear rates, the laboratory wear rates for UHMWPE sliding in water against a similar counterface are somewhat lower and are shown in table 2.2. The higher in situ wear rates have been ascribed to the higher operating speeds and the ingress of highly abrasive quartzite particles in mine water.

TABLE 2.1	
SPECIFIC WEAR RATES FOR ACTUAL ROCKDRILL SEALS	
SEAL	SPECIFIC WEAR RATE [m^3/N/m]
Pa/Pc	4.0×10^{-15}
Pc/Pd	3.0×10^{-15}
Pd/Pr	2.0×10^{-15}
Pr/Pa	1.5×10^{-15}

TABLE 2.2	
SPECIFIC WEAR RATES FOR LABORATORY TESTS WITH UHMWPE ON DIFFERENT COUNTERFACE ROUGHNESSES [material = AISI 431]	
Ra	SPECIFIC WEAR RATE [m^3/N/m]
$0.1\mu m$	2.0×10^{-17}
$0.4\mu m$	5.0×10^{-16}
$0.8\mu m$	4.0×10^{-15}

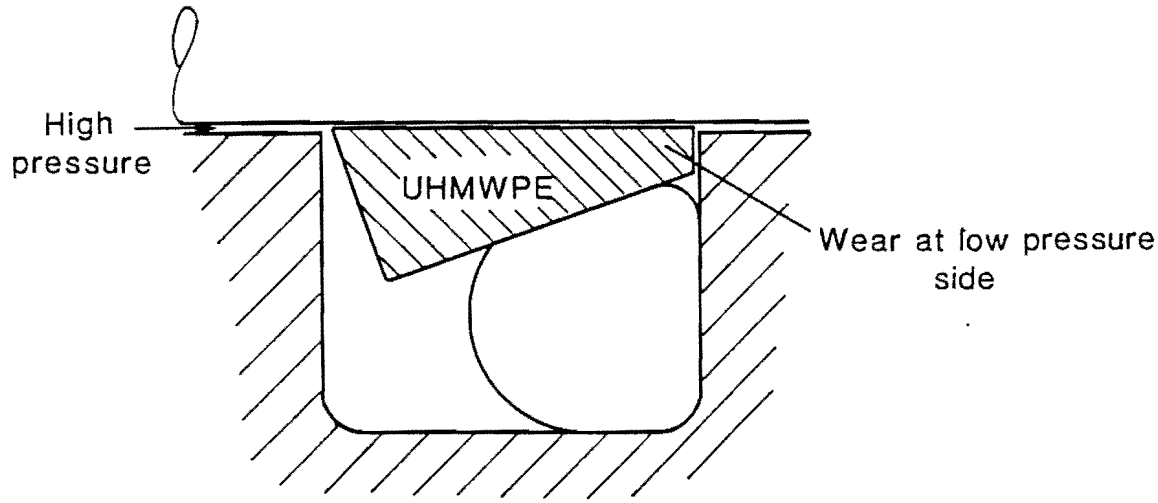

Figure 2.8. WORN SHAPE OF A SEAL

Chapter III. HYDRODYNAMIC LUBRICATION AS MEANS OF IMPROVING SEAL LIFE.

Improving seal life by changing the seal design, rather than changing the seal material or lubricant, can be accomplished in two ways. Either the contact forces at the seal - piston interface need to be reduced, or the functional design of the seal must not be affected by a high seal wear rate. The latter approach incorporates the idea of consumable seals, and although such designs may be feasible, consumable seals have not been dealt with in this thesis.

Reducing the contact forces at the seal face is limited by the nature of the flow of fluid across the seal face. For the case of a rigid seal, the normal contact stresses need to be greater than half the sealed pressure (assuming zero back pressure) to ensure that the seal remains in contact with the piston. For flexible seals the required contact stresses are higher and need to be at least equal to the sealed pressure at some point across the seal face to prevent penetration of the fluid, causing the seal to leak. For the polymeric seals currently used, leakage must occur if high contact pressures and hence wear rates, are to be avoided. In allowing a seal to leak, the leakage needs to be controlled and the simplest, most economical method is to ensure that the seal forms a hydrodynamic film between the polymer seal and piston. In this way the seal will be separated from the piston and not wear at all, while the clearance between the two components will be stable and the leak rate automatically controlled.

While the wear behaviour of rockdrill seals indicates that hydrodynamic lubrication does exist to some degree in current seal designs, the feasibility of full hydrodynamic lubrication for a large portion of the seal cycle has been doubted because of the low viscosity of water. Tests were therefore performed to ascertain whether such lubrication is possible under rockdrill conditions.

The test rig consisted of a modified pin on disk polishing machine in which a polymer slipper was held against a rotating steel counterface, shown in figure 3.1. The angle of the slipper face against the rotating counterface was variable to within 1/100 th of a degree, and measured using a reflected laser beam. With the slipper loaded under

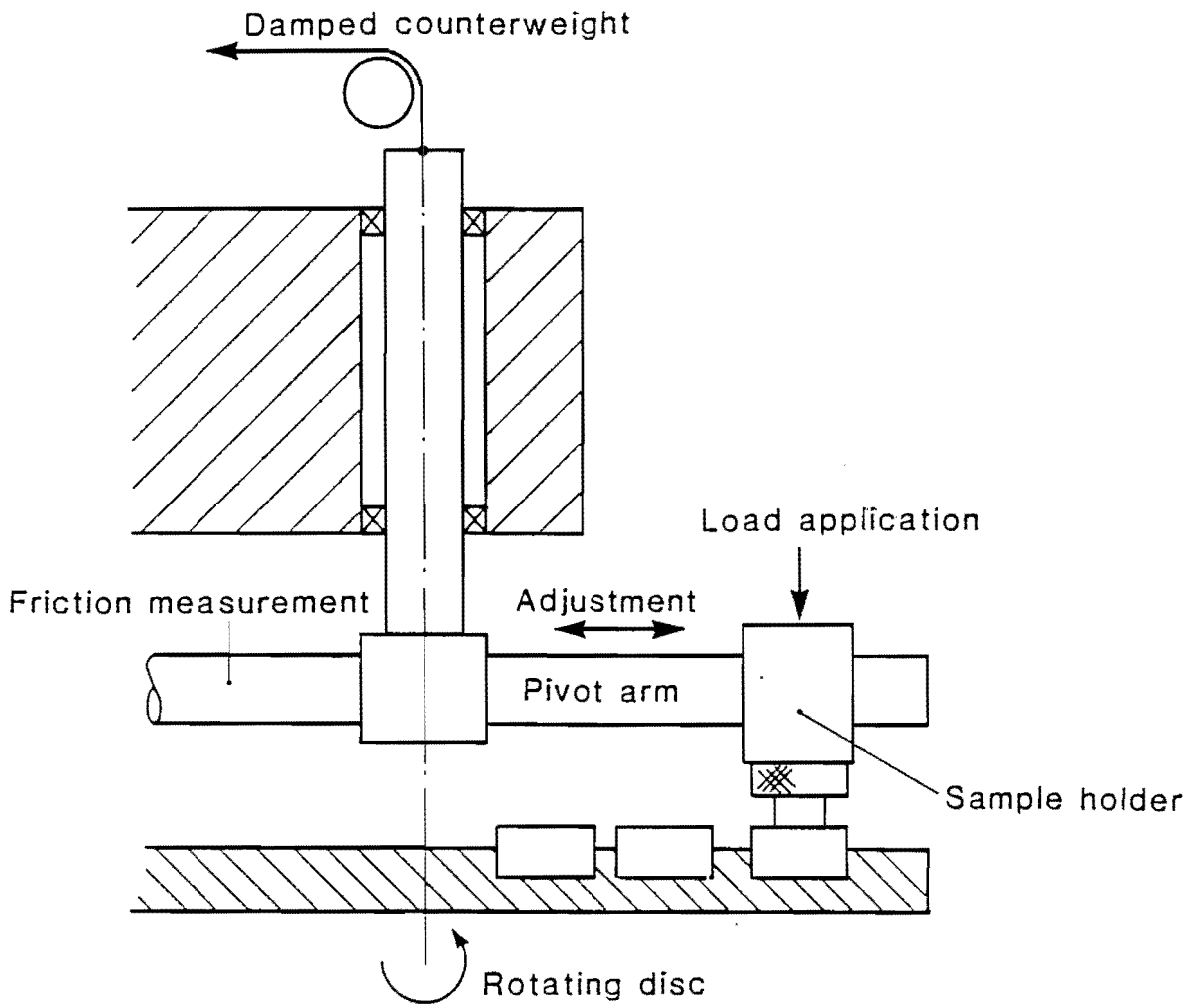

Figure 3.1. MODIFIED PIN ON DISK TEST RIG

a known force, the friction force between the polymer sliding over the counterface in water was measured in order to determine the onset or breakdown of a lubrication film.

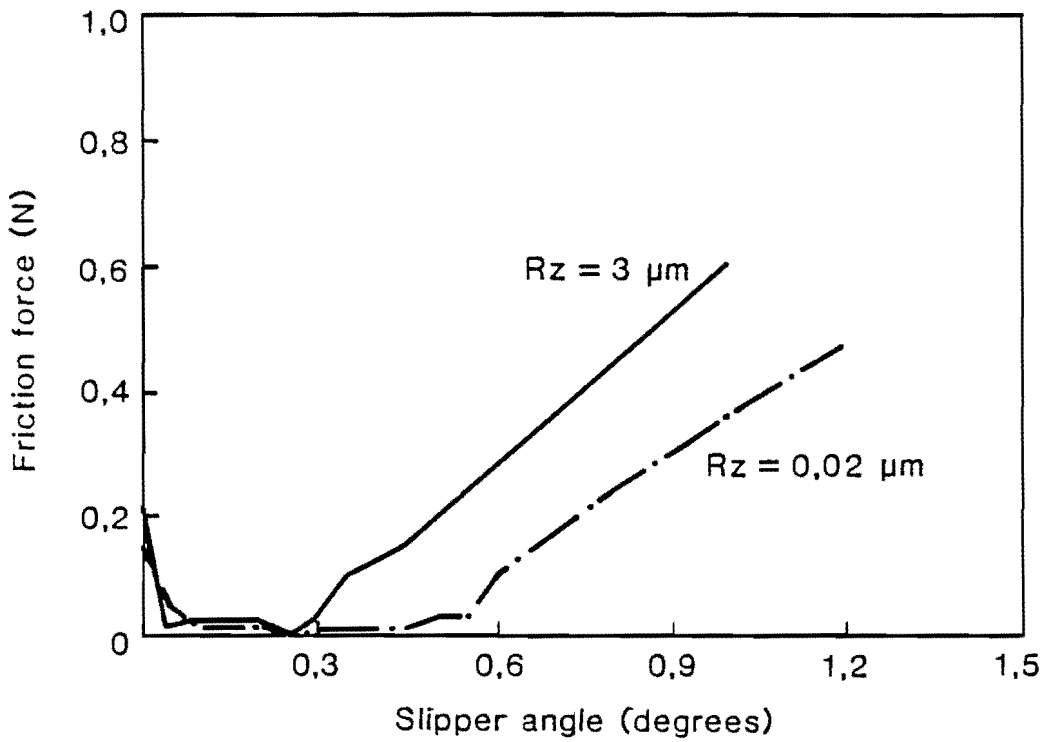

Figure 3.2. FRICTION AT SLIPPER INTERFACE vs SLIPPER ANGLE

The experimental results for the variation of friction force with slipper angle are shown in figure 3.2, and clearly indicate the region of full hydrodynamic lubrication between slipper angles of 0.08° and 0.3° for a speed of 7.8 m/s, normal load of 300 kPa and a counterface roughness of $3\ \mu m$ R_z (mean peak to valley asperity height). A repeat test under identical conditions but after polishing the counterface to $0.02\ \mu m$ R_z showed a similar trend but with a lubrication regime extending to a slipper angle of 0.55°.

A similar experiment to that described above was performed analytically using Reynold's equations for hydrodynamic lubrication, but monitoring the minimum film

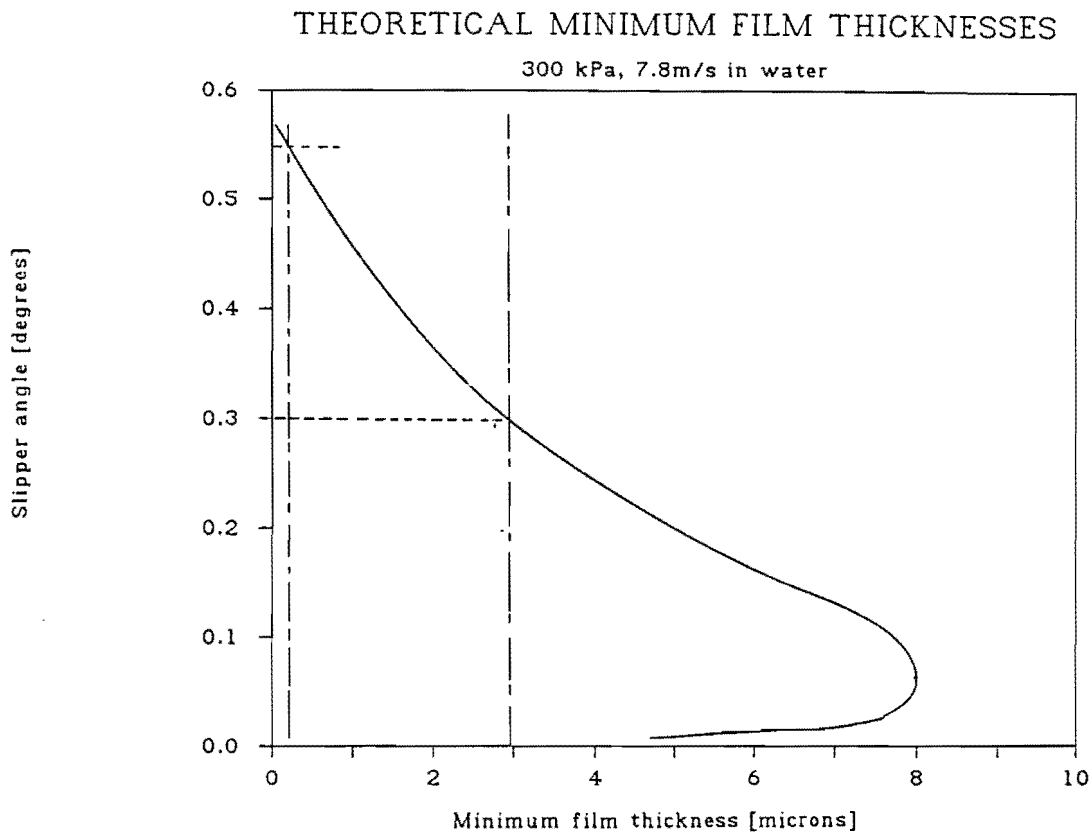

Figure 3.3. MINIMUM FILM THICKNESS vs SLIPPER ANGLE

thickness as a function of slipper angle instead of the friction forces. These results are shown in figure 3.3 and correlate exactly with the physical experimental results. The breakdown of full hydrodynamic lubrication at critical slipper angles corresponds to the minimum film thickness being equal to the mean peak to valley height of the surface asperities (the R_z parameter). Table 3.1 shows the experimentally determined slipper angles and the theoretical angles at which lubrication breaks down for a given surface roughness.

TABLE 3.1 CRITICAL SLIPPER ANGLES IN WATER (Speed = 7.8 m/s load = 300 kPa slipper length = 10 mm)		
Roughness R_z	Experimental angle	Theoretical angle
3.0 μm	0.3°	0.30°
0.02μm	0.55°	0.55°

Both the physical and theoretical experiments show that full hydrodynamic lubrication is possible under certain conditions albeit that the film formed is extremely thin. Current surface finishes on rockdrill are however sufficient to allow films as thin as $0.5\mu m$ to form.

The stability of the lubrication film is however not guaranteed, or at least the above experiments are not able to predict film stability in actual seals since the assumption of a rigid slipper has been made in both cases. To be able to determine more accurate film thicknesses and stable film formation, the deflection of the polymer slipper or seal, under the applied fluid pressure forces, must be taken into account. A full, yet sufficiently simplified elastohydrodynamic lubrication model for flexible seals has thus been constructed, and successfully been used to determine the performance of rockdrill seals.

Chapter IV. AN ELASTOHYDRODYNAMIC MODEL.

The elastohydrodynamic model of the seal has been constructed in order to solve simultaneously, the elasticity equations of the seal and hydrodynamic lubrication equation. Elastohydrodynamic simulations are inherently problematic [7,8], and while solutions have been found for viscous oils, no such work on elastomeric seals in a water medium has been identified by the author.

The model incorporates a finite difference formulation for the deflection of the polymer ring and one dimensional incompressible lubrication equation for steady state flow. In addition the forces exerted on the polymer ring by the o-ring have been determined and used as an input to the model. The implementation of these methods is fairly straight-forward and can be done on a personal computer, making the final numerical model a very versatile and portable tool for designing seals. Although almost any seal shape and type can be modelled under a variety of conditions, limitations do exist owing to assumptions and simplifications in the numerical model. The main assumptions and simplifications are :

1. *Linear elastic behaviour of the polymer.*
2. *Isoviscous, isothermal fluid behaviour.*
3. *Quasi static seal operation. (Inertia effects excluded).*
4. *Pressure differential across seal must be in the same direction as the relative velocity of the seal counterface.*
5. *Piston and seal surfaces are smooth.*

The requirement of smooth surfaces for the seal and counterface does not present a problem. A minimum fluid film thickness less than the counterface roughness will indicate collapse of the hydrodynamic film and high wear of the seal material as a result of the sealed pressure behind the seal.

4.1 Modelling of the o-ring forces

The initial purpose of the o-ring situated behind the polymer ring was to provide a precompression or squeeze of the polymer against the counterface and therefore cause the seal to work. However, a more significant function of the o-ring is that it seals the water pressure behind the polymer ring thereby modifying the pressure profile acting at the rear of the ring. The full effect of the o-ring needs to be understood since the pressure profile behind the polymer ring can stabilize or destabilize any hydrodynamic film that may form. The effect of the o-ring has been determined experimentally by measuring the contact pressures at the face of the seal between the polymer and the counterface. Any contact pressure in excess of the sealed pressure is a direct result of the precompressed rubber o-ring. In addition, the effect of the o-ring on the polymer has been modelled numerically using the finite element method, and the results have been used in the elastohydrodynamic model to determine the deformation of the seal.

4.1.1 Experimental contact pressures.

In the experimental measurement of seal contact pressures, the seal configuration tested was similar to the rockdrill seal configuration except that the polymer was used as a face seal and tested under static conditions. Using a horizontal seal face as opposed to a cylindrical face enabled easier and more accurate measurement of the seal contact pressures. The test rig is shown in figure 4.1 and consists a stationary cylinder which was held in a bench vice during the test. The seal and o-ring were inserted into an eccentric groove in the cylinder face, with varying groove depths and hence o-ring squeezes obtainable by machining the cylinder face. The seal was held in place by a cylinder cap, free to rotate and adjustable to provide the correct clearance between the cylinder once pressure had been applied. A small pin-hole was located in the cap such that the locus of the pin-hole traversed the seal face as the cap was rotated.

An established technique for measuring contact pressures of deformable materials [4] was used to measure the contact pressures of the polymer seal against the counterface. Once the seal had been pressurized to the required pressure, an excess

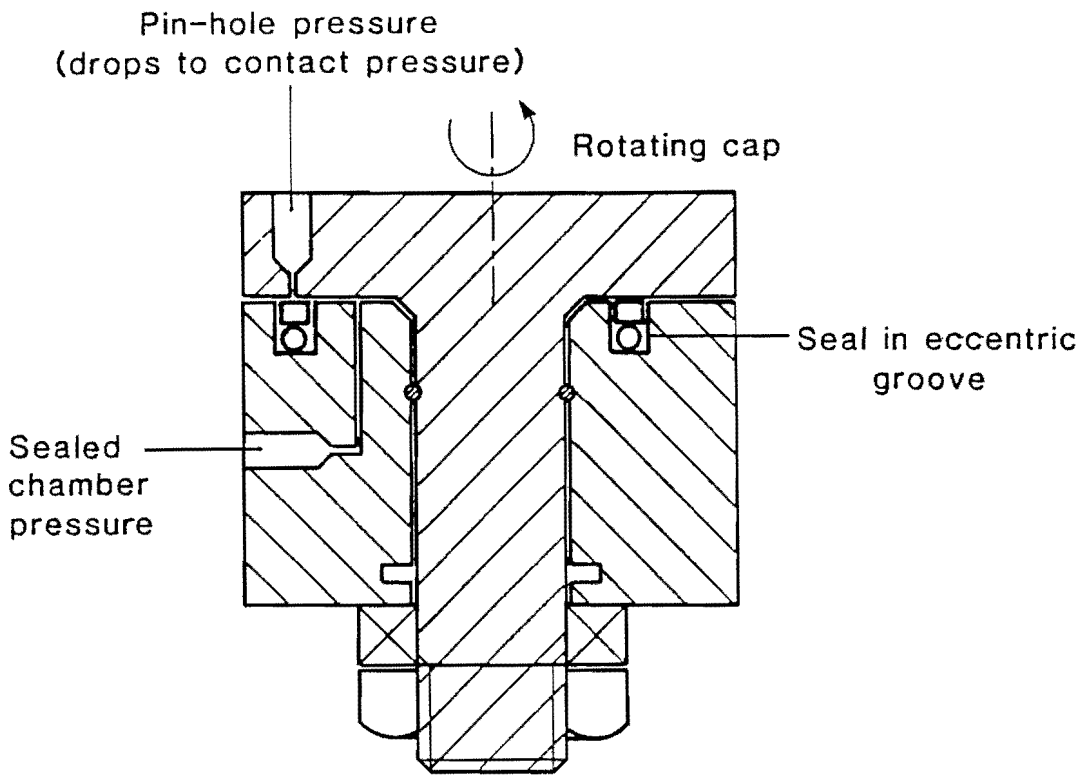

Figure 4.1. CONTACT PRESSURE TEST RIG

pressure was supplied to the pin hole, allowing fluid to leak through the pin-hole over the face of the seal. The seal essentially behaved as a check valve and leakage through the pin-hole stopped when the fluid pressure in the pin-hole equalled the contact pressure of the seal against the counterface. The procedure was repeated at different positions across the seal face until the full contact pressure profile of the seal was determined. The cylinder body was then skimmed to repeat the test using a different o-ring size or squeeze.

The testing procedure described above was especially sensitive to errors and required care in ensuring the correct operation of the small check valve at the pin-hole/seal

interface. Seals used in the as-machined condition produced incorrect results since surface finishes were poor and the seals were not square in section. On pressurization, the seals deformed to the shape of the seal groove causing non-uniform contact pressures at the seal face. Greater consistency in the results was achieved when the seal faces were polished, preventing leakage out of the pin-hole, and the form tolerances on the seal section were increased. A further factor which at first led to inconsistent results was the relaxation of the o-ring stresses with time which is particularly marked in nitrile rubber elastomers and can be overcome by using flouro-elastomers for the o-ring. The stress relaxation in nitrile rubber is however logarithmic, approaching a zero rate of change after about 20 hours, and any adverse effects can be eliminated by using correct design procedures. Figure 4.2 shows the decay of the peak or maximum contact pressure due to o-ring squeeze with time.

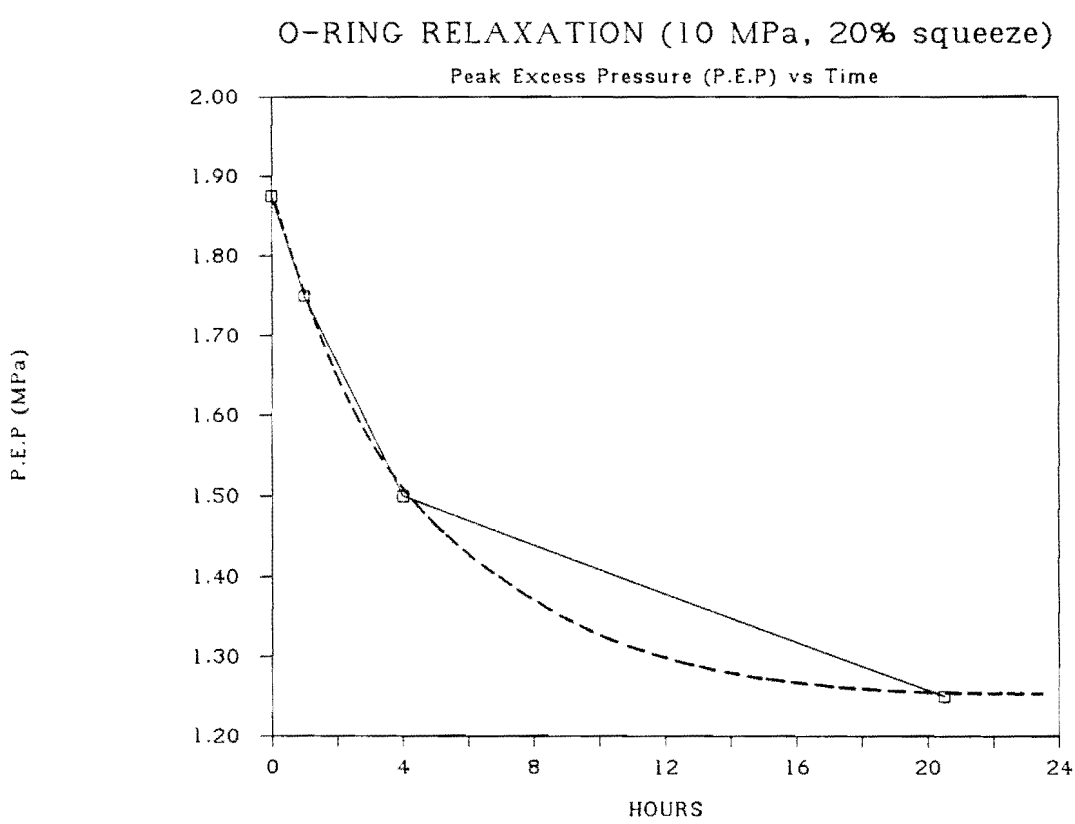

Figure 4.2. O-RING STRESS RELAXATION WITH TIME

side of the o-ring. In a dynamic seal application, there may be insufficient time for the fluid pressure to drop and it is possible that the pressure will remain high at both ends of the o-ring.

The results of the experimental measurement of contact pressures have revealed the fundamental trends in the behaviour of the o-ring, but are incomplete as all of the variables have not been studied. The numerical analysis of the o-ring contact pressures is addressed in the next section, and offers a more coherent analysis of the rubber behaviour.

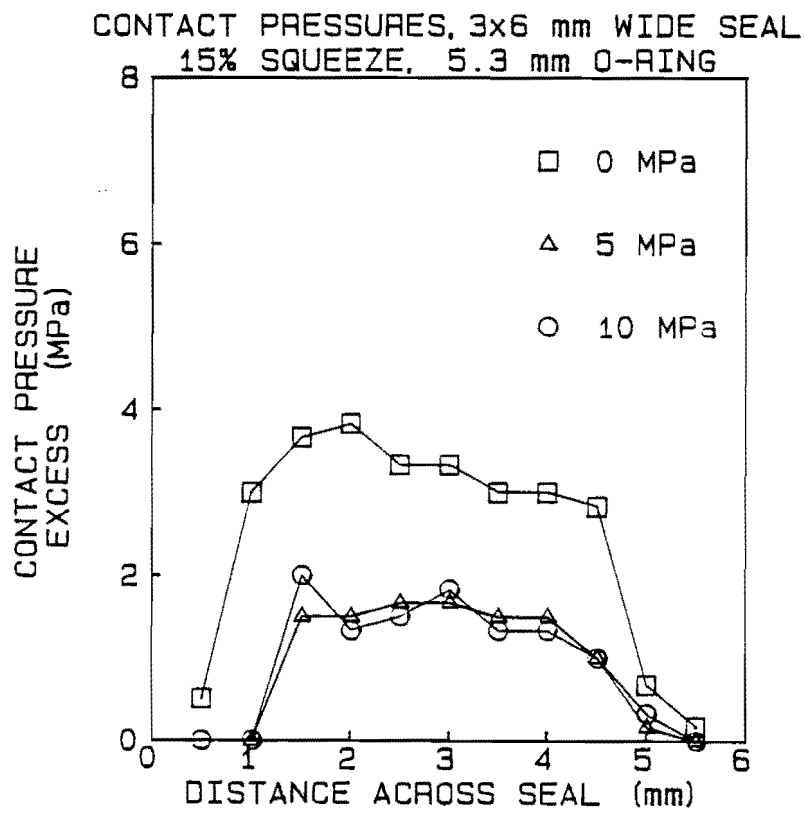

Figure 4.3. TYPICAL CONTACT PRESSURE PROFILES
70 Shore A, 5.3mm o-ring, 15% squeeze

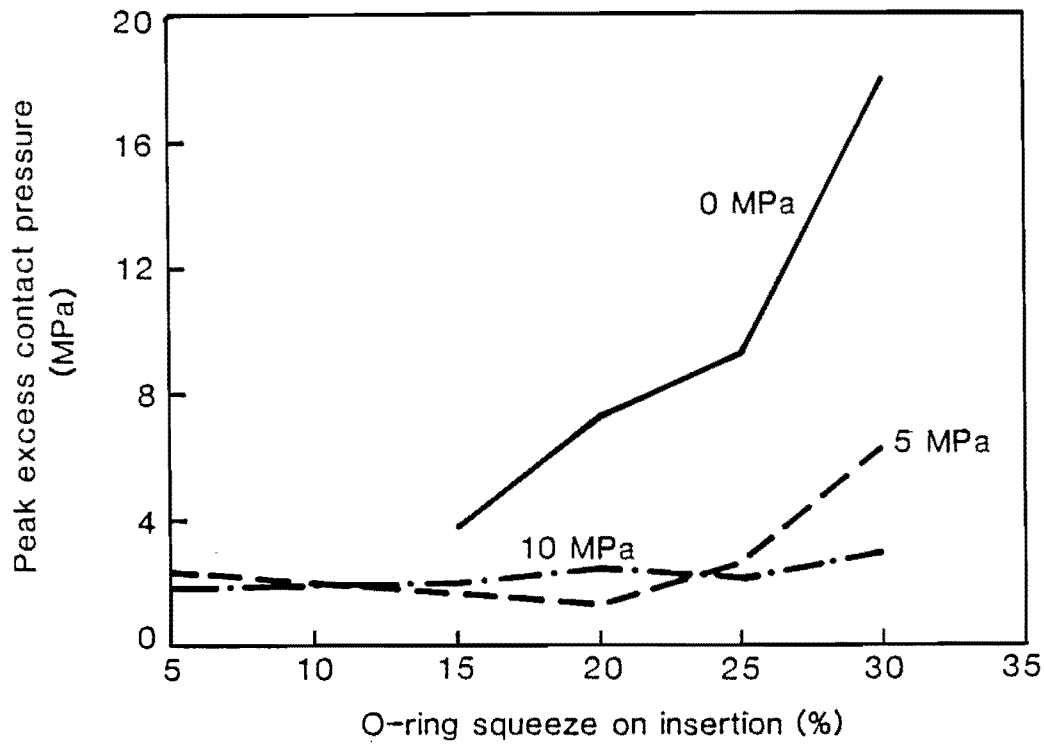

Figure 4.4. MEASURED PEAK CONTACT PRESSURES
70 Shore A, 2mm o-ring

Some results of the experimental measurement of seal contact pressures are shown in figures 4.3 to 4.6, which highlight the main trends observed. All of the results (except those in fig. 4.6) show excess pressure (i.e. contact pressure minus sealed pressure) as a function of the distance across the seal from low pressure to high pressure. The hardness of the rubber was kept constant at 70 shore A.

The influence of the sealed pressure on the effect of the o-ring is marked. Without exception, the contact pressure profile is lowered and shifted towards the low pressure side as the sealed pressure is increased. This would indicate that the deformation of the o-ring to conform to the groove shape under pressure has a reducing effect on the initial o-ring contact pressure. Figure 4.6 shows how the peak excess contact pressure due to 15% squeeze on a 2 mm diameter o-ring varies with sealed pressure. At high pressures, above 4 MPa, there is a minimum peak excess pressure that is reached with increasing sealed pressure for a given seal configuration. This corresponds to the o-ring being compressed and conforming completely to the seal groove shape. As the rubber is nearly incompressible, further increases in sealed pressure above 4 MPa do not deform the o-ring any more, and the excess contact pressures remain constant. The drop in excess contact pressure with sealed pressure is also a function of the friction at the o-ring surface and has been modelled numerically. However the agreement between experimental and numerical results is poor in this area and may be partly due to experimental error in using the test rig. The design of the rig is such that the o-ring squeeze can diminish as pressure is applied, since gap between the rotating cap and rig housing increases with increasing fluid pressure. The reasons for the discrepancy could also lie in the numerical model. However, in using the results in the elastohydrodynamic model, only the results for sealed pressures greater than 4 MPa are of interest since the pressure applied to the seal usually exceeds this value. Above 4 MPa, the effect of the o-ring squeeze appears to have a linear effect on the peak contact pressures, while the area of influence due to the compressed o-ring naturally widens with increasing o-ring squeeze.

At the low pressure side of the seal, the contact pressure drops below the sealed pressure. A similar result is obtained from the numerical analysis of the o-ring deformation, and is caused by pressure leaking out to atmosphere at the low pressure

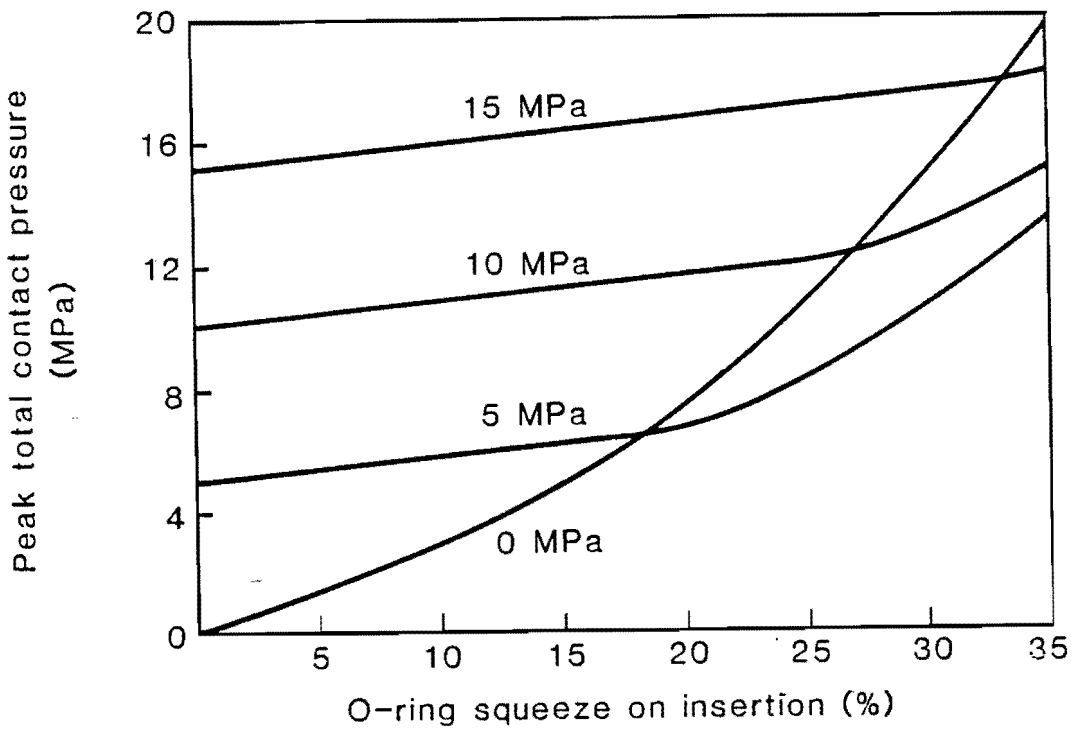

Figure 4.5. POSTULATED TRENDS FROM EXPERIMENTAL DATA
Peak total contact pressures
70 Shore A, 2mm o-ring

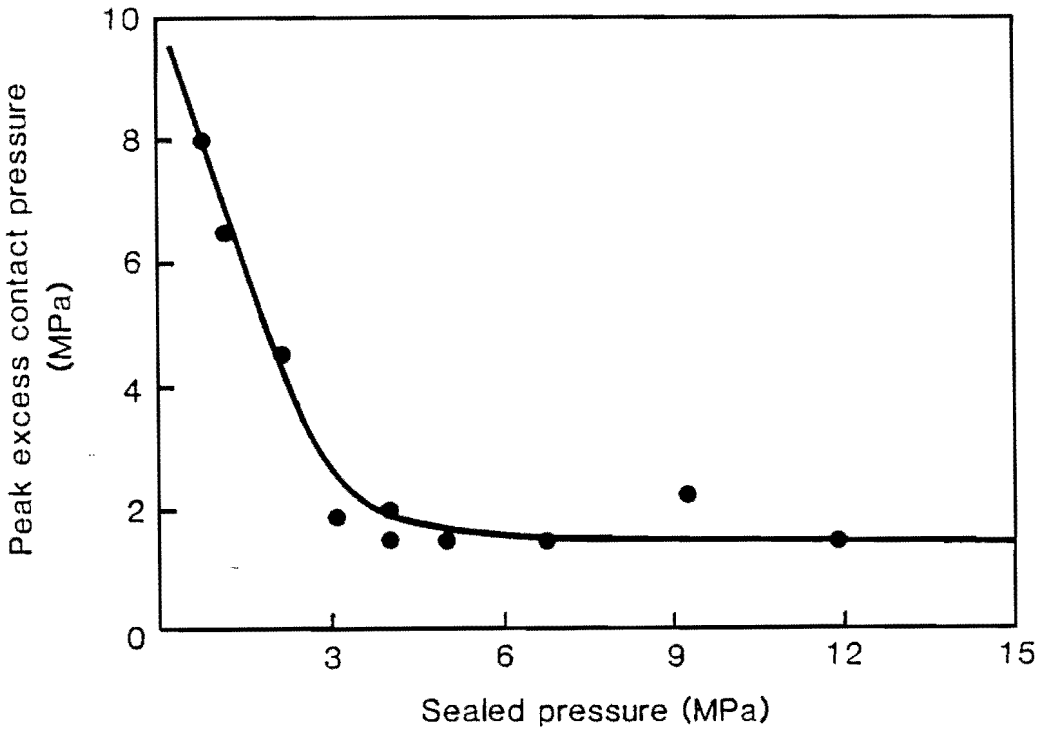

Figure 4.6. PEAK EXCESS CONTACT PRESSURE vs SEALED PRESSURE

4.1.2 Finite element analysis of the o-ring.

A static model that describes the deformation and stresses in a typical cap seal would need to model the behaviour of the o-ring and the polymer cap as well as their mutual interaction and interaction with the piston. However, this approach can be simplified considering the objectives of this thesis. Of use in understanding the lubrication properties of cap seals is the contact pressure profile between the cap and the piston as well as the associated stiffness of the ring during radial deflection. This can be

established in an isolated model of the polymer ring if the boundary conditions are known. The interaction between the o-ring and the polymer ring can be replaced by a shear and normal force profile behind the polymer ring taking note of the fact that the o-ring also limits the effects of fluid pressure behind the seal. The purpose of the finite element analysis of the o-ring has been to determine the interfacial contact pressures between the deformed o-ring and the rear of the polymer seal.

Further justification in modelling the o-ring and seal separately lies in the fact that the elastic modulus of the rubber o-ring is smaller than that of the UHMWPE cap by a factor of 80 (ignoring creep effects in UHMWPE). This, together with the fact that the polymer ring is constrained in the seal groove and by the piston will result in the deflection of the polymer ring at the seal/o-ring interface being of the order of 20 μm. Thus the error in excluding the polymer ring in modelling the o-ring is small and the polymer - o-ring interface can be regarded as a rigid surface.

The behaviour of the o-ring is described in terms of finite elasticity theory since the deformations are large and non-linear effects cannot be ignored, and has been modelled numerically using the finite element method. A satisfactory solution has been obtained with the finite element code ABAQUS, using hybrid elements for hyperelastic materials.

4.1.2.1 The constitutive equations for the rubber o-ring.

Several mathematical constitutive theories of non-linear large elastic deformation based on strain energy density functions have been developed for hyperelastic materials. For isotropic, compressible elastic materials, these are based on the assumption that, once the strain energy density function is known, the constitutive equations are explicit. Many forms of the strain energy density function are available, the most commonly used being the Mooney-Rivlin strain energy function.

The Mooney-Rivlin strain energy function was derived by Mooney in 1940 and is based on a linear relationship between stress and strain in simple shear. The strain energy can be expressed as a function of the principal invariants of the right Cauchy-Green strain tensor, I_k. For incompressible materials $I_3 = 1$ and

$$W = W(I_1, I_2) \qquad (4.1-1)$$

where W is the strain energy density. If we assume that $W = 0$ and that $I_1 = 3$ and $I_2 = 3$ in the reference configuration, it is convenient to regard W as a function of $I_k - 3$. It follows then that the linear form of (4.1-1) is

$$W = C_1(I_1 - 3) + C_2(I_2 - 3) \qquad (4.1-2)$$

where C_1 and C_2 are constants and can be determined experimentally in particular cases. The accuracy in applying the Mooney-Rivlin function to rubber depends significantly on material properties such as the bulk modulus as well as the range and type of deformation incurred.

A methodology for determining the constants in the Mooney-Rivlin function is presented [5] and the results have been incorporated directly into the finite element model.

For the case of simple extension, the constitutive equations can be manipulated such that the constants can be extracted from a tensile test on a rubber specimen according to ASTM D 412.

Simple extension of a homogenous incompressible material can be defined by:

$$x_1 = \alpha X_1$$

$$x_2 = \beta X_2$$

$$x_3 = \beta X_3 \qquad (4.1-3)$$

where α and β are non zero constants and x_i represent the deformed configuration and X_A the reference configuration. Furthermore the requirement that the deformation be isochoric (no volume change) requires

$$J = \frac{dV}{dV_0} = \sqrt{I_3} = \alpha\beta^2 = 1 \qquad (4.1-4)$$

where J is the Jacobian (with respect to the deformation gradient tensor) and dV/dV_0 is the material volume change.

The left Cauchy-Green strain tensor is defined as

$$\mathrm{B} = \mathrm{F}\mathrm{F}^T \qquad (4.1-5)$$

where F is the deformation gradient tensor, and for the case of simple extension is

$$\mathrm{B} = diag[\alpha^2 \quad \beta^2 \quad \beta^2] \qquad (4.1-6)$$

For an incompressible, isotropic, elastic solid, the stress tensor has the form

$$\mathrm{T} = -p\mathrm{I} + 2\frac{\partial W}{\partial I_1}\mathrm{B} - 2\frac{\partial W}{\partial I_2}\mathrm{B}^{-1} \qquad (4.1-7)$$

Where W is the associated strain energy density function and p is an arbitrary constant which can be determined from the boundary conditions, in our case: $T_{22} = T_{33} = 0$. Thus it is easy to show that

$$p = 2\alpha^{-1}\frac{\partial W}{\partial I_1} - 2\alpha\frac{\partial W}{\partial I_2} \qquad (4.1-8)$$

The uniaxial tension can be found in terms of α to be

$$T_{11} = 2(\alpha^2 - \alpha^{-1})\frac{\partial W}{\partial I_1} + 2(\alpha - \alpha^{-2})\frac{\partial W}{\partial I_2} \qquad (4.1-9)$$

For a Mooney-Rivlin material this simplifies to

$$T_{11} = 2(\alpha^2 - \alpha^{-1})C_1 + 2(\alpha - \alpha^{-2})C_2 \qquad (4.1-10)$$

Factorising, we obtain

$$T_{11} = 2(\alpha - \alpha^{-2})(C_1 + C_2\alpha^{-1}) \qquad (4.1-11)$$

In terms of a uniaxial tensile test, T_{11} is the Cauchy stress (ratio of force to original section area) and α is the stretch ratio ($1 + dL/L$). Equation (4.1-11) reveals that if $(T_{11}/2/(\alpha - \alpha^{-2})$ is plotted against α^{-1}, the resulting plot will be a straight line with C_2 as the slope and $(C_1 + C_2)$ as the intercept at $\alpha^{-1} = 1$. In addition, it of interest to note that for an incompressible material the initial tensile elastic modulus E is given by $E = 6(C_1 + C_2)$.

Figures 4.7and 4.8show the resulting Mooney-Rivlin plots for tensile tests performed on samples of 70 and 85 shore A nitrile rubber currently used in cap seal o-rings. For the range of extension which far exceeds that likely to be encountered in practice, the behaviour of the rubber closely follows the Mooney-Rivlin model in that plots are nearly straight lines. The Mooney-Rivlin constants have been extracted from the graphs and are shown in table 4.1.

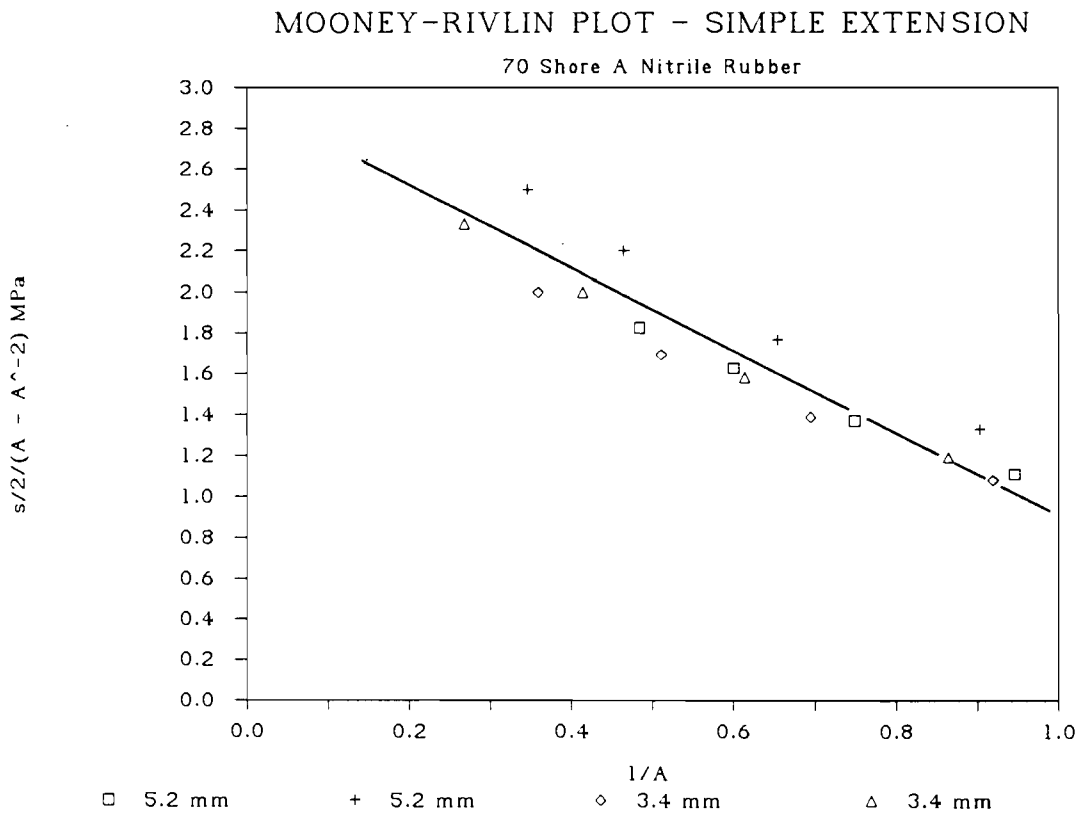

Figure 4.7. MOONEY-RIVLIN PLOT FOR 70 SHORE A RUBBER

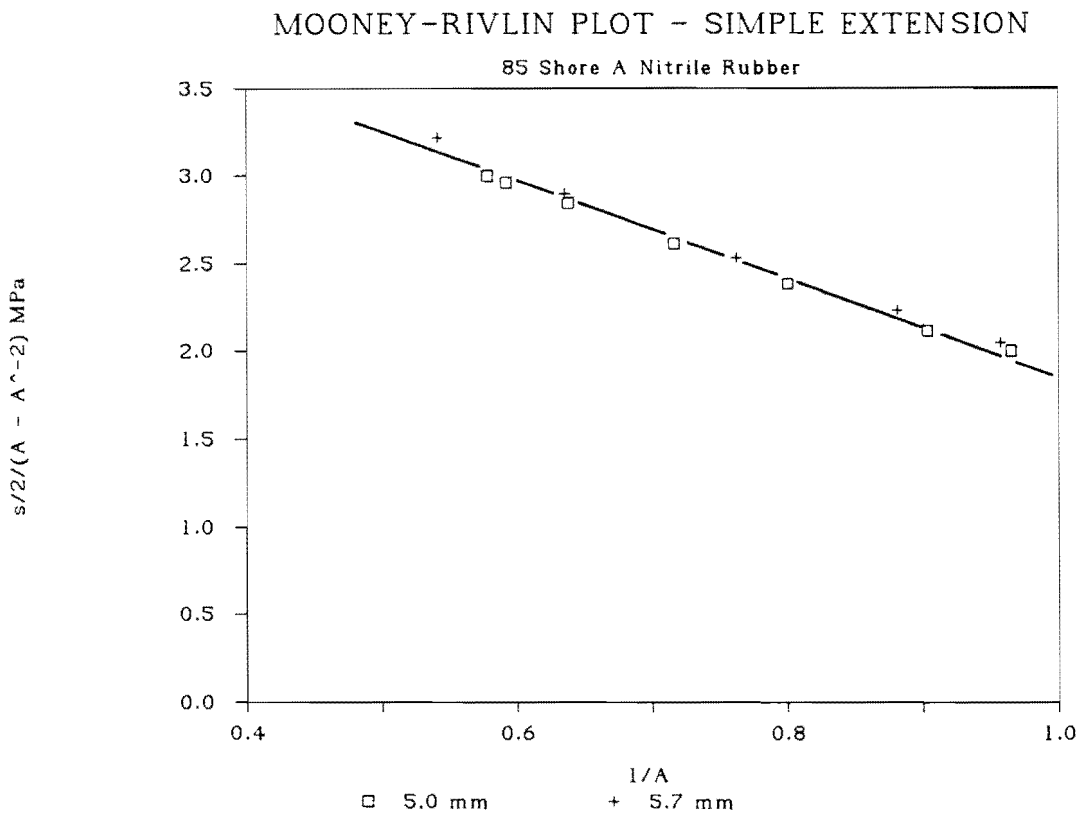

Figure 4.8. MOONEY-RIVLIN PLOT FOR 85 SHORE A RUBBER

TABLE 4.1			
MOONEY-RIVLIN COEFFICIENTS FOR NITRILE RUBBER			
Rubber Type	C_1	C_2	E
70 Shore A Rubber	2.82 MPa	-1.85 MPa	5.82 MPa
85 Shore A Rubber	4.52 MPa	-2.74 MPa	10.6 MPa

4.1.2.2 Finite elements model parameters.

The finite element input data used to model the o-ring consists of two separate input files. The first file relating to the diametral compression of the o-ring section, and the second file to the application of fluid pressure and related boundary conditions to the o-ring. The model for the o-ring is two dimensional axisymmetric using plain strain hybrid elements for hyperelastic behaviour. The model, although small with uncomplicated input files, contains three sources of nonlinearity [6]: material nonlinearity, geometric nonlinearity and boundary nonlinearity

The material nonlinearity is due to the use of hyperelastic elements, wherein the general form of the strain energy function provided simplifies greatly to represent the Mooney-Rivlin form of the strain energy function for incompressible materials. Reduced integration for the 8-noded biquadratic displacement elements is used, which provides significant time savings and little loss in accuracy. In areas where the mesh is refined, 6-noded triangular quadratic elements have been used. The input mesh for the o-ring section is shown in figure 4.9.

The o-ring problem is not truly symmetric about the A-A axis as shown, but the fact that the ratio of o-ring cross section diameter to total o-ring diameter is small, together with relatively high squeezes imposed on the o-ring, guarantees extremely small errors when making this assumption. Furthermore, there is no fixed rule governing the compression or squeeze of o-rings in practice. Depending on available o-ring sizes, the compression can either take place on the inner diameter against the seal, or on the outer diameter against the housing. By making the model axisymmetric about the A-A axis, the mean o-ring diameter is chosen such that the o-ring section is compressed equally on both inner and outer diameters.

The boundaries of the seal groove, as well as the rear of the polymer ring, are defined as rigid surfaces, and interface elements to model the contact condition are defined on all nodes likely to contact the rigid surface. Contact between the nodes and rigid surfaces is then checked for in a direction normal to the rigid surface.

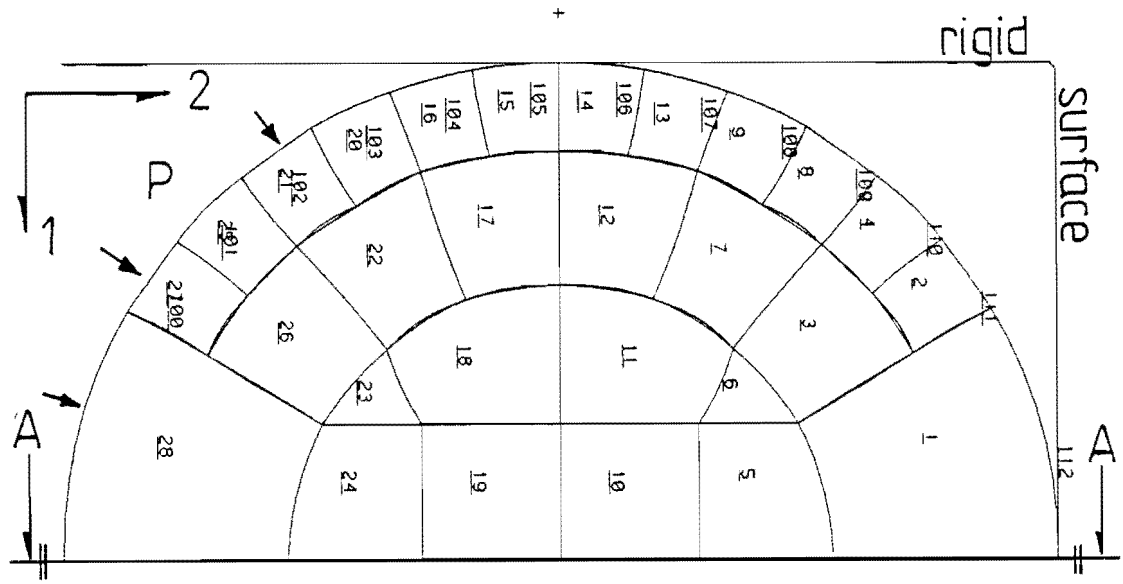

Figure 4.9 FINITE ELEMENT MESH FOR THE O-RING

During the first step of the modelling, the rigid surface is translated towards the A-A axis, while the latter is constrained in the 1st degree of freedom, the incrementation scheme being direct incrementation in fixed time intervals of 0.1 (normalised). In the second step, hydrostatic pressure is applied to the outer element faces of all elements exposed to the fluid pressure but not likely to contact any rigid surface. Elements exposed to the fluid pressure that are likely to contact the rigid surfaces are pressurized with a penetrating pressure. The pressure penetration condition in ABAQUS allows an hydrostatic pressure to penetrate along a series of elements until the mean contact pressure over the exposed side of any particular 'cut-off' element is equal to some factor multiplied by the hydrostatic pressure. The default factor is unity; however, this did not prove realistic in the model since the mean contact pressure over an element side was invariably less than the maximum contact pressure

and the hydrostatic pressure was thus applied throughout the contact area. Rather than refining the mesh in the contact area, which would have solved the problem, the pressure penetration factor was reduced to 0.8 and satisfactory results were obtained. The incrementation scheme in the second step of the model that worked most effectively was automatic incrementation using an initial normalized time step of 0.01.

Friction between the o-ring and both the rigid surfaces was included using a coefficient of 0.6. The coulomb friction model in ABAQUS is implemented by a stiffness method which allows shear forces to be transmitted across the interface so long as these forces are below the friction limit. The friction gap is thus penalized with an artificial stiffness, called the stiffness in stick parameter. A stiffness in stick parameter of 1.0×10^{10} was used, and produced convergent results. The use of a larger parameter caused the solution not to converge, whereas a slightly smaller parameter did not affect the final solution. To aid convergence of the solution, the UNSYMM parameter is also used, forcing the program to include all non-symmetric terms in the matrix algebra.

4.1.2.3 Results.

The results of the finite element model are presented in terms of o-ring/seal interfacial contact pressures, with only the normal components shown since the finite difference formulation for the seal does not allow for the inclusion of shear forces on the one side of the seal. In all cases the section diameter of the o-ring was 2 mm, while the other parameters such as hardness, squeeze and sealed pressure were varied. Figure 4.10 shows the deformed o-ring section and Von Mises stress contours. The region of highest stress lies in the deformed corner of the o-ring some distance from the surface, and it is of interest to note that this is the point from which spiral failure originates in actual o-rings. O-ring failure does not however occur in rockdrill piston seals and the stresses in the o-ring are of no direct importance. Rather, the contact stress profiles at the seal interface have been extracted from the model results and studied as a function of initial o-ring squeeze, sealed pressure and rubber hardness.

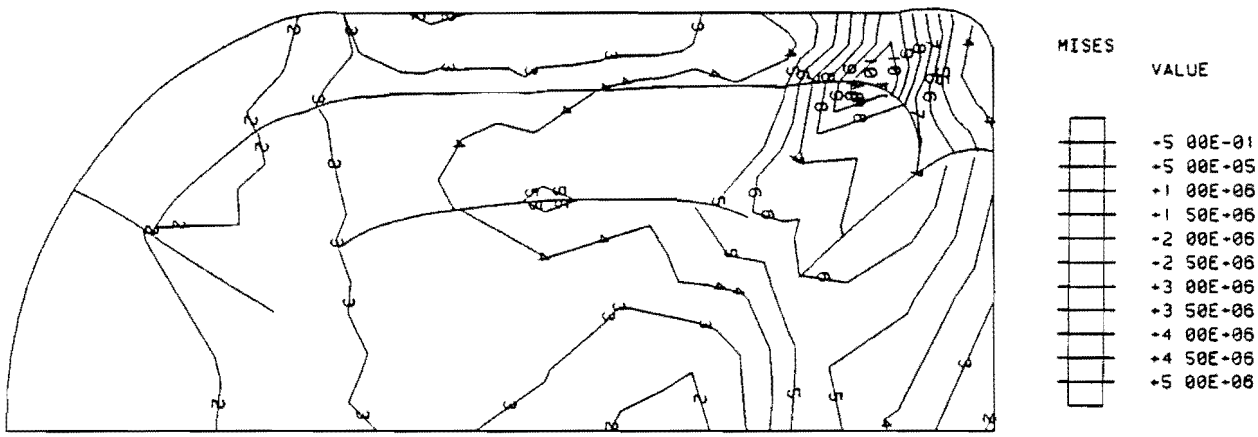

Figure 4.10 O-RING DEFORMATION UNDER PRESSURE

The effect of initial o-ring squeeze is most marked as shown in figure 4.11, with the normal contact pressure between the seal and the o-ring plotted on the ordinate.

The interface distance from high to low pressure corresponds to the initial o-ring section diameter, with the rigid boundary of the seal housing at +1.0mm. The drop off in contact pressure at the low pressure side of the interface (0 - 1.0mm) is a result of the pressure behind the o-ring not being allowed to build up, but rather to leak out at the back of the seal. The contact profiles shift towards the high pressure side of the interface with increasing squeeze since at low squeezes the o-ring has not deformed much and is still able to deform under the sealed pressure. The peak excess

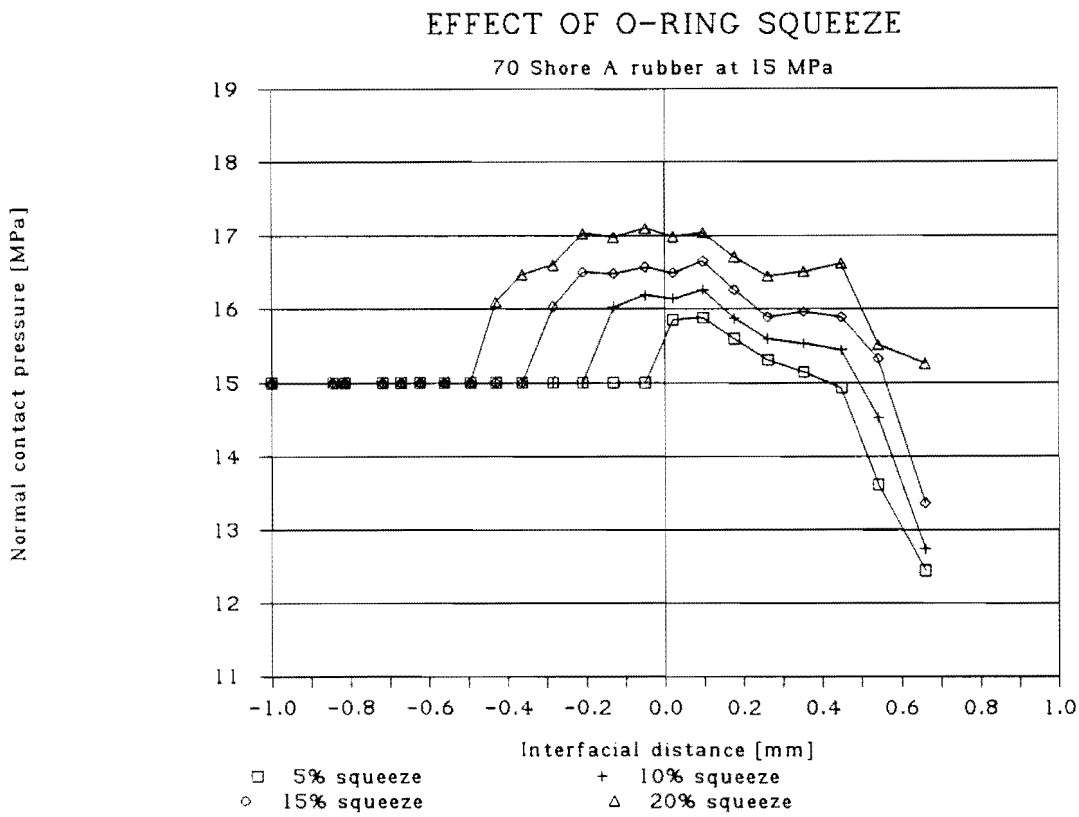

Figure 4.11. THE EFFECT OF O-RING INITIAL SQUEEZE

contact pressures (total contact pressure less the sealed pressure) correspond well to the experimental measurements and are shown as a function of o-ring squeeze in figure 4.12.

The effects of sealed pressure (figure 4.13) are less prominent in the finite element model, compared with the experimental results. The lowering of the contact pressure as well as the shift of the profile towards the low pressure side with increasing sealed pressure, do occur in the model as seen in the exploded view of the contact profiles in figure 4.14. The fact that these trends were more pronounced in the experiments has been ascribed to the face seal configuration that was used in obtaining the experimental results, which allowed for a drop in initial squeeze of the o-ring. The

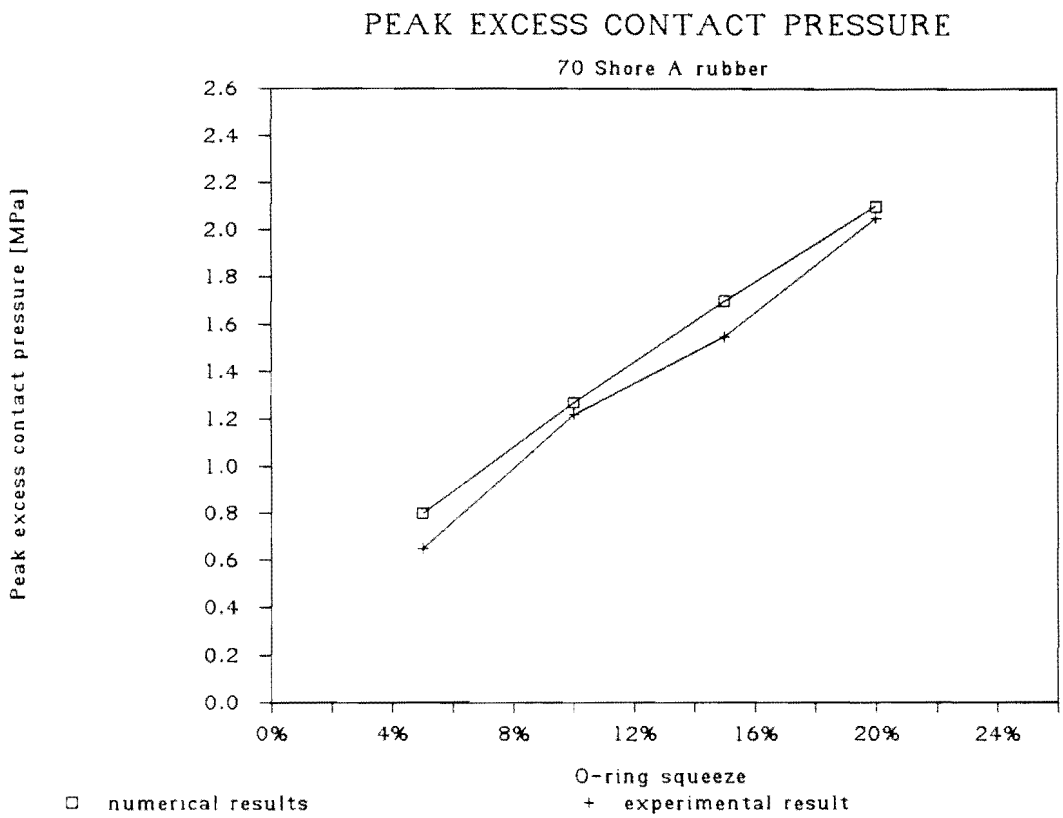

Figure 4.12 PEAK EXCESS PRESSURES AS A FUNCTION OF SQUEEZE EXPERIMENTAL AND FINITE ELEMENT RESULTS

finite element model does however reveal that these trends are a result of friction forces at the o-ring - seal interface. Figure 4.15 shows the effects of modelling friction at the interface, where the associated drop in contact pressure and slight shift of the profile correspond to the trends shown as a result varying the sealed pressure.

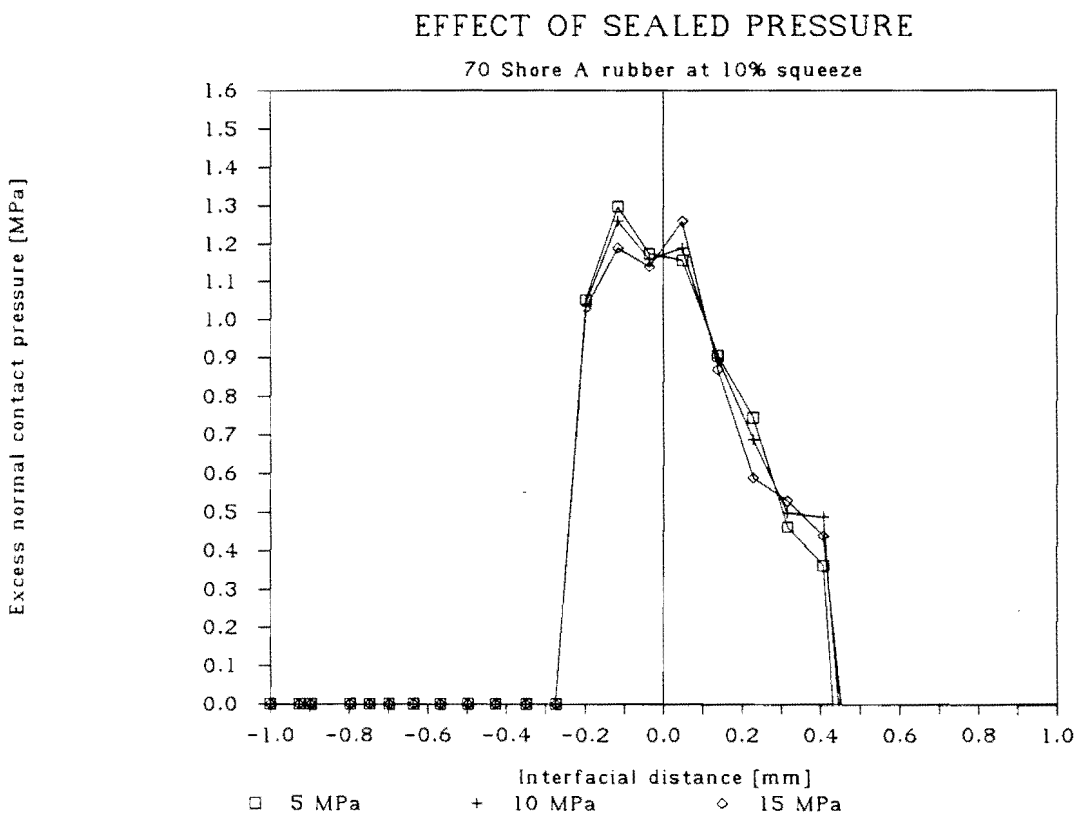

Figure 4.13. THE EFFECTS OF SEALED PRESSURE

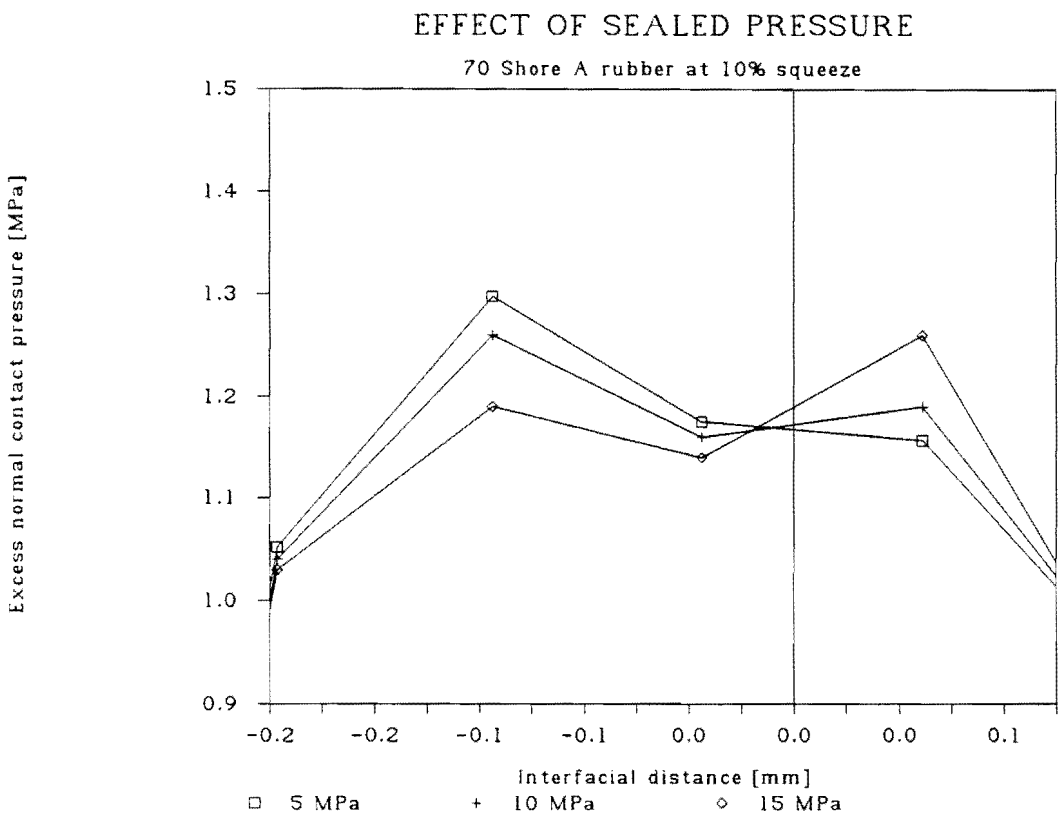

Figure 4.14. THE EFFECTS OF SEALED PRESSURE (ENLARGED)

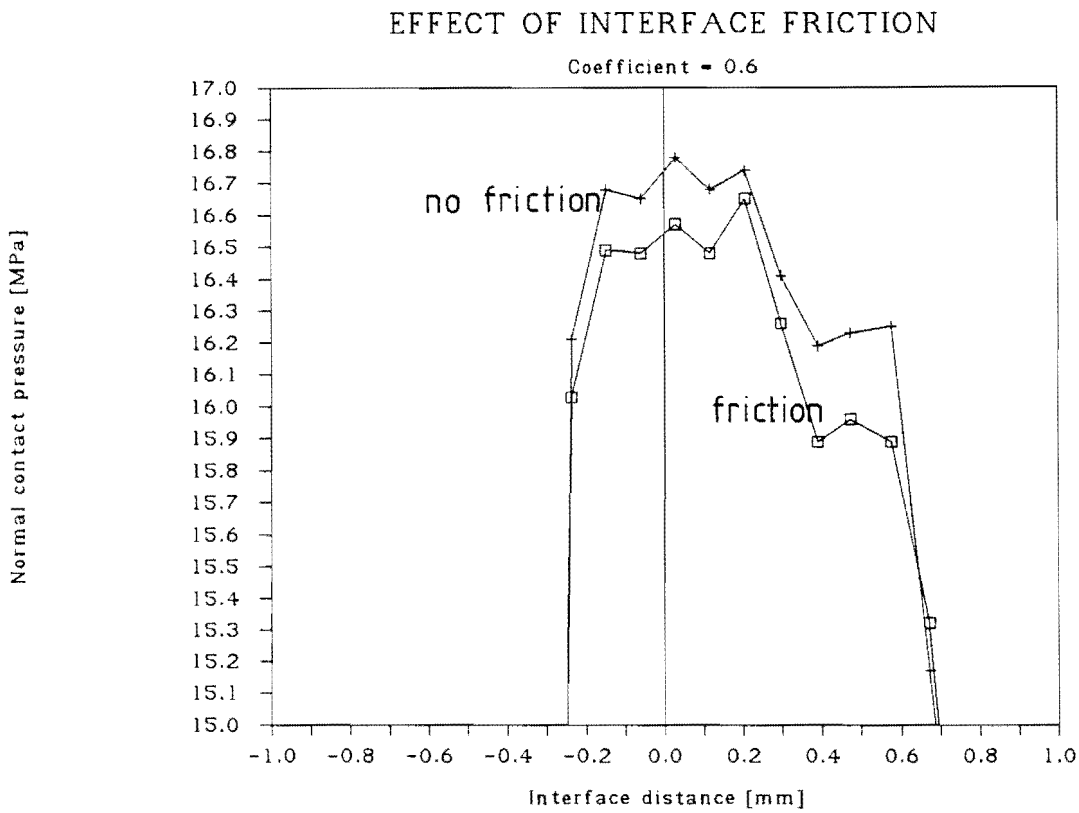

Figure 4.15. THE EFFECT OF FRICTION ON CONTACT PRESSURES

Increasing the hardness of the rubber o-ring also has a significant effect in raising the contact pressures, especially at high initial squeezes. Figure 4.16 shows the pressure profiles for 70 and 85 Shore A rubber at a sealed pressure of 15 MPa.

The trends and profiles presented have shown the effect of the o-ring in limiting the extent of pressure penetration at the rear of the seal, and provide the necessary information required as an input into the finite difference model of the seal described in the following section.

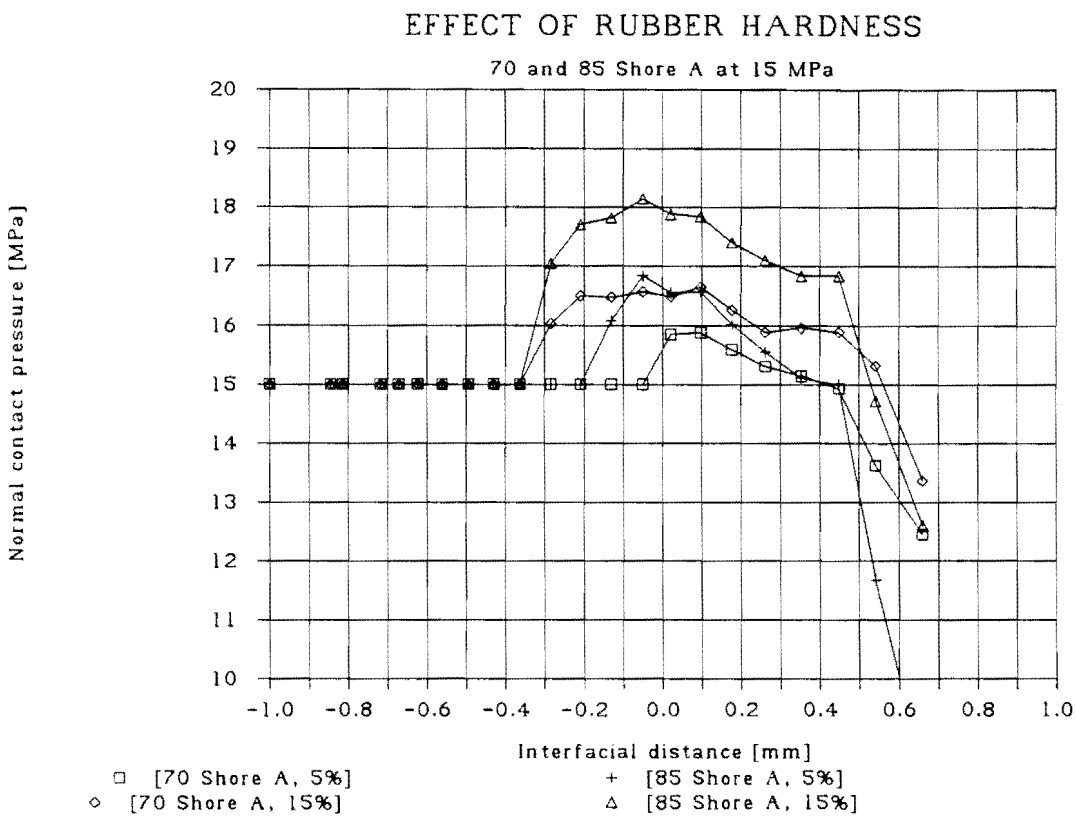

Figure 4.16. THE EFFECT OF RUBBER HARDNESS

4.2 A finite difference analysis of the seal.

The finite difference method has been chosen primarily because of its easy implementation on a personal computer, and the ability to combine the algorithm with other functions in a computer program.

The polymeric seal can be considered to be thin walled elastic cylinder subject to axisymmetrical radial loading due to the energiser, hydrodynamic film and sealed pressure. Because of symmetry, any section of the shell perpendicular to the cylinder

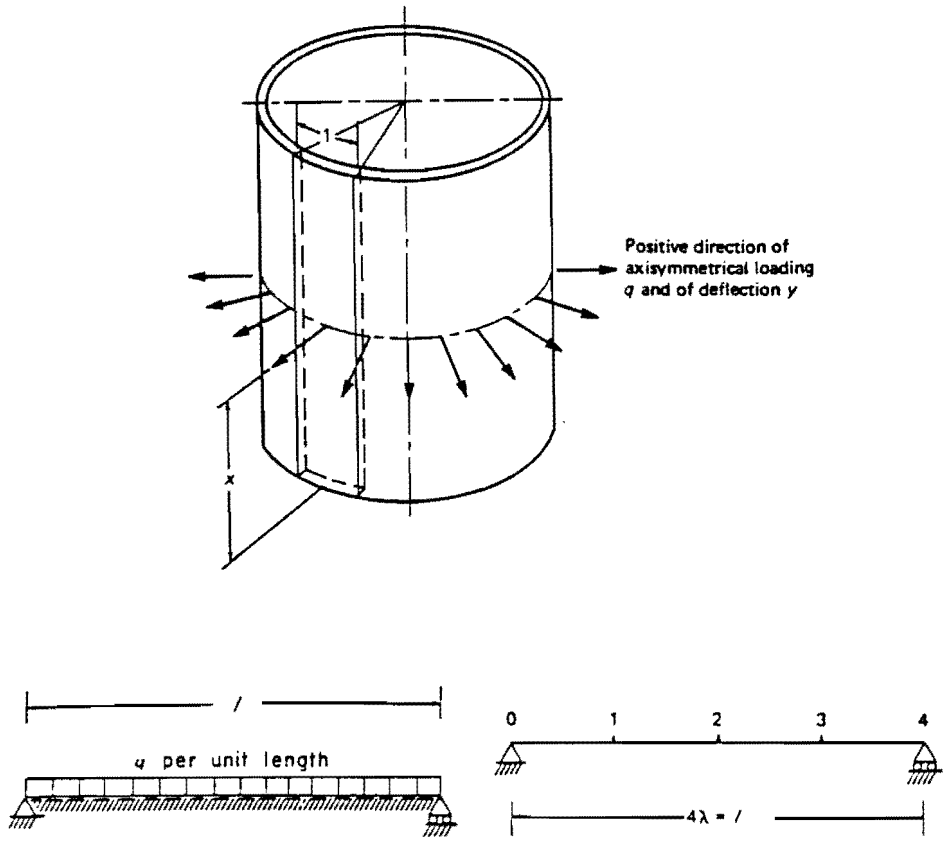

Figure 4.17. A FINITE DIFFERENCE MODEL FOR THE SEAL

axis will remain circular while the radius will undergo a change $\Delta r = y$. We need therefore to consider the deformation of only one strip parallel to the cylinder axis with unit width (figure 4.17).

The radial displacement y, must be accompanied by a circumferential force whose magnitude per unit length of the axis is

$$N = \frac{Eh}{r} y \qquad (4.2-1)$$

where h is the cylinder thickness and E the elastic modulus. The circumferential forces are considered positive when tensile and the radial deflection is positive outward. Dividing equation 4.2-1 by $(-r)$ the resultant hoop force per unit length in a direction opposing the deflection is

$$-\frac{N}{r} = \frac{-Eh}{r^2} y \qquad (4.2-2)$$

Hence the strip can be modelled as a beam on an elastic foundation whose modulus is

$$k = \frac{Eh}{r^2} \qquad (4.2-3)$$

Because of the axial symmetry of the wall deformation, the edges of any strip must remain in a radial plane and lateral extension or contraction is prevented. This restraining influence is equivalent to a bending moment in a circumferential direction.

$$M_\phi = \nu M \qquad (4.2-4)$$

where M is the bending moment parallel to the axis and ν is Poisson's ratio. It can be shown that the stiffening effect of M_ϕ on the bending deformation of the beam strip can be taken into account by increasing the moment of inertia of the strip in the ratio $1/(1-\nu^2)$, hence the flexural rigidity of the strip is

$$EI = \frac{Eh^3}{12(1-\nu^2)} \qquad (4.2-5)$$

The differential equation for the deflection of a beam resting on an elastic foundation,

$$\frac{d^2}{dx^2}\left(EI\frac{d^2y}{dx^2}\right) = q - ky \quad , \qquad (4.2-6)$$

can be used for the cylinder with y indicating the radial deflection and x the axial distance along the cylinder. The intensity of radial pressure on the wall is defined as q and k is the foundation modulus (ie the foundation reaction per unit length of the beam per unit deflection).

The finite difference form of equation (4.2-6) when applied to a general point i is

$$\frac{E}{\lambda^4}[I_{i-1}\,|-2(I_{i-1}+I_i)\,|\,(I_{i-1}+4I_i+I_{i+1})\,|-2(I_i+I_{i+1})\,|\,I_{i+1}]$$

$$\times\begin{Bmatrix} y_{i-2} \\ y_{i-1} \\ y_i \\ y_{i+1} \\ y_{i+2} \end{Bmatrix} \cong q_i - k_i y_i \qquad (4.2-7)$$

where λ represents the distance between two nodes and I_i the local second moment of area of the beam section. Using the equivalent concentrated load Q_i to replace $q_i\lambda$ and rearranging terms, equation (4.2-7) becomes

$$\frac{E}{\lambda^3}\left[\, I_{i-1} \,|\, -2(I_{i-1}+I_i) \,|\, \left(I_{i-1} + 4I_i + I_{i+1} + \frac{k_i\lambda^4}{E} \right) |\, -2(I_i + I_{i+1}) \,|\, I_{i+1} \,\right] \times \begin{Bmatrix} y_{i-2} \\ y_{i-1} \\ y_i \\ y_{i+1} \\ y_{i+2} \end{Bmatrix} \cong Q_i \qquad (4.2-8)$$

Since I is defined locally, seals of varying longitudinal section may be modelled. The above equations apply to internal nodes of the beam (section of the cylinder) and need to be modified for the end nodes, assumed to be freely supported, and for the nodes immediately adjacent to the end nodes. A freely supported end node is only truly applicable to the high pressure side of the seal, whereas radial deflection at the low pressure end of the seal is constrained by a friction force between the seal and housing. This force can however be incorporated into the concentrated load at that node. The coefficients of the deflection terms of E/λ^3 change for the end nodes as shown in table (4.2).

TABLE 4.2					
Coefficients of the deflection in terms of $\frac{E}{\lambda^3}$ for a free support					
Position of node i	y_{i-2}	y_{i-1}	y_i	y_{i+1}	y_{i+2}
end node	0	0	$I_i + k_i\lambda/2$	$-2I_{i+1}$	I_{i+2}
second from end	0	$-2I_{i-1}$	$(4I_i + I_{i-1} + k_i\lambda)$	$-2(I_i + I_{i+1})$	I_{i+2}

Once the stiffness matrix and resultant load vector have been set up the deflections y_i are found by Gaussian elimination.

4.3 The hydrodynamic lubrication equations. (Reynold's equations).

The one dimensional Reynold's lubrication equation is merely a simplification of the Navier-Stokes equations for an incompressible and isothermal fluid given in vector notation by

$$\rho \frac{D\omega}{Dt} = F - \text{grad } p + \mu \nabla^2 \omega \qquad (4.3-1)$$

When the inertia terms are neglected the incompressible Navier-Stokes equations assume the form

$$\text{grad } p = \mu \nabla^2 \omega \qquad (4.3-2)$$

$$\text{div } \omega = 0 \qquad (4.3-3)$$

These equations of creeping motion (viscous flow) can be further simplified for the case of an infinitely wide slipper or seal sliding over a piston (figure 4.18). The equation for the y-direction can be omitted altogether because the velocity component v is very small compared to the component u. Furthermore, in the equation for the x-direction $\partial^2 u/\partial x^2$ can be neglected with respect to $\partial^2 u/\partial y^2$, because the former is smaller than the latter by a factor $O(h^2/l^2)$. The pressure distribution must satisfy the boundary conditions and whereas the pressure gradient in the direction of motion, $\partial p/\partial x$ is not constant, the very small pressure gradient in the y-direction can be neglected. With these simplifications the equation (4.3-2) reduces to

$$\frac{dp}{dx} = \mu \frac{\partial^2 u}{\partial y^2} \qquad (4.3-4)$$

The equation of continuity can be satisfied by the condition that the volume of flow throughout the section must remain constant,

$$Q = \int_0^{h(x)} u\,dy = constant \qquad (4.3-5)$$

The boundary conditions for the seal or slipper are

$$\begin{aligned} y = 0 &\rightarrow u = V \\ y = h &\rightarrow u = 0 \\ x = 0 &\rightarrow p = P_1 \\ x = l &\rightarrow p = P_2 \end{aligned} \qquad (4.3-6)$$

The solution of equation (4.3-4) satisfying the velocity boundary conditions is

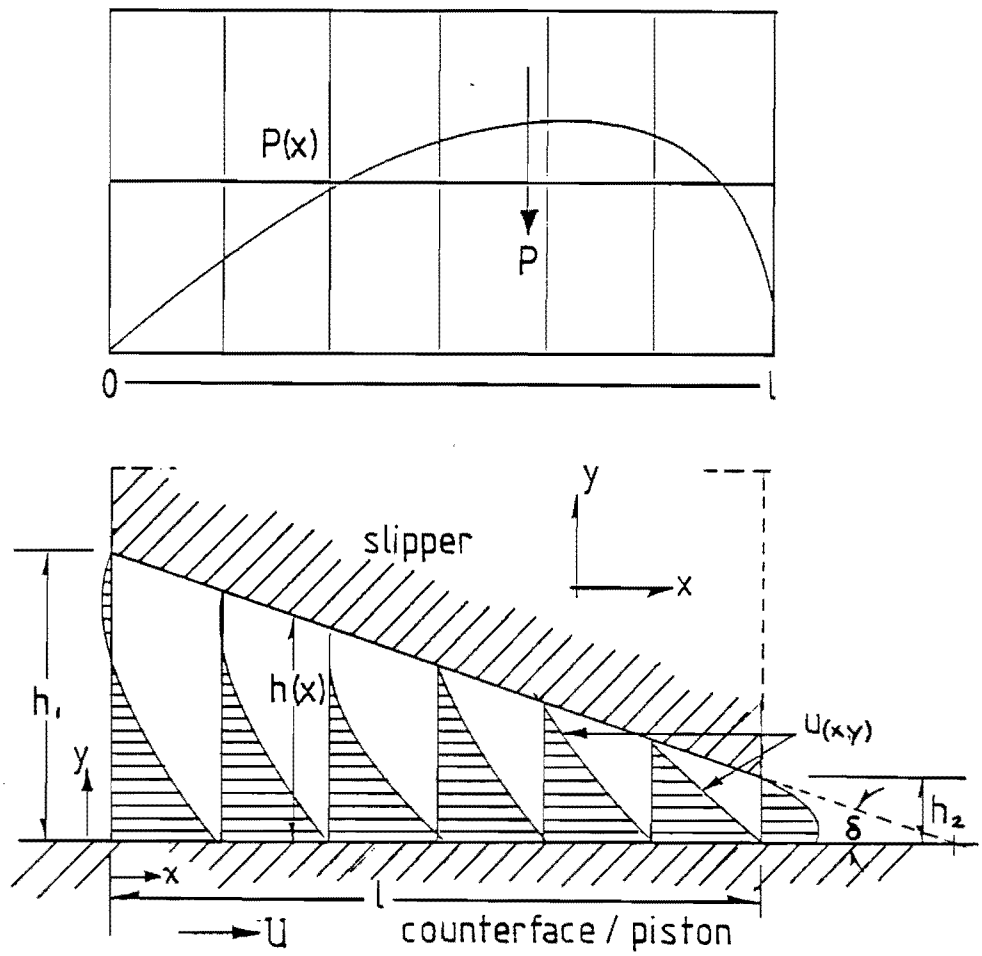

Figure 4.18 HYDRODYNAMIC LUBRICATION BENEATH A SLIPPER

$$u = V\left(1 - \frac{y}{h}\right) - \frac{hy}{2\mu}\frac{\partial p}{\partial x}\left(1 - \frac{y}{h}\right) \qquad (4.3-7)$$

Substituting equation (4.3-7) into the continuity equation we obtain

$$Q = \frac{Vh}{2} - \frac{h^3}{12\mu}\frac{\partial p}{\partial x} \qquad (4.3-8)$$

Solving for $\partial p / \partial x$ and integrating we obtain

$$p(x) = P_1 + 6\mu V \int_0^x \frac{dx}{h^2} - 12\mu Q \int_0^x \frac{dx}{h^3} \qquad (4.3-9)$$

Inserting the condition that $p = P_2$ at $x = l$, we obtain the volume flow

$$Q = \frac{P_1 - P_2 + 6\mu V \int_0^l \frac{dx}{h^2}}{12\mu \int_0^l \frac{dx}{h^3}} \qquad (4.3-10)$$

Thus, given the profile of the seal over the counterface or piston, $h(x)$, the volume flow rate is known and the pressure at any point x can be calculated by equation (4.3-9).

4.4 A solution algorithm.

The solution to the seal problem involves solving the elasticity equations simultaneously with the hydrodynamic lubrication (HDL) equation to determine the deflection of the polymer and the associated leakage of water through the seal. In the finite difference solution the forces acting on the seal are required to determine the seal deflection and in the hydrodynamic solution the seal deflection is required to determine the fluid pressure profile and hence the forces acting on the seal. An iterative procedure involving alternate solution of the two equations is the obvious choice; however serious problems of instability arise.

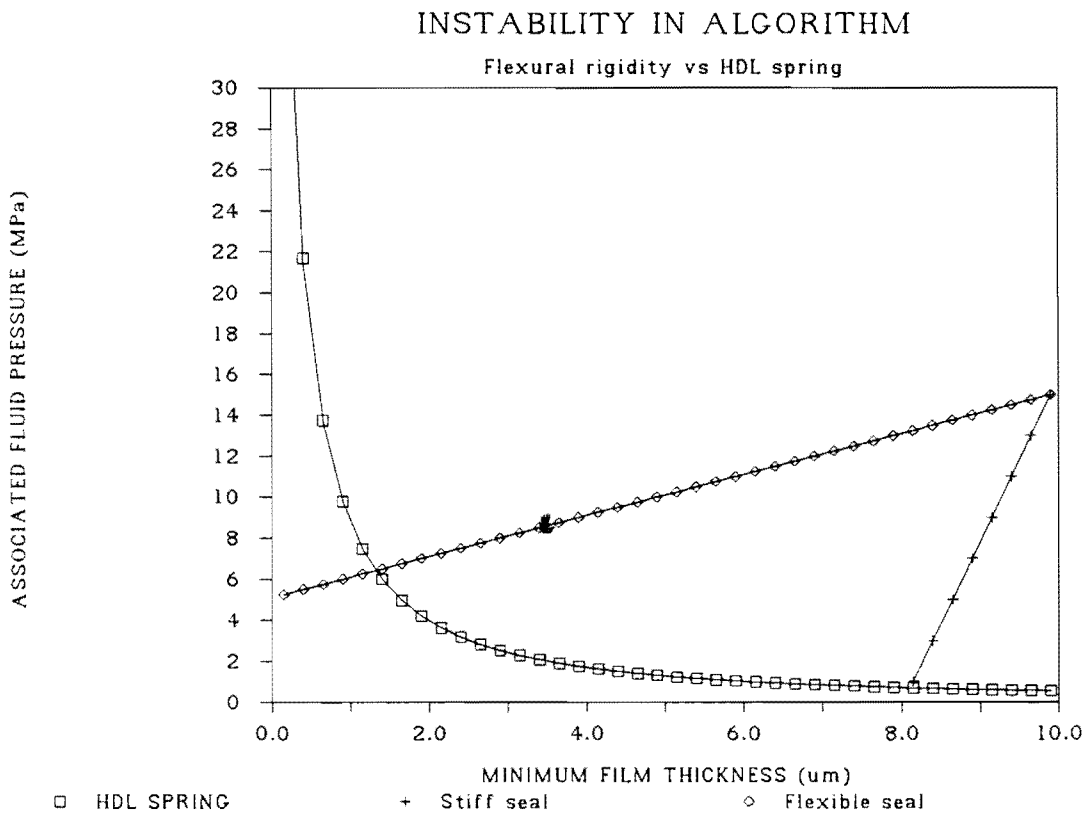

Figure 4.19. EFFECTIVE STIFFNESSES OF SEAL AND HDL FILM

Figure 4.19 shows the stiffness of the hydrodynamic film at a given position along the seal as a function of the film thickness. In addition the stiffness or flexural rigidity for two hypothetical seal materials is shown. The influence of the hydrodynamic film is essentially that of a non-linear spring or set of springs exerting a force on the polymer ring. As the clearance between the seal and the counterface diminishes, the hydrodynamic spring stiffness increases rapidly whereas the flexural rigidity of the polymer ring remains low.

The iterative algorithm involves beginning with an assumed film thickness (or film thickness profile in the case of the entire seal length) and solving the lubrication equation to establish a fluid pressure (or profile). The fluid pressure is used as an

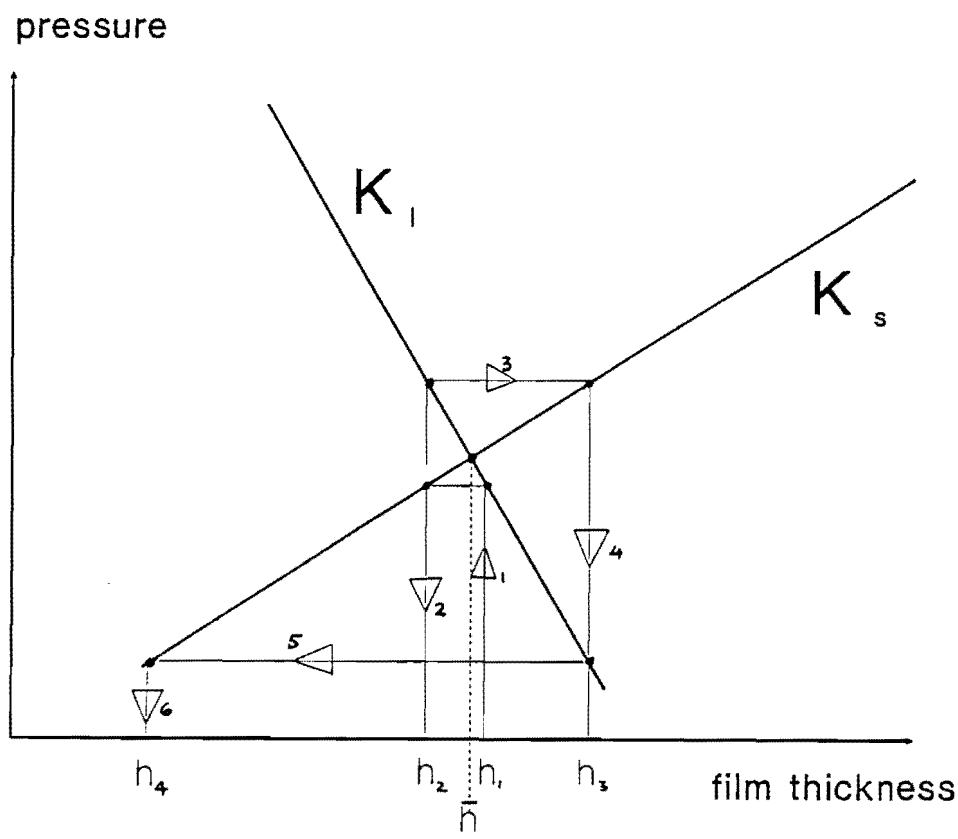

Figure 4.20. INSTABILITY IN THE ALGORITHM AS A FUNCTION OF SEAL FLEXURAL RIGIDITY

input to the finite difference method and a new film thickness profile is calculated for the seal. The iterative procedure can be followed in figure 4.20 using the HDL spring and the seal flexural rigidity alternatively. The solution is reached when the two stiffness curves intersect, while stability in actual seals is ensured by the fact that the gradients of the two curves at the intersection have differing signs.

The exact solution of film thickness is shown as $\bar{h}$ in figure 4.20,and the film thickness at the n th iteration is labelled h_n. Owing to the order of iteration, ie. first solving the HDL equation using a known film thickness, it will be clear from the figure that

$$K_s\left|h_{n+1}-\bar{h}\right| = K_l\left|h_n-\bar{h}\right|$$

and thus the criterion for convergence is

$$|K_s| > |K_l| \qquad (4.4-1)$$

where K_s is flexural stiffness of the seal material and K_l is the stiffness associated with the lubrication film (see figure 4.19). It is clear that this criterion is met for a very stiff seal material but not for a soft material such as the polymer currently used for seals (UHMWPE). The only way to guarantee convergence and stability is to introduce a form of artificial control in the iteration algorithm. To further encourage stability, convergence towards a node must be asymptotic and monotonic if the same algorithm is to be applied to all nodes along the seal length.

Several algorithms were tried in solving the elastohydrodynamic problem, all beginning with a uniform film thickness across the seal. The first was to increase the pressure differential across the seal during each iteration until the desired sealed pressure was reached. This algorithm was extremely unstable since the HDL spring stiffness varies significantly with sealed pressure and the convergence criterion viz. $|K_s| > |K_l|$ was soon violated. The second attempt was to start at the correct pressure differential but using a stiff seal material, and decrease the seal stiffness over each iteration. The solution was stable and convergent for high elastic moduli or extremely thick seal sections, but once again stability was lost as the stiffness of the seal decreased. A final and working algorithm was used during which the film shape was adjusted by underrelaxation of the polymer ring. In other words, the film shape emerging from the finite difference analysis was adjusted prior to being used in the

hydrodynamic equation to ensure that the film thickness decreased asymptotically and monotonically towards the solution at each node. Similar algorithms have been used in modelling the lubrication properties of thin strips on rubber rollers in the printing industry [9] and in modelling lip seals in an oil medium [10]. The adjustment was applied uniformly at all of the nodes as follows:

$$h_{n+1} = h_n - C_u |h_n - h_{n+1}| \qquad (4.4-2)$$

The factor C_u used in underrelaxation had to be sufficient to ensure that the converging film thickness did not overshoot the exact solution and was typically 0.999. The algorithm could be made to work even if $|K_s| < |K_l|$ since a sufficiently large underrelaxation factor could always ensure stability to within a specified error margin. A flow chart of the computer program implementing this algorithm is shown in figure 4.21.

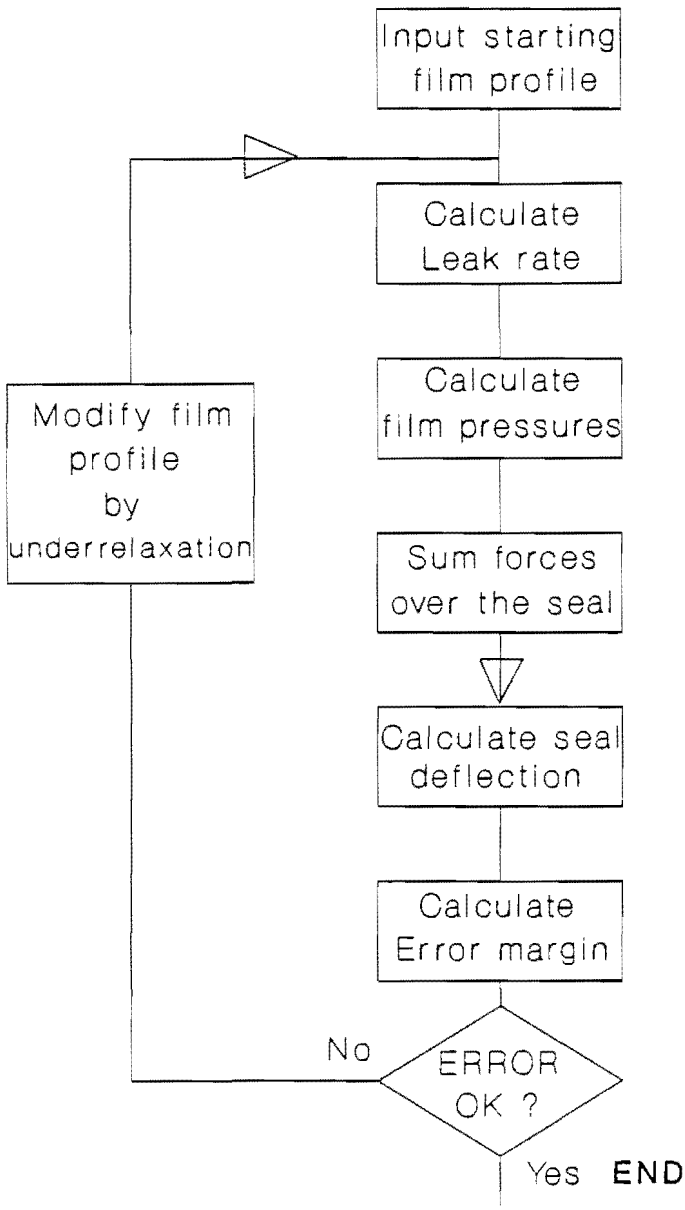

Figure 4.21 A FLOW CHART FOR THE SOLUTION ALGORITHM

Chapter V. THE ANALYSIS OF PISTON SEALS.

The analysis of rockdrill piston seals has been done experimentally and analytically using the elastohydrodynamic model described above, and fair correlation between the results has been obtained. The two methods of analysis are complementary, and shed light on different aspects of the seal behaviour. The numerical model only describes that portion of the seal cycle wherein the pressure differential is in the same direction as the relative piston velocity, and can only model full hydrodynamic lubrication. Partial elastohydrodynamic lubrication or boundary lubrication can, however, exist if the minimum film thickness is less than the surface roughness of the counterface, and is stable. The numerical model defines the equilibrium position of the seal in relation to the counterface and the associated leakage across the seal. An advantage of the model is the ability to note the effect of changing design parameters, not easily variable in an experimental set-up, and a near optimum design solution can be found.

The experimental testing of seals is less flexible, given budget and time limitations, but does model some important real features of seal behaviour. In the test rig described below, the pressure differential across the seal remains constant in magnitude and direction, and as the seal reciprocates relative to the piston, conditions favourable for hydrodynamic lubrication exist during only half the cycle. The natural assumption regarding seal life is that if a seal is able to form a lubricating layer, even at low speeds, the effective life of the seals can only double since the layer will break down during half the seal cycle. This, however, did not occur during the tests. Several seals did not wear at all over extended tests of 5 million cycles, indicating that the seal was separated from the counterface at all times during the cycle. The reason for this behaviour is assumed to lie in the dynamic response of the seals to the changing boundary conditions. With a frequency of 50 Hz, the seal needs to respond within 10 milliseconds if it is to deform and touch the counterface during part of the cycle. Without having investigated the dynamic response of seals in this thesis, it has been assumed that in such cases, the equilibrium position of the seal above the counterface is somewhere between that predicted by the numerical model, and contacting the counterface. This assumption is in agreement with leakage and wear rates obtained in experimental tests.

The high speed seal test rig that was designed and used to test piston seals is described in the following section and the results for existing and new seal designs are presented.

5.1 Test rig and experimental procedure.

The test rig consists of a reciprocating piston moving in and out of a pressure chamber, with two piston seals at either end. Both the pressure chamber and seals are stationary while the piston reciprocates at a frequency of 50 Hz with a stroke of 30 mm. The piston is crank driven with the needle roller bearings splash lubricated from a water cooled oil reservoir.

Despite the high frequency and large stroke of the piston, vibration has been minimised by effective balancing of the primary forces and partial balancing of secondary forces in the rotating crank and connecting rod. The mass of the reciprocating components has also been kept to a minimum thereby helping to reduce vibration and ensure an acceptable fatigue life.

The piston is separable and consists of a primary piston permanently fixed to the connecting rod and a secondary piston which can be freely removed and forms the counterface sliding over the two piston seals. The primary piston floats in an oil-fed bronze bush, which linearizes the motion of the piston. As a result, the secondary piston remains concentric with the piston seals and pressure chamber and eliminates the possibility of side loading of the seals by the piston. The secondary piston was made from AISI 431 stainless steel, hard chrome plated and surface ground in a circumferential direction to a finish of 0.1 R_a. The pressure chamber is fed with a constant flow of tap water under pressures of up to 20 MPa and maintained at a constant temperature of 20°.

The test procedure for each different seal consisted of repeated weighing of the seal at intervals of 500 000 cycles to determine seal wear, and measurement of the leakage through the seal. Runs were usually terminated at 5 million cycles (approximately 30 hours), as this is greater than the current expected life of piston seals, unless the seal wear was excessive and conclusive results could be obtained in a shorter period.

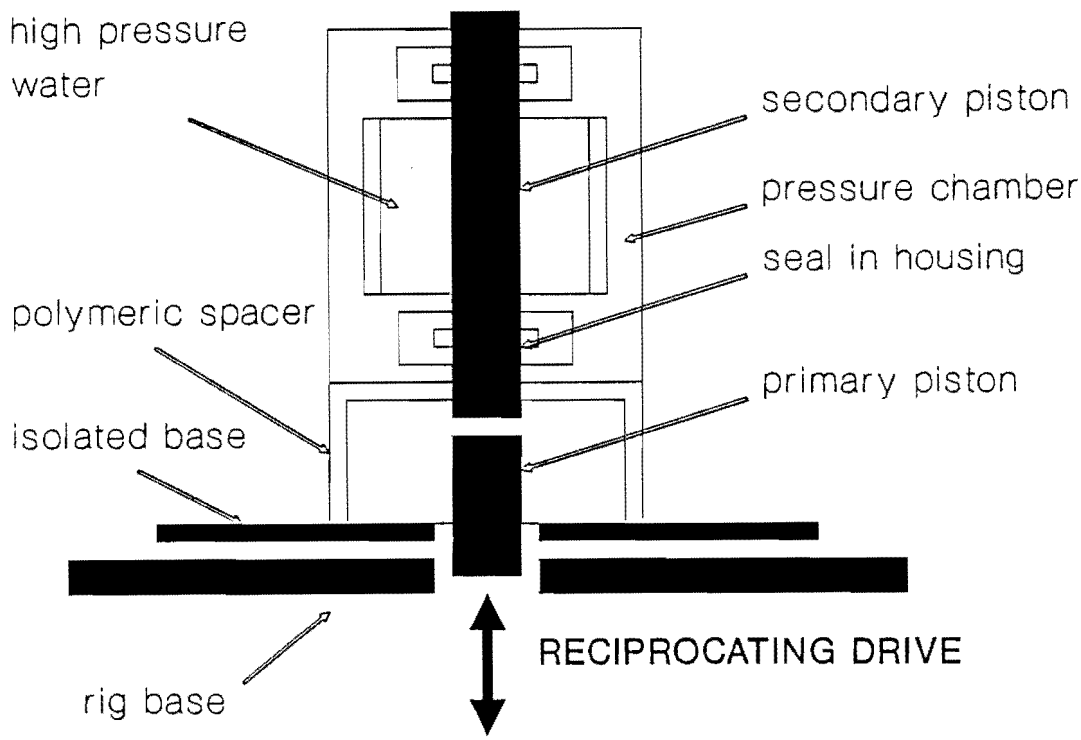

Figure 5.1 HIGH SPEED SEAL TEST RIG

Seal lives beyond 5 million cycles were extrapolated from the wear measurements as by this stage the wear rate was uniform. It will be noted that weighing of the seals at the first interval often showed a slight mass gain corresponding to water absorption by the polymer. It is possible to adjust the mass measurements to account for

absorption, but the mass gain is so small that it lies within the bounds of normal experimental error and has therefore not been compensated for in the presentation of the results.

5.2 The performance of existing piston seals.

The seals currently used in water powered rockdrills wear at a high rate because they remain in contact with the piston during the entire, or at least the majority of the seal cycle. Whether the seal wear process is abrasive wear, adhesive wear, or whether the wear process is dominated by hard particle contamination in the mine water, the wear takes place due to contact between the seal and counterface. The elastohydrodynamic model does not yield solutions for the current seal designs and the high speed tests in the experimental rig produces seal wear rates similar to those obtained in polymer wear studies under conditions unfavourable for the formation of hydrodynamic lubrication. Although no solutions emerged for the existing seals it may still be possible that a lubrication film exists during a portion of the seal cycle since all the possible combinations of forces that may act upon the seal have not been modelled. Effects such as o-ring relaxation, variations in dimensional tolerances of the seal and piston, and the normal wear of seals may at some stage favour elastohydrodynamic lubrication.

The input data for the o-ring forces in the narrow seal configuration was taken from the finite element results for a 70 Shore A nitrile rubber o-ring at 15% squeeze. The remaining input data for the elastohydrodynamic model pertaining to the currently used narrow seal is tabulated in table 5.1.

TABLE 5.1	
MODEL INPUT PARAMETERS FOR CURRENT NARROW SEAL	
PARAMETER	VALUE
Elastic modulus	750.0×10^{6} Pa
Poisson's ratio	0.4
Thickness	1.8 mm
Length	10 mm
Sliding speed	3.3 ms^{-1}
Viscosity of water	$10^{(-3)}$ $Pa\ s$
Seal inner diameter	30 mm
Radial clearance	10 μm
Sealed pressure	15 MPa
Back pressure	0 MPa $(guage)$

The current seals do not form a lubricating layer because of an imbalance in the forces acting on the seal, which is best made clear if the model of the seal is further simplified to resemble a rigid slipper ring sliding over the piston. The slipper surface is regarded as smooth and flat, while the slipper face is free to rotate and assume any angle in relation to the counterface. In using the theory of hydrodynamic lubrication, possible fluid films, and equilibrium positions of the seal are modelled.

Assuming that the hydrodynamic film is to support an average pressure of 17 MPa due to o-ring and fluid at the rear of the seal, contours for a mean hydrodynamic pressure of 17 MPa can be plotted for the seal. Figure 5.2 shows such contours for a narrow 2mm wide seal, in which the required angle of the slipper is plotted as a function of the minimum film thickness for different sliding speeds. It is clear that the minimum film thickness is in excess of the normally used roughness parameter R_z, which means that full hydrodynamic lubrication is possible for a range of slipper angles, even at low piston speeds occurring at the ends of the seal cycle. However, the film that may form is unstable, and may be seen if the respective centres of pressure for the fluid film and forces acting at the rear of the seal are plotted for the range of

feasible slipper angles in figure 5.3. The two centres of pressure do not coincide, which implies an unstable condition since the seal is only in equilibrium when the hydrodynamic film centre of pressure crosses the centre of pressure caused by the remaining forces acting on the seal, in a right handed manner as shown in figure 5.4. The effect of the separation in centres of pressure is to apply a right handed twisting moment to the seal, causing it to deflect and touch the counterface at the low pressure trailing edge of the seal. This deflection of the seal against the counterface is the cause of the characteristic wedge shaped wear that is seen on worn seals.

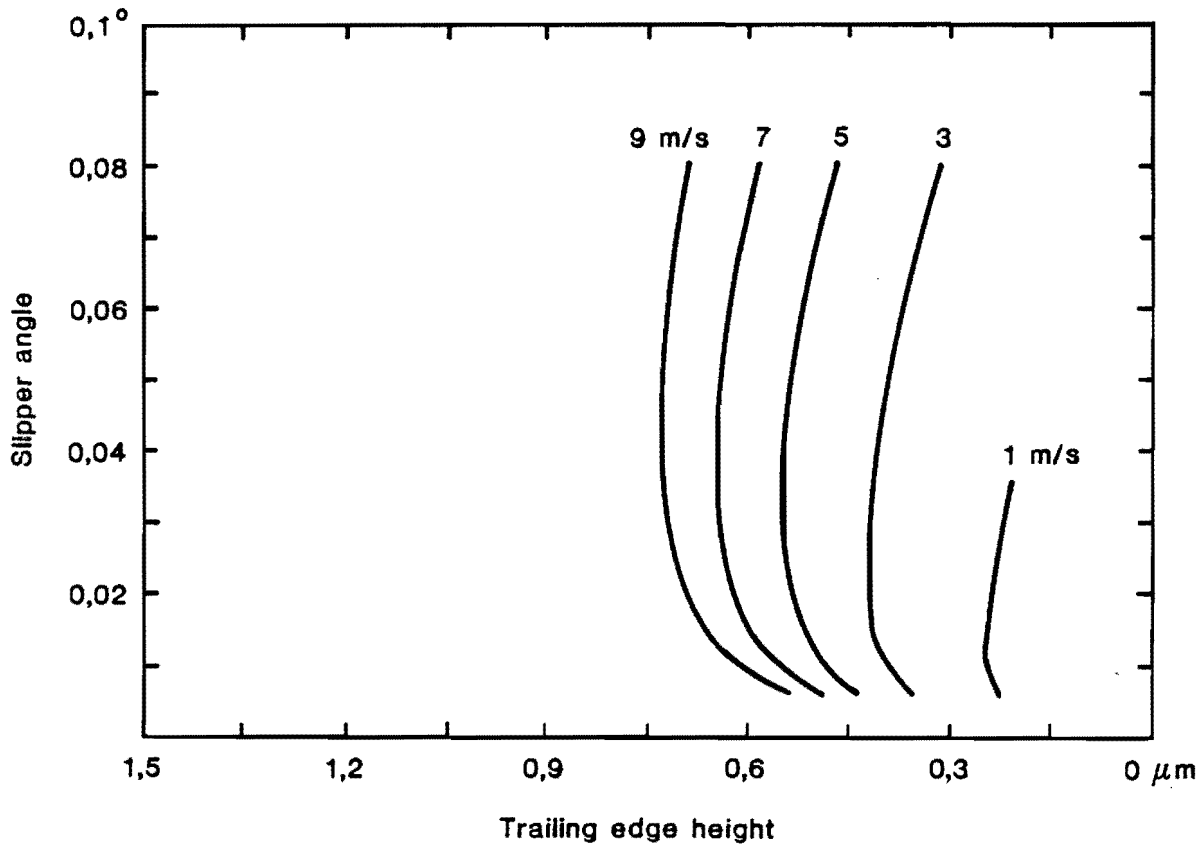

Figure 5.2 17 MPa CONTOURS FOR NARROW SEALS

If the effect of the flexural rigidity of the seal in twisting as a ring over the piston is included in the forces acting on the seal, the centre of pressure of forces behind the seal shown in figure 5.3 moves towards the high pressure side of the seal for increasing slipper angles. This in effect increases the possibility of forming a stable lubrication film. The elastic modulus of UHMWPE is, however, too low to have any significant effect on the film stability, and the desired improvements can only be achieved by using a seal material with a far higher modulus than UHMWPE. Stable solutions using the full elastohydrodynamic model for narrow seals in the current configuration have been found for seal materials with a modulus of elasticity approximately one hundred times greater than UHMWPE. A similar analysis reveals that the lubrication layer that may form in the case of wide piston seals is also unstable, although to a lesser degree.

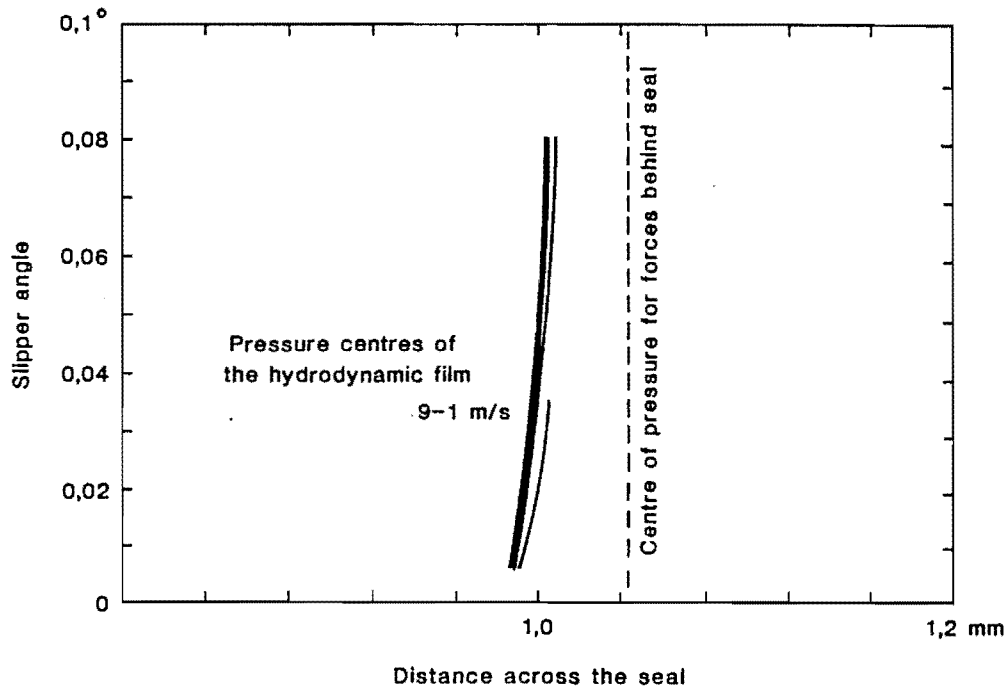

Figure 5.3 CENTRES OF PRESSURE FOR FORCES ACTING ON THE SEAL

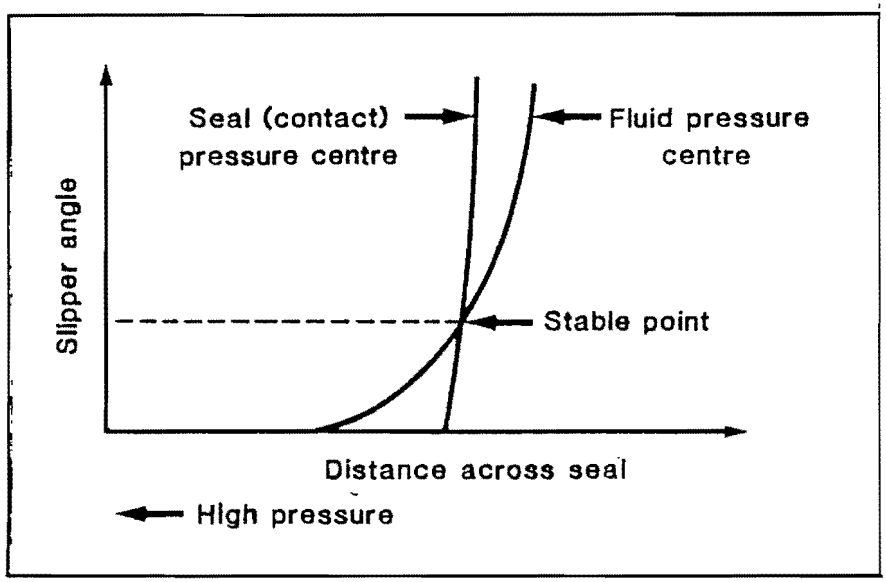

Figure 5.4 A CONDITION FOR STABILITY IN HYDRODYNAMIC LUBRICATION FILMS

The above explanation for the instability of hydrodynamic films that may form in piston seals did not take into account the elasticity of the seal, which further destabilizes the fluid film. Typical pressure profiles for the hydrodynamic film that may form are shown in figure 5.5, together with the pressure loading profiles due to the forces acting at the rear of the seal. At the trailing edge of the seal, the difference in the two pressure profiles is extreme and, in the case of an elastic seal, will cause the trailing edge to deflect towards the counterface, possibly touching and causing breakdown of the hydrodynamic film. If the seal face is to be kept flat then the pressure profiles for the different forces acting in the seal are to be identical. Rather,

the trailing edge of the seal can be made to deflect away from the counterface by suitably modifying the pressures acting at the rear of the seal. This method for improving the lubrication behaviour of seals is exploited further in the next section, using the elastohydrodynamic model for the behaviour of the seals.

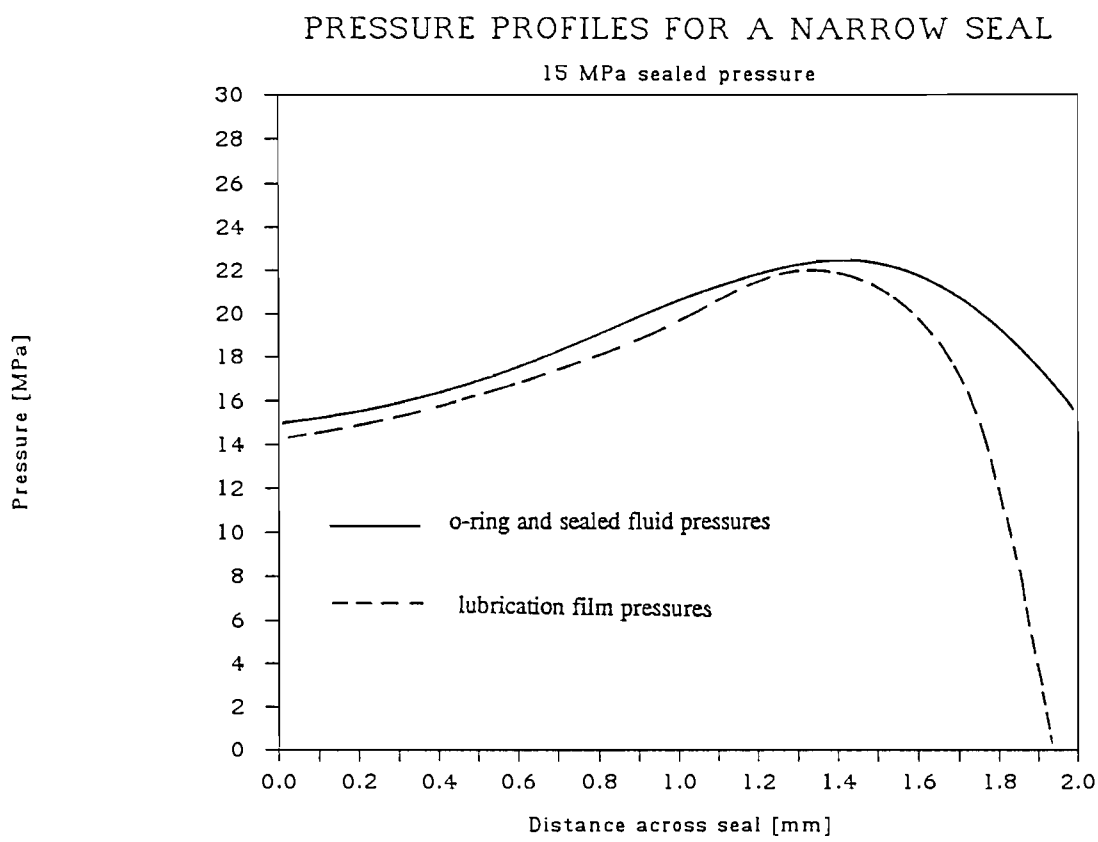

Figure 5.5 TYPICAL PRESSURE PROFILES FOR A NARROW SEAL

5.3 Modifications to encourage elastohydrodynamic lubrication.

An infinite number of seal designs are possible, many of which may represent an improvement over current seal types in terms of wear rate. The selection of alternate

seal designs has therefore been based on modifications likely to offer the greatest improvements, and that are feasible in terms of implementation in existing machines. The modifications are simple, namely

1. *Increase the seal length.*
2. *Provide an initial radial clearance between the seal and counterface.*
3. *Use the position of the o-ring to limit the extent of pressure behind the seal.*

Before the influence of each parameter was established, a new seal incorporating all of the above modifications was modelled, and the details are presented below. This modified seal forms a hydrodynamic film easily, even at low speeds, and although the seal does leak (essential if the seal does not wear), the leakage rate is extremely low and does not present a problem at all. Experimental verification of the seal performance has shown the seal wear to be 8 times less than existing seals made from the same material.

The new seal is shown if figure 5.6. The seal is 10 mm wide and 1.8 mm thick, with the usual o-ring precompressed to 15% but offset from the low pressure side of the seal by 2mm. Behind the o-ring is an anti-extrusion ring made of poly-acetal. The seal itself is manufactured from Solidur DS, a filled UHMWPE having superior wear properties to virgin UHMWPE. The seal is cylindrical and floats freely on the piston with a radial clearance of $10 \mu m$. The purpose of the o-ring is to force the seal against the piston to ensure that the seal always seals as the pressure is applied, and to modify the pressure profile acting at the rear of the seal in order to encourage the formation of a stable hydrodynamic film. The increased length of the seal further encourages the film formation. The resultant pressure profile that acts at the rear of the seal, used as an input to the model, is shown in figure 5.7 and has been obtained from the finite element analysis of the o-ring (70 Shore A nitrile rubber). No pressure build up has been allowed behind the seal since the pressure differential does not switch in the test rig. This results in the gauge pressure dropping to zero at the trailing edge of the seal.

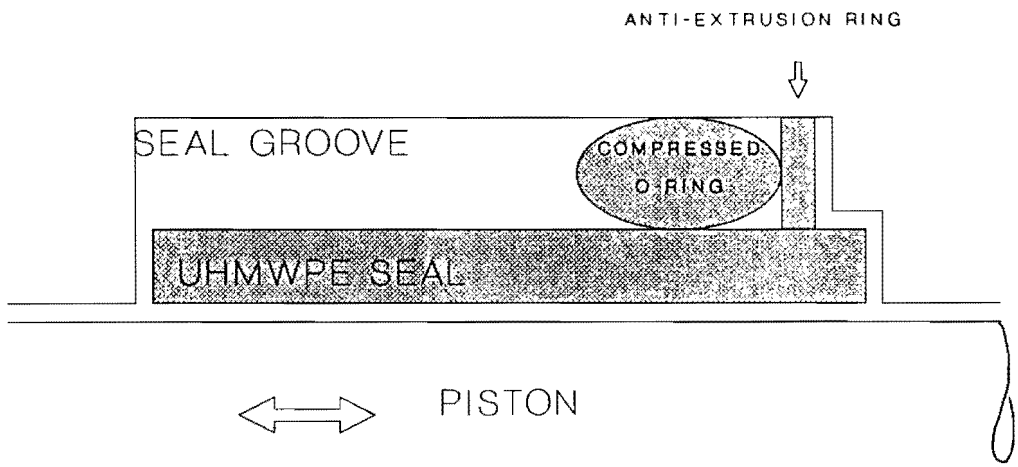

Figure 5.6 CONFIGURATION OF AN IMPROVED SEAL

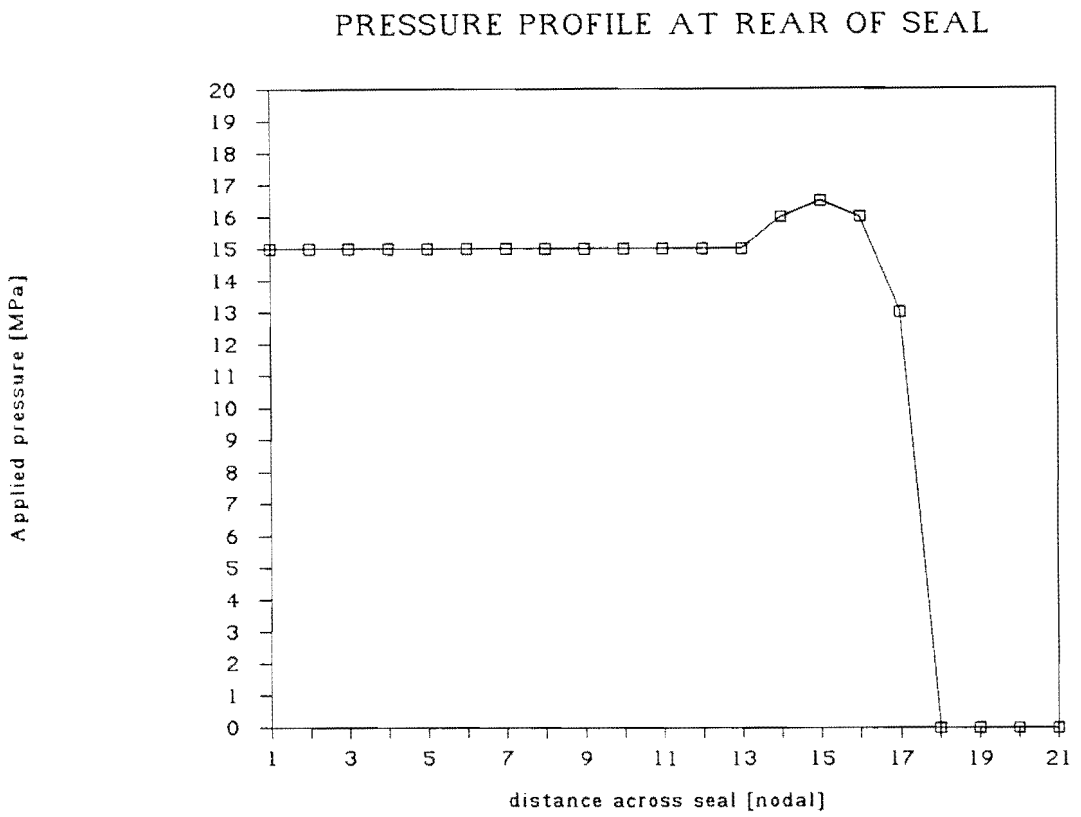

Figure 5.7 THE PRESSURE PROFILE AT THE REAR OF THE MODIFIED WIDE SEAL

The final result of the deformed seal profile over the counterface, sliding at 3.3 m/s, is shown in figure 5.8.

The minimum clearance above the counterface at the sliding speed of 3.3 m/s (average speed of the test rig piston) is $1.35\,\mu m$ and is in excess of the normally existing roughness parameter R_z which implies that the lubricating film formed is feasible and stable. The leading edge of the seal is well clear of the counterface, and this movement must be permissible in the seal design. Should the hydrodynamic film break down as the piston velocity approaches zero or opposes the direction of the

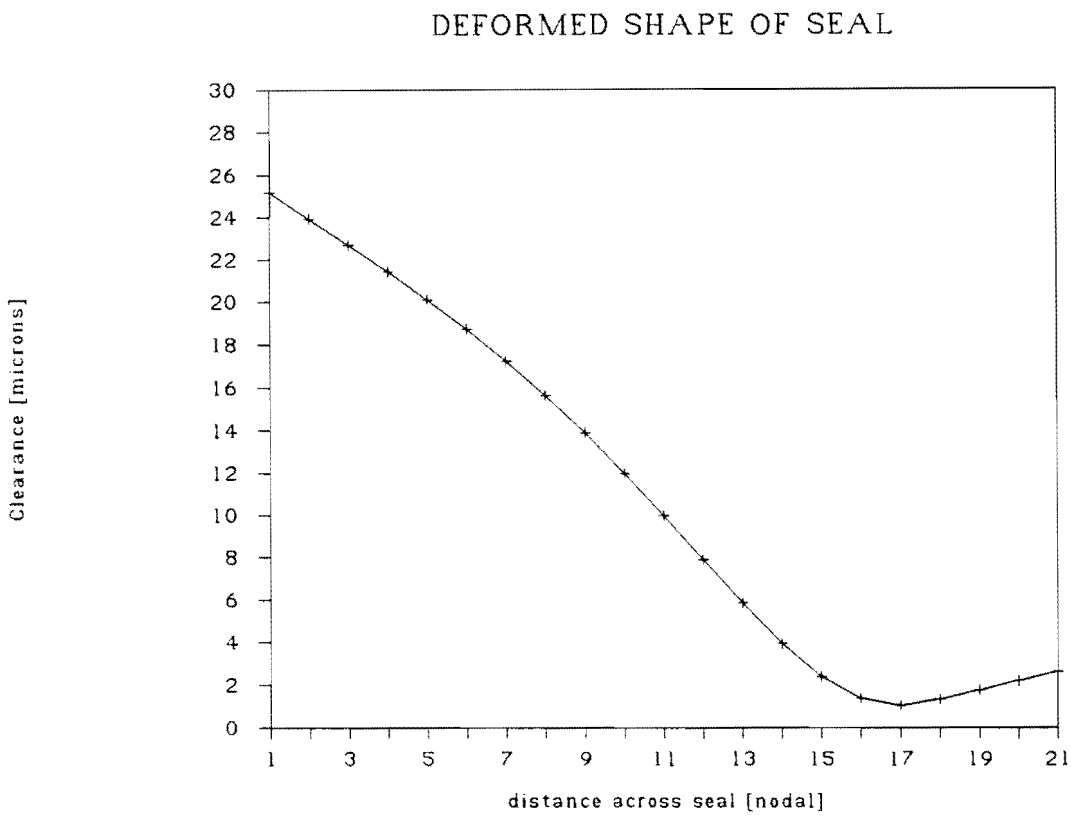

Figure 5.8 THE DEFORMED SHAPE OF THE MODIFIED WIDE SEAL

pressure drop across the seal, wear of the polymer seal will occur in a narrow band at the low pressure side of the seal. The calculated leak rate across the seal is 21 ml per minute.

The question as to how the seal will perform when the piston velocity is in an opposite direction to the pressure drop across the seal is important since this condition frequently arises in rockdrill seals. Should the response time of the seal be less than the 10 ms it takes for the pressure to cycle, the seal may contact the counterface during half the total piston cycle. The true leakage rate of the seal will then possibly be half that predicted by the model, ie. 10 ml per minute. This corresponds to the experimental leak rate obtained for the seal described above. What may happen to the seal

if it cannot respond fast enough so as to fully contact the counterface is not known, but the seal may assume an intermediate position above the counterface; somewhere between fully contacting and that described by the model. The condition will still ensure an adequate clearance above the counterface. In this case it may again be postulated that the leakage rate will be approximately 10 ml per minute. Notably the wear of the seal will be extremely low if the seal assumes this intermediate position during the entire cycle, being an advantage of using the seal in high frequency reciprocating applications.

In the following sections, the effects of changing the seal design parameters are studied with the elastohydrodynamic model. Unless otherwise mentioned, the seal is 1.8 mm thick, with an initial radial clearance above the piston of 10 μm. The piston speed has in most instances been kept constant at 3.3 m/s which corresponds to the average speed of the test rig, and of the rockdrill piston.

5.3.1 Seal length.

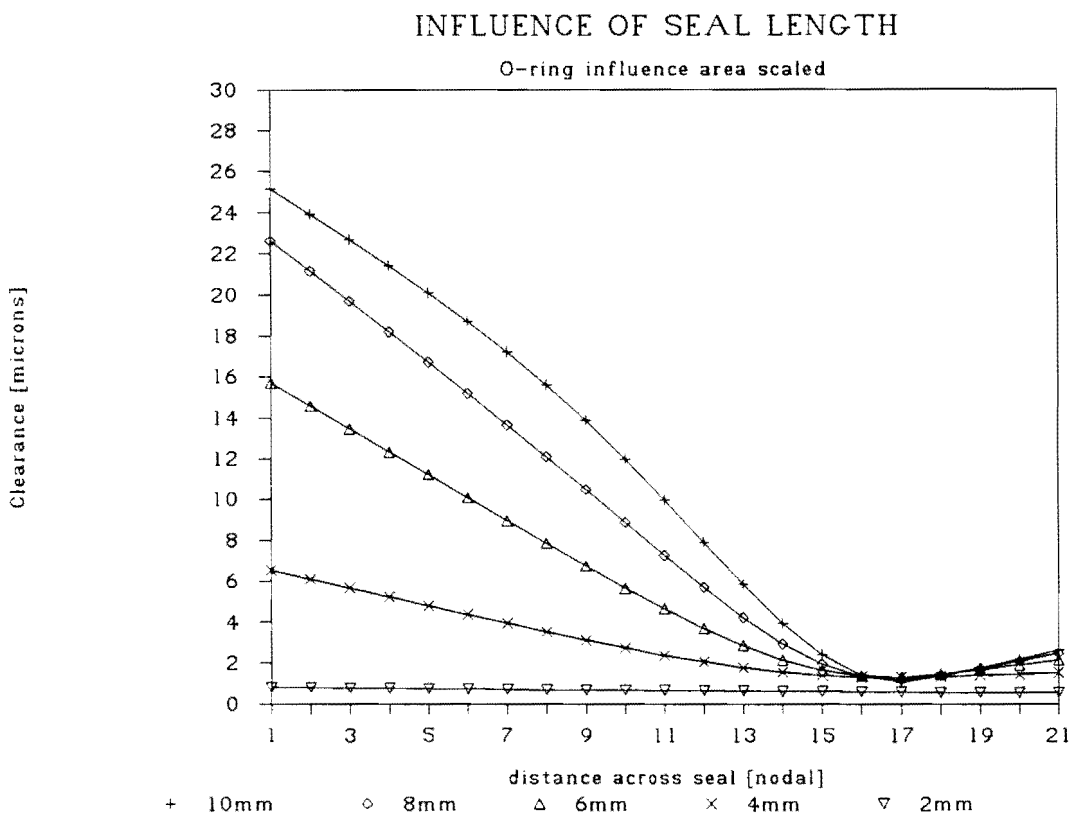

Figure 5.9. DIFFERENT SEAL LENGTHS
O-RING AREA OF INFLUENCE SCALED

The influence of the seal length is difficult to isolate, as is the case with several other of the parameters. In some instances increasing the seal length improves its lubrication performance, while at other times no benefit is gained. Figure 5.9 shows the deformed profiles of seals ranging from 10 mm long, down to 2 mm, where the pressure behind the seal was allowed to extend up to node number 17 (out of a total of 21 nodes along the seal length). This position corresponds to a distance of 2 mm from the low pressure side in the case of the 10 mm seal, but only 0.4 mm from the same side in the 2 mm seal. In other words, the effect of the o-ring has been scaled in proportion to the length of the seal. The minimum film thickness does not change

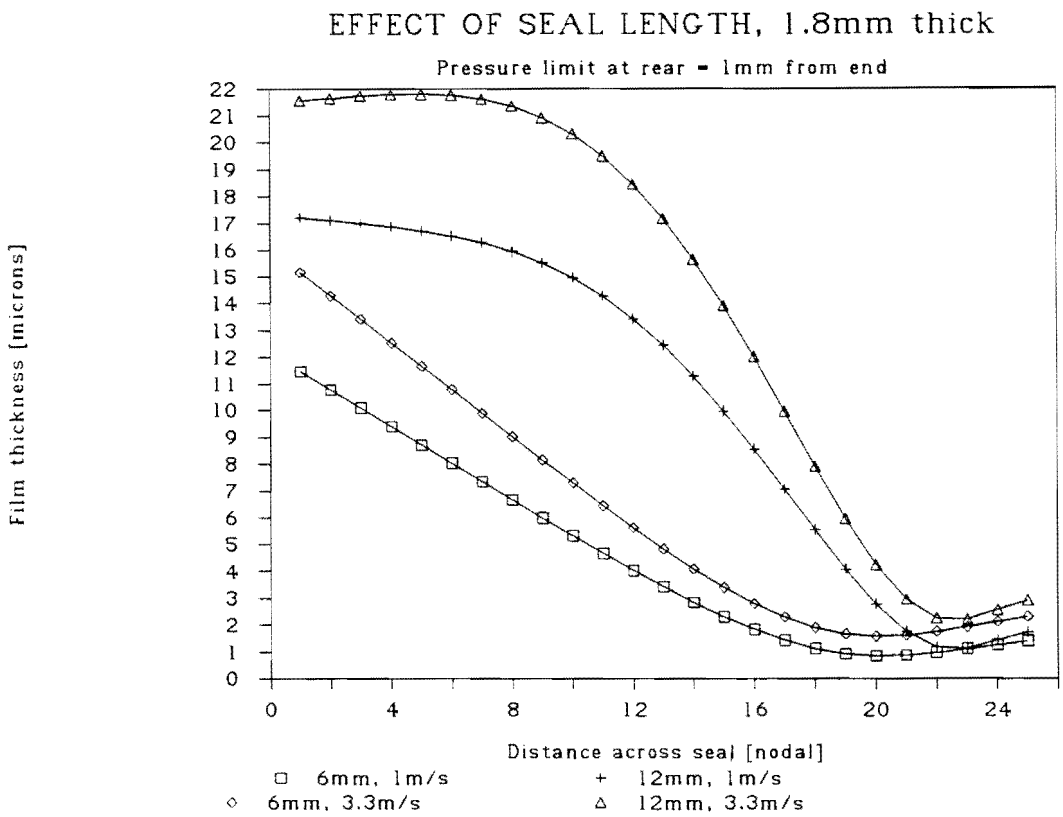

Figure 5.10 DIFFERENT SEAL LENGTHS
O-RING 1 mm FROM LOW PRESSURE SIDE

with decreasing length up to a length of 4 mm, in fact it increases slightly. However the leading film thickness drops rapidly with decreasing length which may adversely effect the dynamic behaviour of the seal as the lubricating film will collapse faster if pressure and velocity conditions become unfavourable. The leak rates for the seals longer than 2 mm were all between 21 and 27 ml/min. The lubricating film of the 2 mm seal is far thinner with a minimum film thickness of $0.5\,\mu m$ which may break down owing to the surface finish of the piston. The thin film is accompanied by a low leak rate of 7 ml/min.

If the area of influence of the o-ring is not scaled as the seal length is reduced, then the minimum film thickness decreases with decreasing seal length as is shown in figure 5.10 for two seals, 12 and 6 mm long, sliding at speeds of 1 and 3.3 m/s.

Thus increasing the seal length does improve the nature of the elastohydrodynamic film, but the benefits are dominated by the more important variable, namely the position of the o-ring, or extent of pressure penetration at the rear of the seal.

5.3.2 Seal thickness and elastic modulus.

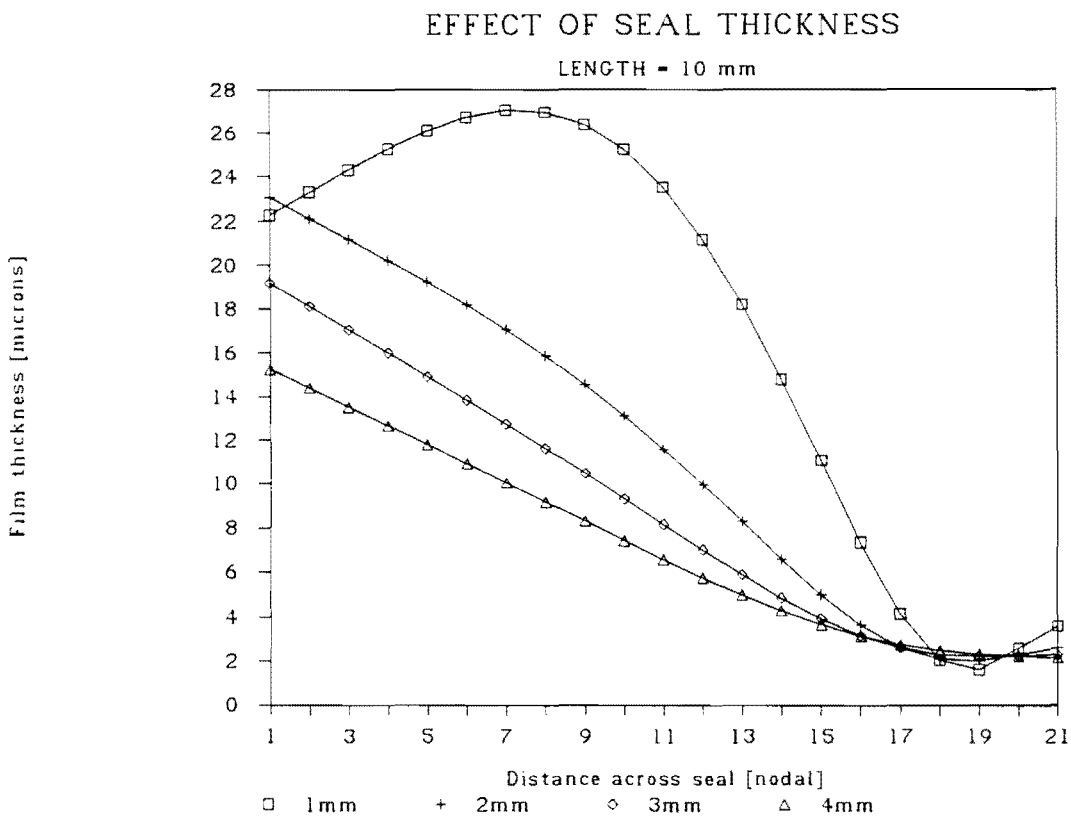

Figure 5.11 THE EFFECT OF SEAL THICKNESS

Seal thickness (figure 5.11), and elastic modulus have a similar effect on the deformation of the seal since the flexural rigidity of the polymer strip being modelled is a function of both parameters. Assuming that UHMWPE is the current optimal seal material, the only variable parameter is the seal thickness which is favourable since the flexural rigidity is proportional to the cube of the thickness and only linearly proportional to the modulus. The effect of increasing the seal thickness is to stiffen the seal, resulting in a less pronounced deflection towards the counterface. The performance of the seal with respect to wear rate will improve owing to a larger contact area if the seal touches the counterface. In addition, the response of the seal to rapidly changing pressures or velocity, will be slower and the seal may remain separated from the counterface for a greater portion of the cycle. The disadvantage in increasing the seal thickness, is that of space occupied in the rockdrill housing and difficulty in inserting the seals.

5.3.3 Piston speed.

Increasing piston speed has a favourable effect on the seal performance apart from increasing the leakage rate slightly. A seal designed about a lower speed limit will ensure the formation of a lubricating film at all higher speeds since the total force exerted on the seal by the lubricating film increases with increasing speed thus increasing the film thickness. There are in addition two other effects, opposing one another, that ensure the stability of the lubricating layer as the speed increases. Firstly as the speed of the piston increases in the direction of the pressure differential, the centre of pressure in the lubricating film shifts towards the seal trailing edge (low pressure side), thereby decreasing the angle of tilt of the seal. Opposing this, and ensuring that a stable angle is always achieved, is the effect that the centre of pressure in the film shifts towards the leading edge as the angle of tilt decreases. The effects of varying the counterface speed are shown in figure 5.12. By increasing the speed from 2 to 9 m/s, the minimum film thickness nearly doubles (shown at node 18 for the wide seals).

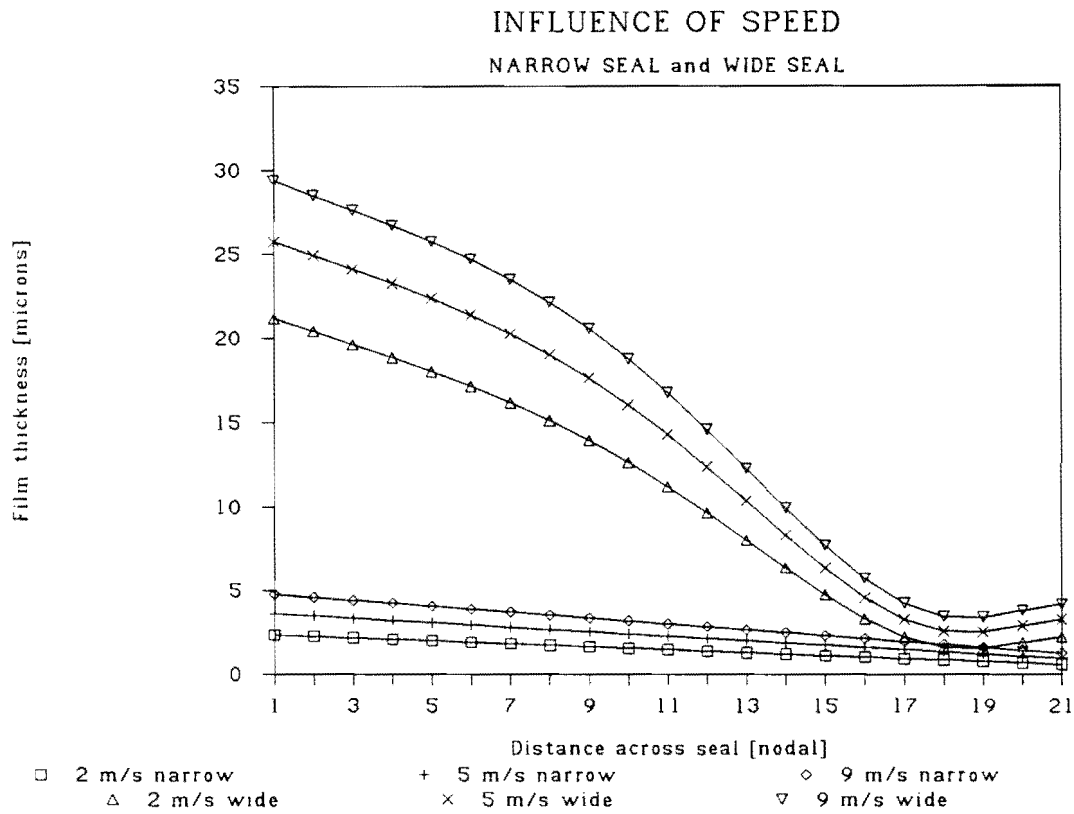

Figure 5.12 THE EFFECT OF PISTON SPEED

5.3.4 Radial clearance.

Increasing the initial radial clearance of the seal does not affect the minimum film thickness nor does it alter the leak rate significantly as illustrated in figure 5.13. In addition the problems of initial sealing are eliminated by the use of an energiser which ensures that the seal is in contact with the counterface before pressure is applied to the seal. Machining tolerances of the inner seal diameter can thus be relaxed, so long as there exists some radial clearance between the seal and counterface. The dynamic behaviour of the seal is beyond the scope of this thesis, but the effects of lowering the initial clearance to below 5 or 10 μm may be adverse. The leading edge of the

seal starts to move closer to the counterface with decreasing initial seal clearance, and no stable solution for elastohydrodynamic film formation was found using an initial radial clearance of $2\,\mu m$.

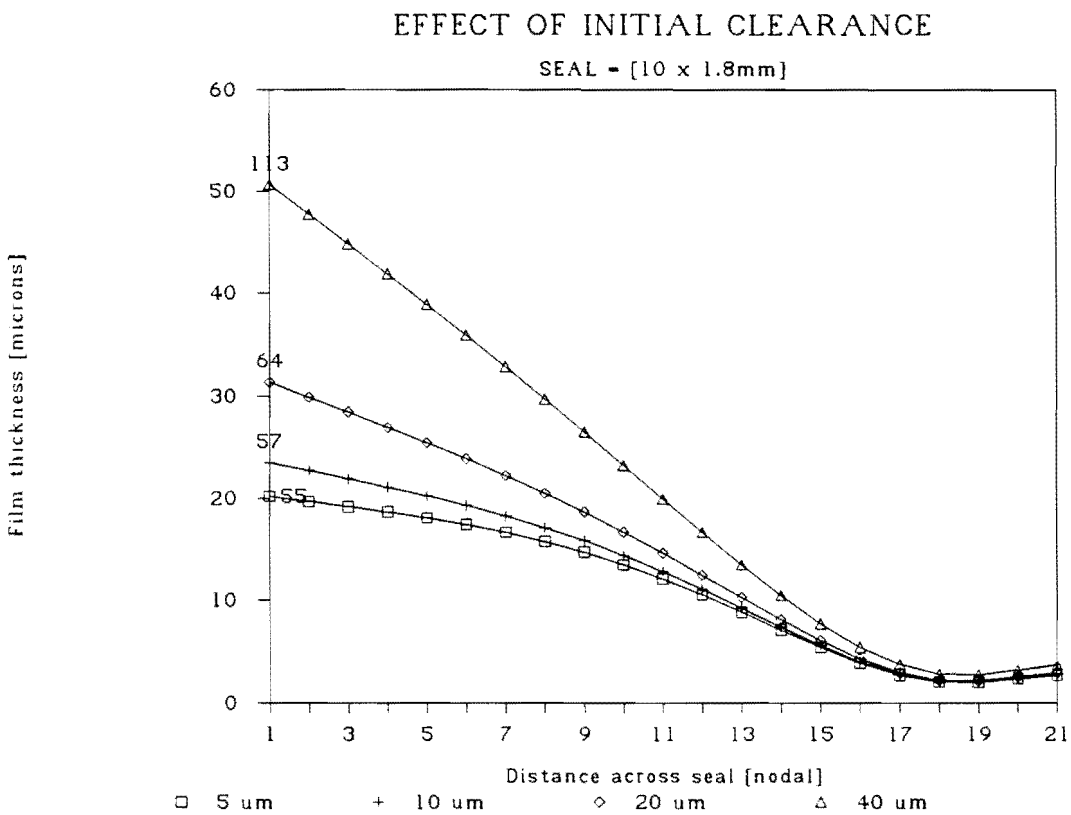

Figure 5.13 THE EFFECT OF INITIAL RADIAL SEAL CLEARANCE

5.3.5 Counterface roughness.

The counterface roughness is crucial in encouraging lubrication of the seal, and while the elastohydrodynamic model does not include roughness effects on the counterface, the influence is clear and has been learned from earlier experiments on hydrodynamic film formation. An elastohydrodynamic film will break down, in part or in full, if the

counterface roughness (R_z), exceeds the minimum film thickness. The critical regime where the counterface roughness is approximately equal to the minimum film thickness is often termed micro-elastohydrodynamic lubrication. In this region the friction and wear of the polymer is still limited, as the interaction between the polymer and counterface asperities is small [11].

In terms of wear mechanisms between the seal and counterface, the established optimum surface roughness of $0.2\mu m$ R_a should be sufficient to allow film formation. Below this roughness, adhesive wear of the polymer dominates, whereas abrasive wear dominates in rougher counterfaces. However, it is felt that the lubrication advantages to be gained by polishing the counterface may outweigh any increased effects of adhesive wear between the two components.

5.3.6 Sealed pressure.

Sealed pressure seems to have little effect on the film formation, as shown in figure 5.14. Increasing the pressure to 30 MPa, compared with the normal 15 MPa, decreased the minimum film thickness from $2\mu m$ to $1.2\mu m$ while also decreasing the leak rate by 20 ml/min to 38 ml/min. Lowering the sealed pressure to 7.5 MPa had the reverse effect, increasing the film thickness by $1\mu m$ and the leak rate by 20 ml/min.

In general, however the changed seal performance as predicted by the model is not significant as the film remains fairly thick, and the leak rates low.

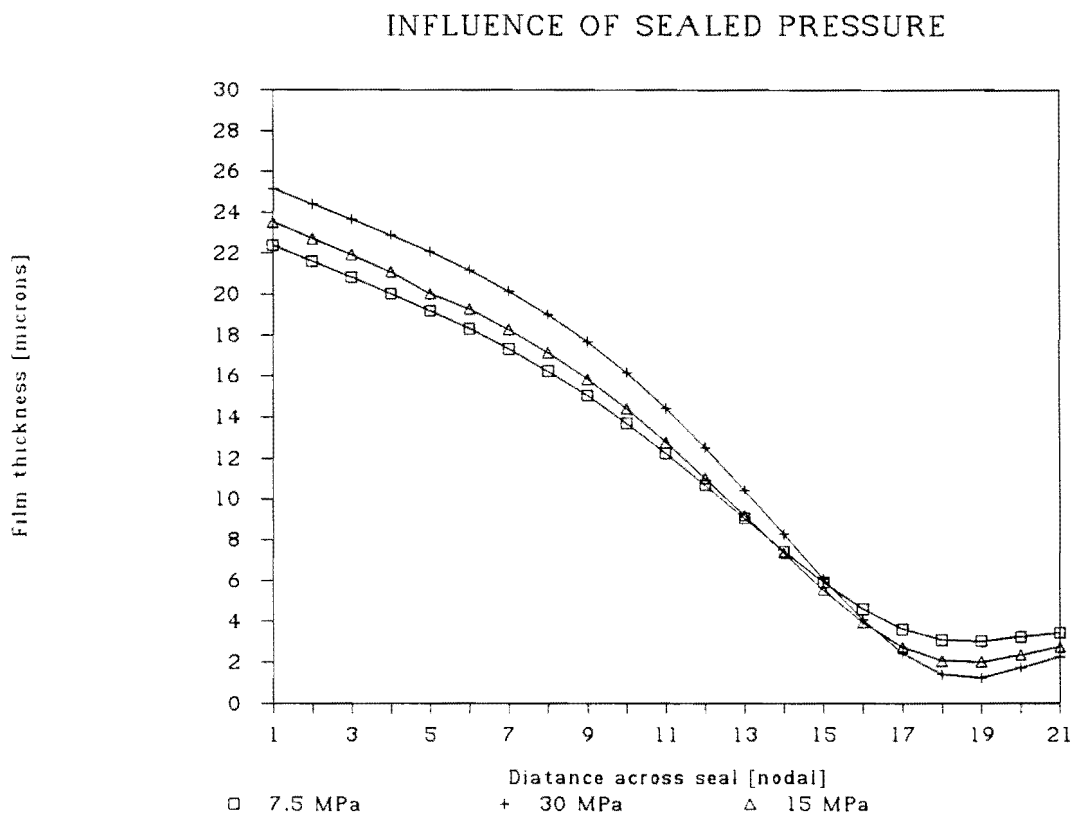

Figure 5.14 THE EFFECT OF SEALED PRESSURE

5.3.7 O-ring positioning.

The position of the o-ring behind the seal limits the extent of pressure penetration and thus modifies the fluid pressure profile at the rear of the seal. It will be clear from earlier discussions that it is desirable for the pressure profile behind the seal to match that of the hydrodynamic film. Thus the optimum position of the o-ring lies between two extremes: namely in the centre of the seal and at the trailing edge of the seal (low pressure side). For an o-ring placed in the centre behind the seal, the centre of pressure of the lubricating layer is always downstream of the resultant of the other forces acting on the seal. No stable lubricating film is therefore possible due to the resultant moment on the seal tending to tilt the leading edge of the seal against the counterface. The wear of the seal will occur at a high rate on the leading

half of high pressure side of the seal. The optimum position for the energiser is offset from the low pressure side of the seal a distance of between 5% and 20% of the seal's length. Figure 5.15 shows film profiles for 10 mm wide seals [or 21 nodes long] with the o-ring situated at different nodal positions across the seal face, measured from the high pressure side of the seal. With the o-ring at nodal positions of 16 and less, no film formation was possible (according to the model results). For the o-ring placed at node 20, the seal trailing edge starts deflecting towards the counterface, and when placed at node 21, no solution is possible.

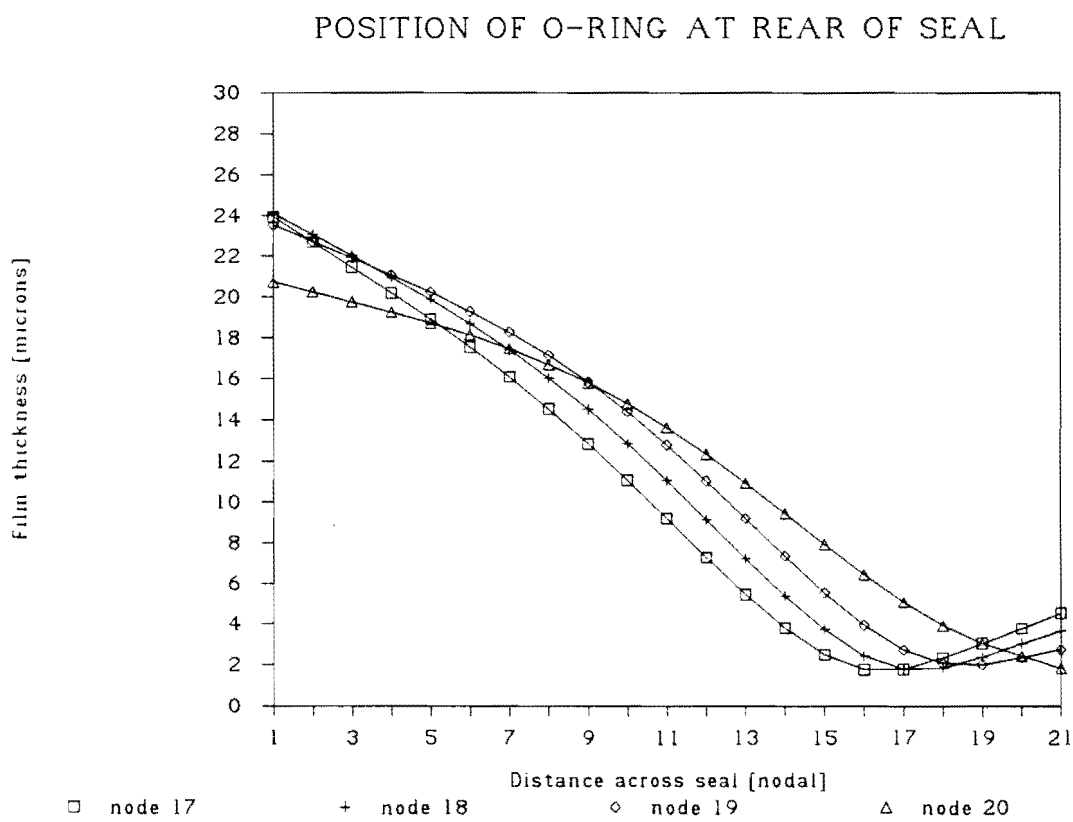

Figure 5.15 THE EFFECT OF O-RING POSITION

5.3.8 The effects of initial o-ring precompression or squeeze.

No significant effects were noted in the elastohydrodynamic film as the squeeze of the o-ring was varied. This is due to the high stiffness of the elastohydrodynamic film at the equilibrium position shown in figure 4.19. The only important requirement is that the o-ring forces the seal against the counterface with some pressure to prevent leakage of the seal on start-up of the rockdrill.

Chapter VI. HIGH SPEED SEAL TEST RIG RESULTS

The experimental test results are given for a series of different tests designed to confirm the predictions of the elastohydrodynamic model and produce experimental wear rates for the different seals.

In all the tests the sealed pressure was kept constant at 15 MPa, and the counterface was always hard-chrome plated and ground to a roughness of $0.2\mu m$ R_a perpendicular to the sliding direction.

Figure 6.1 shows wear data for a narrow virgin UHMWPE seal in the standard configuration with a square energiser. The increased volume wear loss over mass loss is due to water absorption by the polymer. The wear rate of the seal in the test is 2.8×10^{-16} $m^3N^{-1}m^{-1}$ which is in agreement with laboratory wear data obtained for UHMWPE at low speeds in the absence of any hydrodynamic lubrication. The seal test data therefore indicates that the seal remains in contact with the piston at all times, never forming any lubricating film, and this is in agreement with the results from the elastohydrodynamic model. No leakage occurred across the seal face which is further indication of the absence of a lubricating film.

Figure 6.2 shows a similar test using the same seal configurations but changing the seal material from UHMWPE to the filled material, Solidur DS. The wear rate for Solidur DS is approximately 10 times lower than the virgin UHMWPE, which is again in agreement with laboratory wear data for the two materials. Again the results indicate no formation of a hydrodynamic film.

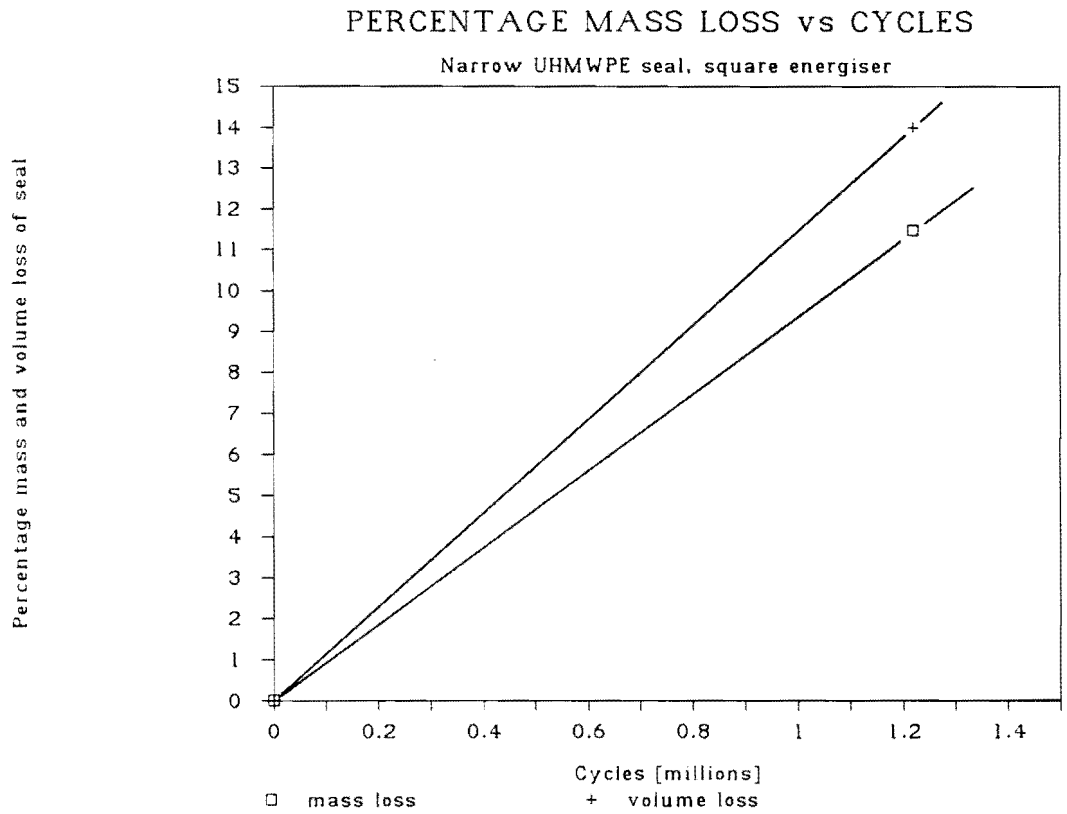

Figure 6.1 WEAR RATES FOR NARROW STANDARD SEALS [virgin UHMWPE]

Figure 6.3 shows four similar results for the mass loss of 10 mm wide Solidur DS seals using a 70 Shore A round energiser, compressed to 15% and offset a distance of 2 mm from the low pressure side of the seal. The initial radial clearance between the seal and piston was approximately $10\mu m$. Two of the results show a relatively higher wear rate, and this is confirmed by lower leak rates of the same seals shown later in figure 6.5. It is probable that the radial clearances were slightly less in these two seals as it is difficult to measure to within $10\mu m$ in the case of a polymer seal. The overall wear rates of the seals are extremely low, with the seal not wearing at all in two of the tests. The results indicate that elastohydrodynamic lubrication is dominant during the entire seal cycle and the seal leak rates of nominally 10 ml/minute are in close agreement with the predictions of the elastohydrodynamic model.

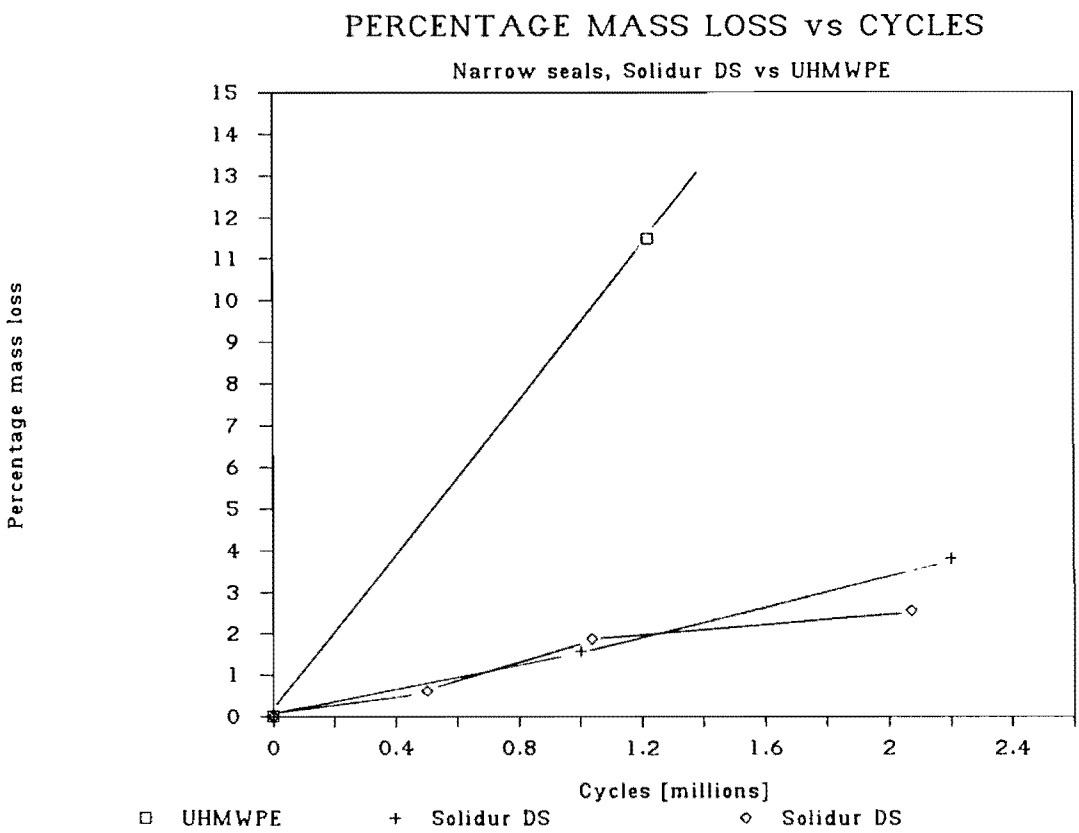

Figure 6.2 WEAR RATES FOR NARROW STANDARD SEALS [Solidur DS]

On observation, the inner seal surface was polished along the last third of its length at the low pressure side indicating that the lubrication film did at some stage collapse, either initially or repeatedly during the cycle. The area of the seal that contacted the counterface is in agreement with the portion of the seal lying closest to the counterface in the model predictions. The leading two thirds of the seal surface did not touch the counterface at all and the original machining marks on the polymer were undamaged.

By changing the position of the o-ring, or in this case a square energiser ring, it was possible to destroy the elastohydrodynamic layer completely as predicted by the model. Figure 6.4 shows the previous results for the wide seal with off-set o-ring together with the results wherein the o-ring was situated right up against the low

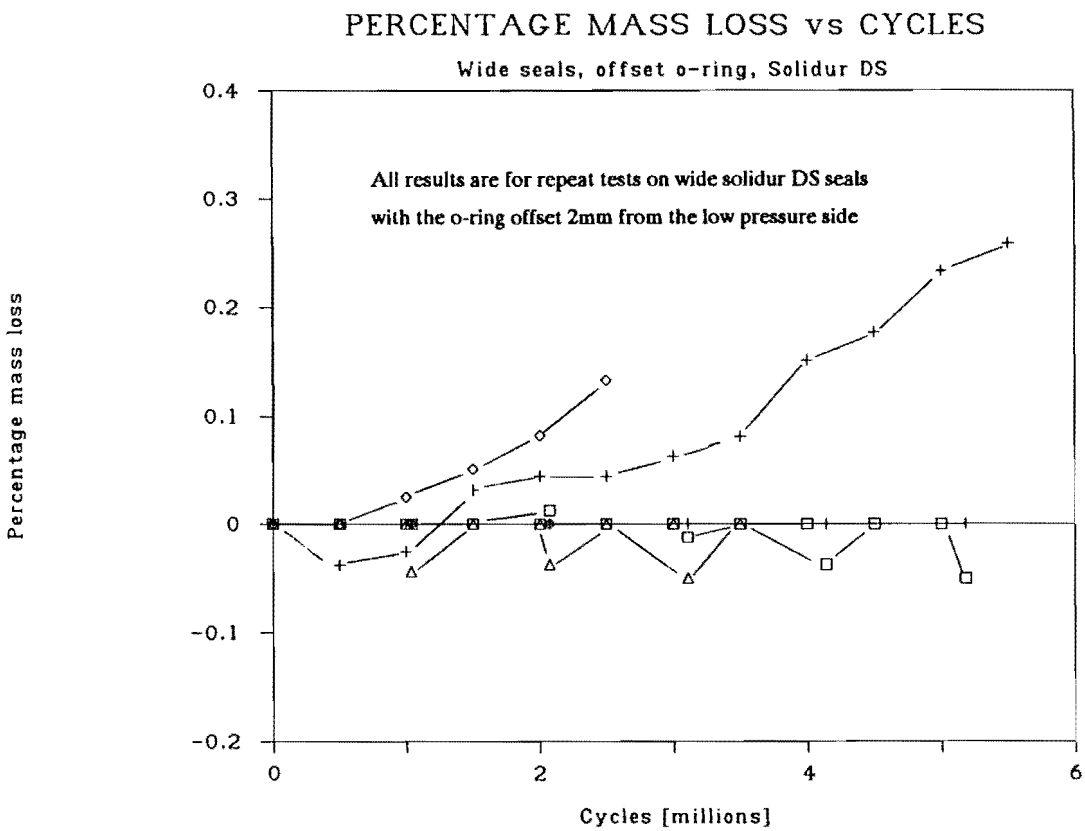

Figure 6.3 WEAR RATES FOR WIDE MODIFIED SEALS [Solidur DS]

pressure side of the seal. With no o-ring off-set, the wear results for the seal, correspond to those for narrow seals with lubrication film. For the purposes of comparison, the percentage mass loss data for the narrow seals have been divided by 3 since the wide modified seals only wore along the lower third of the seal length. The improvement in using wide seals with an offset o-ring is approximately eight (8) fold, compared to existing narrow seals of the same material. Compared to existing narrow seals made from virgin UHMWPE, the improvement in performance is eighty (80) fold using the experimental seal test rig.

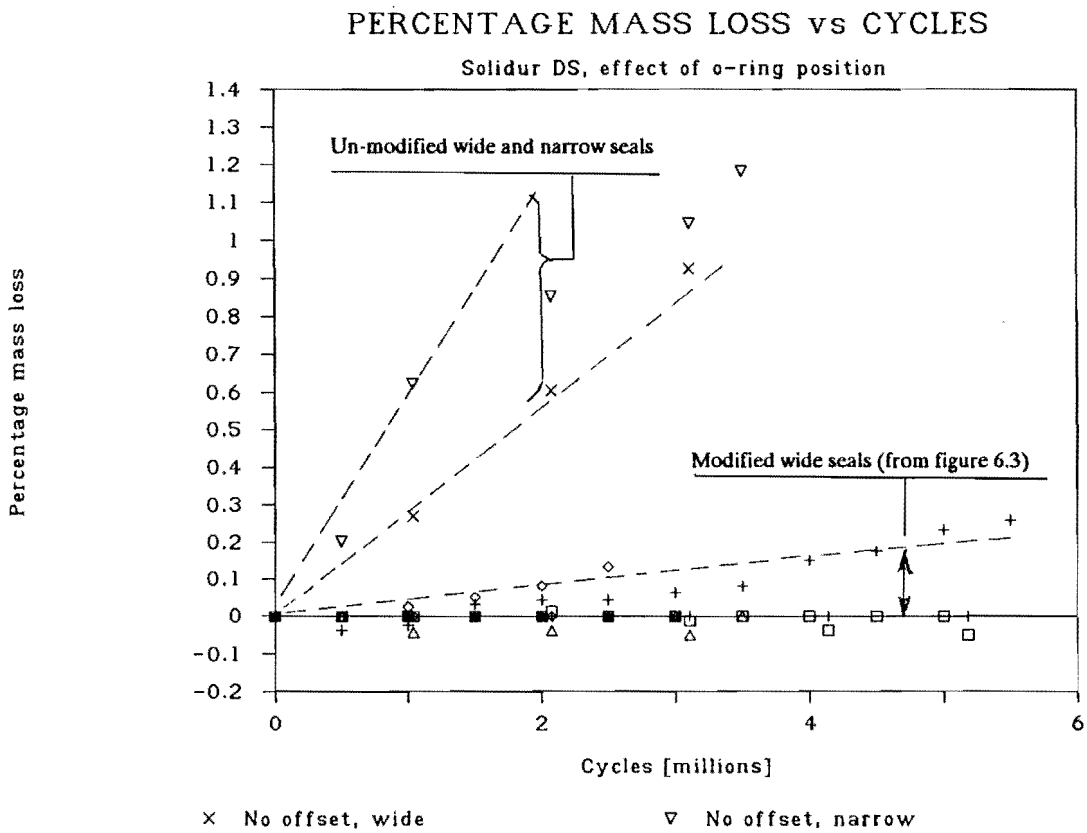

Figure 6.4 WEAR RATES FOR WIDE AND NARROW SEALS

As a result of the formation of an elastohydrodynamic film, the seals must leak, and the range of measured leak rates for the four modified wide seals tested in the rig are shown in figure 6.5. Even the higher leak rates are acceptable though, for use in rockdrills.

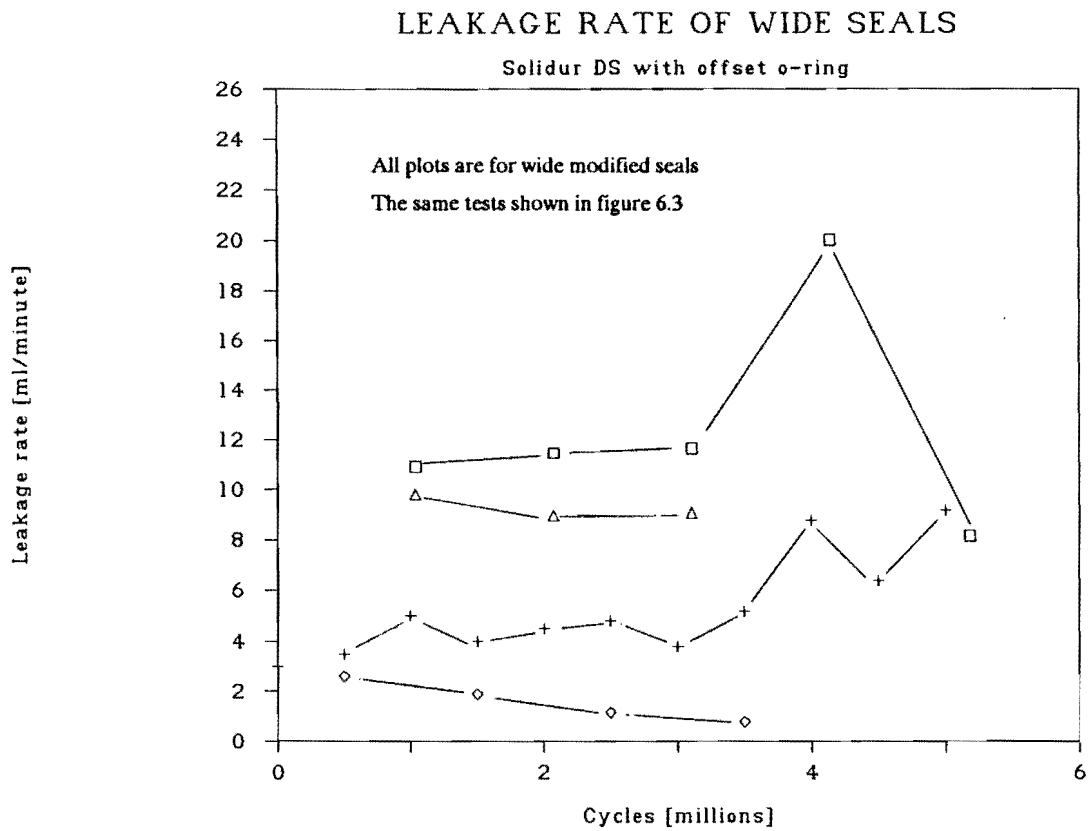

Figure 6.5 LEAK RATES OBTAINED FOR THE MODIFIED WIDE SEALS

Chapter VII. CONCLUSIONS.

The performance of rockdrill piston seals in relation to the formation of an elastohydrodynamic film has been determined. In essence, the poor wear properties of the seals can be attributed, in part, to the lack of formation of such a film, resulting in high contact stresses at the sealing face. An elastohydrodynamic model has been developed to simulate the behaviour of the seals, and has identified reasons for the instability of the elastohydrodynamic film. As a result, design modifications have been implemented in new seals and shown to improve the wear rate of seals by a factor of eight under laboratory conditions. The conclusions drawn from the analysis of existing and modified rockdrill piston seals can be listed as follows:

1. Existing piston seals (both narrow and wide seals) do not form any elastohydrodynamic film. This is due to the fact that the forces acting on the seal are not balanced, and the resultant moment causes the low pressure side of the seal to contact the counterface.

2. Seals can form a stable and sufficiently thick lubricating film if suitable changes are made with regard to the following:

   The position of the o-ring at the rear of the seal.
   The length of the seal.
   The initial radial clearance between the seal and piston.
   The counterface roughness of the piston.

3. The most significant improvement in the elastohydrodynamic behaviour of seals can be achieved by modifying the pressure profile acting at the rear of the seals. This can be achieved by shifting the o-ring away from the low pressure side of the seal by a distance of between 5 and 20 percent of the seal length.

4. Increasing the length of the seal increases the average thickness of the lubricating film, but does not necessarily increase the leak rate across the seal. If the o-ring is positioned in accordance with the distances given in conclusion 3 above, the minimum film thickness does not change for seals of 4mm and longer.

5. There must exist an initial radial clearance between the seal and counterface (excluding the effect of the o-ring) for a lubricating layer to form. This initial clearance must be between 5 and 40 μm.

6. The o-ring squeeze is of little consequence in modifying the lubricating properties of the seals. However, an initial squeeze must be sufficient (taking into account the relaxation of o-ring stresses with time) to ensure that the seal contacts the piston before operation to prevent excessive leakage.

7. The mean peak to valley asperity height of the counterface (R_z) must always be less than the minimum film thickness.

8. The lubricating film is not significantly affected by changes in sealed pressure (dynamic effects excluded).

9. Modified wide piston seals have shown experimental wear rates 8 times lower than existing piston seals made of the same material, Solidur DS.

The elastohydrodynamic model is implementable on a personal computer and may be used for the analysis of future seal designs as a screening test before actual testing in rockdrills.

Chapter VIII. RECOMMENDATIONS.

The seal modifications required to encourage elastohydrodynamic lubrication differ depending on the operating conditions of the seal. If conditions are favourable for the formation of a lubricating film at all times, that is the pressure drop is always in the direction of the relative velocity of the piston, then the following recommendations are made:

1. Increase the seal width to 4 mm or longer, while maintaining existing thicknesses of approximately 1.8 mm. The seal material should be Solidur DS.

2. Shift the position of the o-ring so that it lies a distance of 12% of the seal length, away from the low pressure side of the seal. Precompress the o-ring by 10 to 15% and ensure that 70 Shore A nitrile rubber is used. Flouro-elastomers of similar hardness may also be used.

3. Ensure an initial radial clearance between the seal and counterface (excluding the o-ring effects) of between 5 and 40 μm.

4. The counterface hardness is of less importance than the surface finish which should be less than 0.1 μm R_a.

If conditions favourable for lubrication exist during only a portion or half of the total cycle, the above recommendations apply except for the following two modifications:

1. The length of the seal should be between 7 and 10 mm.

2. The initial radial clearance between the seal and counterface should be in excess of $10\,\mu m$, but less than $40\,\mu m$.

Chapter IX. REFERENCES.

1. **Bohm, H., Betz, S., Ball, A.** (1990). The wear resistance of polymers. Tribology International, v23, n6, pp 399-406.

2. **Hampson, L.G.** (1989). Wear of polymers in water: Stage 1 report. NCT Report 3689/606. Risely, UK.

3. **LLoyd, A.I.G.** (1986). The sliding wear of UHMWPE against steel. MSc thesis, University of Cape Town.

4. **Johannesson, H.** (1980). On the optimization of hydraulic cylinder seals. Doctoral thesis. University of Lulea.

5. **Finney, R.H., Kumar, A.** (1988). Development of material constants for non-linear finite element analysis. Rubber Chemistry and Technology, v61, n11, pp 879-891.

6. **ABAQUS User's Manual,** (1987). Hibbitt, Karlsson and Sorenson, Inc., Providence, Rhode Island.

7. **Hooke, C.J., O'Donoghue, J.P.** (1972). Elastohydrodynamic lubrication of soft, highly deformed contacts. J. Mech. Eng. Sci, v14, n1, pp 34-48.

8. **Field, G.J., Nau, P.S.** (1973). The lubrication of rectangular rubber seals under conditions of reciprocating motion. BHRA Fluid Eng. Report RR 1200.

9. **Jaffar, M.J.** (1990). Two-dimensional elastohydrodynamic lubrication of elastic strips. Wear, v139, n2, pp 335-350.

10. **Prati, E., Strozzi, A.** (1983). Elastohydrodynamic lubrication in elastomeric reciprocating seals; Part 2: Theoretical, experimental and numerical methods. Plastics and Rubber Processing and Applications, v3, n1, pp 1-8.

11. **Evans, C.R.** (1987). The influence of surface roughness on elastohydrodynamic traction. Proc. Instn. Mech Engrs. v201, nC2, pp 145-150.